

LIFE CYCLE ASSESSMENT OF MARINE COATINGS

by

Ryan Ingham

Submitted in partial fulfilment of the requirements  
for the degree of Master of Applied Science

at

Dalhousie University  
Halifax, Nova Scotia  
April, 2022

Dalhousie University is located in Mi'kma'ki,  
the ancestral and unceded territory of the Mi'kmaq.  
We are all Treaty people.

© Copyright by Ryan Ingham, 2022

This thesis is dedicated to my mom, dad, three brothers, girlfriend, dog, and housemates: Cindy, Andrew, Alex, Harrison, Brooklyn, Ellie, Benson, Ian, and Cooper. Thank you for your love and support throughout my degree and for keeping life interesting.



# Table of Contents

LIST OF TABLES .....	v
LIST OF FIGURES.....	vii
ABSTRACT.....	ix
LIST OF ABBREVIATIONS USED.....	x
ACKNOWLEDGEMENTS .....	xi
<b>CHAPTER 1 INTRODUCTION.....</b>	<b>1</b>
1.1 Global Shipping .....	1
1.2 Marine Coatings.....	2
1.3 Life Cycle Assessment.....	6
1.4 Research Motivation .....	7
1.5 Structure of this Thesis.....	8
<b>CHAPTER 2 FUEL &amp; GHG ANALYSIS OF A SMALL FISHING FLEET .....</b>	<b>9</b>
2.1 Introduction .....	9
2.2 Materials & Methods.....	11
2.2.1 Vessel dimensions and specifications .....	11
2.2.2 Sea Trials.....	13
2.2.3 Fuel Oil Consumption Analysis.....	15
2.2.4 Analysis Method #1: One-Way ANOVA Normalized 8 knots.....	15
2.3.4 Analysis Method #2: All Speed Runs.....	16
2.4 Results and Discussion.....	17
2.4.1 Hull Biofouling Results .....	18
2.4.2 Fuel Data Results from Analysis Method #1 .....	23
2.4.3 Fuel Data Results from Analysis Method #2 .....	24
2.4.4 Max Throttle Speed Comparison for All Boats .....	26
2.5 Sources of Error .....	27
2.6 Avoided Green House Gas Emissions .....	29
2.7 Limitations and Recommendations for Future Work.....	32
2.8 Conclusions .....	33
<b>CHAPTER 3 FRICTIONAL DRAG MEASUREMENTS IN A FULLY</b>	
<b>TURBULENT FLOW CHANNEL .....</b>	<b>34</b>
3.1 Introduction .....	34

3.2 Materials & Methods.....	36
3.2.1 Experimental Apparatus.....	36
3.2.2 Test Panel Design & Preparation.....	37
3.3.3 Panel Surface Roughness Profiles.....	39
3.3.4 FTFC Pressure Drop Measurements.....	40
3.3.5 Experimental Uncertainty.....	43
3.4 Results and Discussion.....	44
3.4.1 Wall shear stress comparison.....	44
3.4.2 Skin friction coefficients.....	45
3.4.3 Determination of the Roughness Functions.....	48
3.4.4 Granville Similarity Law Scaling Procedure.....	52
3.5 Conclusions and Recommendations for Future Work.....	58
CHAPTER 4    LIFE CYCLE ASSESSMENT OF MARINE COATINGS.....	61
4.1 Introduction.....	61
4.2 LCA Methodology.....	64
4.2.1 Goal and scope definition.....	64
4.2.2 LCA boundary and model assumptions.....	65
4.3 Life Cycle Inventory.....	67
4.3.1 Marine Coating Production.....	67
4.3.2 Application of Marine Coatings.....	69
4.3.3 In-Service Operation of the KRISO containership.....	71
4.4 Life Cycle Impact Assessment.....	78
4.4.1 Results for Marine Coating Production & Application.....	78
4.4.2 Results for In-Service Scenarios #1 & #2.....	80
4.5 Life Cycle Interpretation.....	83
4.5.1 Other LCA Limitations.....	86
CHAPTER 5    CONCLUSIONS, LIMITATIONS AND RECOMMENDATIONS FOR FUTURE WORK.....	88
Appendix A: Supplementary Sea Trial Data.....	90
Appendix B: Supplementary Fully Turbulent Flow Channel Data.....	98
Appendix C: Supplementary LCA Data.....	101
BIBLIOGRAPHY.....	102

# LIST OF TABLES

Table 1: Historical developments of anti-fouling paints adopted from Dafforn et al. (2011). .....	3
Table 2: Overview of the main marine coating types, adapted from Van Rompay (2012). .....	5
Table 3: Attributes of the four Cape Islander fishing vessels. ....	11
Table 4: Instrumentation and parameters recorded during the sea trials.....	13
Table 5: Sea trial hull conditions and nominal speed runs for all vessels.....	15
Table 6: NSTM fouling ratings adopted from Oliveira and Granhag (2020) for this study. ....	18
Table 7: Hull inspection results for each vessel including coating type and hull fouling coverage/condition. .....	21
Table 8: Resulting hull fouling NSTM ratings and corresponding $k_s$ values for each vessel.....	22
Table 9: Cruising speed FOC results from the interval plot of the average speed adjusted FOC.....	24
Table 10: Cruising speed FOC results from exponential fit.....	25
Table 11: List of GHG pollutants from the combustion of marine diesel oil according to the Fourth IMO GHG Study (2020).....	29
Table 12: Relative fuel and GHG emissions savings based on hull condition.....	29
Table 13: Overview of each test panel set, marine coating systems applied, coating types and method of application.....	38
Table 14: Average surface roughness parameters for each test surface from profilometer. ....	40
Table 15: Relative change in $C_f$ values of the test panels with respect to the Reference Panel. ....	46
Table 16: $\Delta U^+$ and $k^+$ values for each coated panel set. ....	50
Table 17: Design parameters for the KRISO Container Ship (KCS), adapted from (Song et al., 2021a). ....	54
Table 18: Granville scale-up results using the previously determined roughness functions compared to those found in literature. ....	54
Table 19: Granville scale-up results for the KVLCC2 compared to CFD simulated results (Zhang et al., 2021). ....	56
Table 20: OpenLCA inventory for BRA640 hazardous raw material components. ....	68
Table 21: Product specifications including dry film thickness, VOC content, coverages, and amounts to coat the hull of the newbuild case vessel. ....	71
Table 22: GWP comparison per $m^2$ surface area with biocide-based anti-fouling coatings found in literature. ....	79
Table 23: LCA results for each coating system in both in-service scenarios (in terms of Global Warming Potential ( $GWP_{100}$ ), Acidification Potential (AP), Photochemical Oxidation Creation Potential (POCP), and Marine Aquatic Ecotoxicity Potential ( $MAETP_{inf}$ )). ....	82
Table 24: LCA data quality rating system for the Ecoinvent database using four indicators (Reliability, Completeness, Temporal Correlation, and Further Technological Correlation) .....	83
Table 25: Overview of all speed trial dates and vessel hull conditions. ....	94

Table 26: OpenLCA inventory for INT1100SR hazardous raw material components. ....	101
Table 27: OpenLCA inventory for XGIT-Fuel hazardous raw material components. ....	101

# LIST OF FIGURES

Figure 1: Classifying fouling organisms commonly found on ship hulls; adapted from Demirel (2015) .....	3
Figure 2: The life cycle assessment framework according to ISO 14040 (2006). .....	6
Figure 3: Typical relationship between total resistance coefficient and vessel speed, adopted from (USNA, 2002) .....	12
Figure 4: Image of the sea trial location (denoted by the red star), obtained from <i>Mapcarta</i> (2022).....	14
Figure 5: Image of vessel Delta heading out for a sea trial on a calm day, typical of other testing conditions. ....	14
Figure 6: Estimated hull fouling rating over time based on environmental conditions and number of idle days. ....	20
Figure 7: Idle time of vessels Alpha and Bravo over 12-months. ....	21
Figure 8: Alpha 8 knot Speed Adjusted Fuel Oil Consumption for Various Hull Conditions.....	23
Figure 9: Bravo 8 knot Speed Adjusted Fuel Oil Consumption for Various Hull Conditions.....	23
Figure 10: Exponential Fit for Alpha Fuel Oil Consumption vs. Speed .....	24
Figure 11: Exponential Fit for Bravo Fuel Oil Consumption vs. Speed .....	25
Figure 12: Max throttle speed comparison for all boats in various hull conditions. ....	26
Figure 13: Visual representation of collective GHG emissions for each hull condition.....	30
Figure 14: The FTFC facility and experimental apparatus taken by Roberto Ravenna (PhD. candidate) at the University of Strathclyde. ....	36
Figure 15: Solid Works drawing of the high-density polyethylene panels design for the FTFC test section. ....	37
Figure 16: HDPE panels after surface preparation and coating application .....	38
Figure 17: VTSYIQI surface roughness gauge used for panel roughness measurements (Ra, Rz, Rq, Rt). ..	39
Figure 18: Visual of the pressure tap distribution along the test section of the FTFC.....	41
Figure 19: Centrifugal pump frequencies and corresponding mean bulk velocities at the test section of the FTFC with the hydraulically smooth acrylic reference (uncoated) panel. ....	41
Figure 20: WSS achieved in FTFC compared to a 200m long flat plate using the ITTC formulation. ....	44
Figure 21: Skin friction coefficients vs. Reynold’s number ( $Re_M$ ) for all marine coating surfaces. ....	46
Figure 22: Plot of $\sqrt{(2/C_f)}$ vs. $\text{Log}(Re_M\sqrt{(C_f)})$ for each set of coated panels.....	48
Figure 23: Exaggerated difference between the roughness functions of the smoothest and roughest coated panels. ....	50
Figure 24: Roughness functions for all coated panel surfaces using $R_t$ as the roughness length scale. ....	51
Figure 25: Outline of the Granville similarity law scaling procedure.....	53
Figure 26: Added resistance diagram for FR01 for 100m, 200m and 300m ship lengths. ....	58
Figure 27: LCA phases and system boundary included for comparison.....	67
Figure 28: OpenLCA Unit Process Flow Diagram for production of BRA640.....	69

Figure 29: Hull coating schemes with the number of layers and required dry film thickness on the newbuild case vessel.....	70
Figure 30: Annual surface water temperature and salinity for Port Canaveral, Florida testing site (adapted from (Swain et al., 2022)).....	72
Figure 31: Data adapted from (Demirel, 2015) for the % effective power increase for KRISO container ship at 19knots.....	74
Figure 32: In-service biofouling growth scenario #1 using static panel data with minimal fouling release performance for an active vessel. ....	76
Figure 33: In-service biofouling growth scenario #2 using weekly groomed panel data to represent fouling release performance for an active vessel .....	76
Figure 34: Relative environmental impact categories for application of marine coatings.....	78
Figure 35: Relative environmental impact categories for marine coating production. ....	78
Figure 36: Relative environmental impact categories for In-Service Scenario #1 (BRA640 is the baseline for comparison).....	81
Figure 37: Relative environmental impact categories for In-Service Scenario #2 (BRA640 is the baseline for comparison).....	81
Figure 38: Avoided GHG emissions for each In-Service Scenario using BRA640 as the baseline. ....	82
Figure 39: Tjärnö fouling region adapted from Oliveira et al. (2021). ....	90
Figure 40: Kristineberg fouling region adapted from Oliveira et al. (2021).....	90
Figure 41: Shaft RPM vs. Speed for Vessel Alpha .....	91
Figure 42: Shaft RPM vs. Speed for Vessel Bravo .....	91
Figure 43: Shaft RPM vs. Speed for Vessel Charlie .....	92
Figure 44: Shaft RPM vs. Speed for Vessel Delta .....	92
Figure 45: Photos of Alpha and Bravo after a season of summer fouling growth. ....	93
Figure 46: Photos of Charlie and Delta after a season of summer fouling growth. ....	93
Figure 47: Images of each coated panel tested in the fully turbulent flow channel. ....	98
Figure 48: Added resistance diagram for FR01 for 100m, 200m and 300m ship lengths. ....	99
Figure 49: Added resistance diagram for BL01 for 100m, 200m and 300m ship lengths. ....	99
Figure 50: Added resistance diagram for AF01 for 100m, 200m and 300m ship lengths. ....	100
Figure 51: Added resistance diagram for IB01 for 100m, 200m and 300m ship lengths. ....	100

## **ABSTRACT**

In this thesis I present two unique studies to capture the environmental performance of a new marine coating, XGIT-Fuel. A small-scale fishing boat study was analyzed and a relationship between the hull condition of the vessels (fouled, clean, and coated) and their fuel efficiency, was successfully identified through performing speed trials. A fully turbulent flow channel was used to determine the roughness functions of a controlled-depletion polymer, a silicone foul release, a gelcoat barrier, an ice breaking coating and the XGIT-Fuel coating. The obtained data was used in a scaling procedure to determine the effects of each coating on the frictional resistance and powering of a full-scale containership in its applied condition. The results from this study were used to perform a comparative life cycle assessment on the production, application, and in-service phases of BRA640, INT1100SR, and XGIT-Fuel when applied to the hull of a 3,600 TEU containership.

## **LIST OF ABBREVIATIONS USED**

AF	Anti-Fouling
AP	Acidification Potential
CII	Carbon Intensity Indicator
CDP	Controlled Depletion Polymer
DFT	Dry Film Thickness
EEDI	Energy Efficiency Design Index
FR	Foul Release
GHG	Greenhouse Gas
GWP	Global Warming Potential
HFO	Heavy Fuel Oil
ISO	International Standard of Organization
LCA	Life Cycle Assessment
LNG	Liquified Natural Gas
MAETP	Marine Aquatic Ecotoxicity Potential
MDO	Marine Diesel Oil
POCP	Photochemical Ozone Creation Potential
SEEMP	Ship Energy Efficiency Management Plan
TBT	Tributyltin
TEU	Twenty-Foot Equivalent Unit
VOC	Volatile Organic Compound



## **ACKNOWLEDGEMENTS**

I would like to thank my supervisor, Dr. Clifton Johnston for giving me the opportunity to work with him and for his support and guidance over the past two and a half years. I would also like to thank my supervisory committee members, Dr. Darrel Doman, and Dr. Adam Donaldson, for their thoughtful consideration of my thesis. Moreover, I would like to thank the members of the Graphite Innovation & Technologies (GIT) team, most specifically Mo AlGermozi, Marciel Gaier, Grant Heddon, Mehedi Hasan, Clayton Galvan, Ilia Rodionov, Maggie Kennedy and Joseph Murphy for their continued support and guidance throughout my research. Lastly, I would like to thank my friends, girlfriend, and family for their endless love and support throughout my degree.

## CHAPTER 1 INTRODUCTION

### 1.1 Global Shipping

The global shipping industry is responsible for the transportation of around 80% of the world's goods by volume and about 70% of trade value (UNCTAD, 2019). If we compare to other methods of transportation, it is the most energy-efficient method for moving large volumes of cargo as it has the lowest carbon emissions per ton kilometer. Despite this fact, global shipping was still responsible for 2.89% of the global anthropogenic greenhouse gas (GHG) emissions in 2018, according to the Fourth IMO GHG Study (International Maritime Organization, 2021). GHG emissions from ships are a result of the combustion of carbon-based fuels, most common being heavy fuel oil (HFO), marine gas/diesel oil (MGO/MDO) and liquified natural gas (LNG). The combustion of shipping fuels emits CO<sub>2</sub>, CH<sub>4</sub>, N<sub>2</sub>O along with nitrogen oxides (NO<sub>x</sub>) and sulfur oxides (SO<sub>x</sub>), which can have impacts on acidification, eutrophication of the ocean environment and are detrimental to air quality, especially near port communities.

GHG and other harmful gas emissions due to shipping operations are becoming a greater issue for ship owners and operators, as the global pressure to implement energy efficiency measures is ever-increasing. To this end, the International Maritime Organization (IMO) has implemented regulations such as the Ship Energy Efficiency Management Plan (SEEMP) (IMO, 2012) for all ships and the Energy Efficiency Design Index (EEDI) (IMO, 2012) for newly built ships. The EEDI requires newly built ships to have a minimum level of energy efficiency per capacity mile based on the ship type and size category. From an operational standpoint, the IMO has recently come out with a few measures to enforce a year-over-year improvement in the energy efficiency of ships such as the Carbon Intensity Indicator (CII) which will come into force on January 1st, 2023 (IMO, 2021). Shipping owners are now constantly looking for more effective ways to improve the efficiency of their ships, by means of optimized vessel routing, retrofitting, ship maintenance and implementing new technologies such as energy saving devices

(IMO, 2021). The use of marine coatings has been identified as a suitable energy saving method (ITTC, 2017) by reducing the frictional resistance experienced by the hull of a ship.

## **1.2 Marine Coatings**

The underwater hulls of marine vessels are coated with marine coatings to provide general protection and to prevent biofouling and corrosion. The amount of energy required to propel marine vessels through the water is proportional to their hydrodynamic performance. A vessel's marine coating can significantly affect hull performance, which relies on both the surface nature of the coating and its interaction with fouling organisms. For example, a coating system with a smooth finish contributes little frictional resistance to a vessel's hull moving through the water. Moreover, a marine coating system that negatively influences the adhesion of fouling organisms (whether by killing them with biocides or by making it difficult for them to properly adhere) allows the underwater hull to remain relatively free of fouling which would otherwise increase its frictional resistance. Frictional resistance can account for up to 80% of total ship resistance for merchant ship types when cruising at lower speeds (Sindagi et al., 2019). Hence, the importance of identifying suitable technologies that can reduce frictional drag, which in turn will substantially reduce fuel consumption and GHG emissions.

The age of a ship's hull, the application method, and wear of marine coatings over time have all been identified as factors that contribute to increasing hull roughness (Yeginbayeva and Atlar, 2018)(Schultz, 2007). The attachment of marine organisms to a ship's hull, is a phenomena called biofouling, which is also known for increasing the associated roughness of a hull (Schultz, 2007). There are two main types of biofouling, plant and animal, which can be seen in Figure 1. Within each category of biofouling, there is a plethora of species. Soft (shell-less) animal forms most commonly found on ship hulls often include hydroids, anemones, and tunicates (sea squirts) (USNA, 2002).

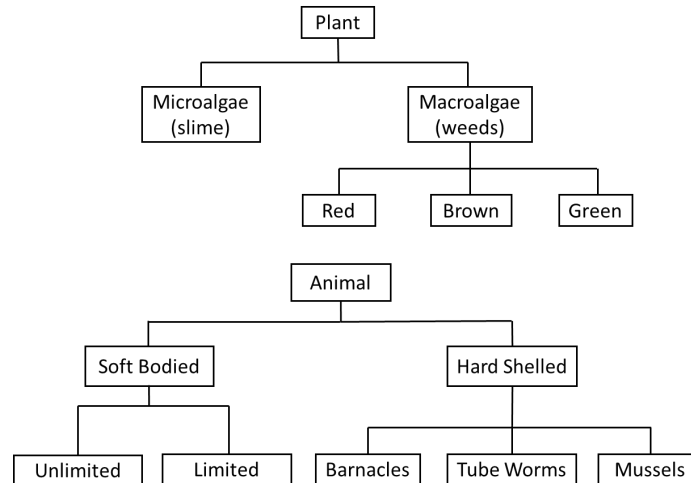


Figure 1: Classifying fouling organisms commonly found on ship hulls; adapted from Demirel (2015)

Historically, marine coating systems leached biocides such as tributyltin, copper, and zinc to kill off fouling organisms and keep vessel hulls clean (Dafforn et al., 2011). A breakdown of the significant events throughout the history of anti-fouling paints is shown in Table 1.

Table 1: Historical developments of anti-fouling paints adopted from Dafforn et al. (2011).

Time Period	Significant events
1500–300 BC	Use of lead and copper sheets on wooden vessels
1800–1900s	Heavy metals (copper, arsenic, mercury) incorporated into coatings
1800s - present	Continued use of copper in anti-fouling coatings
1960s	Development of tributyltin (TBT) conventional coatings
1974	Oyster farmers report abnormal shell growth
1977	First foul release anti-fouling (AF) patent
1980s	Development of TBT SPC coatings allowed control of biocide release rates
1980s	TBT linked to shell abnormalities in oysters and imposex in dogwhelks
1987–90	TBT coatings prohibited on vessels <25m in France, UK, USA, Canada, Australia, EU, NZ, and Japan
1990s-present	Copper release rate restrictions introduced in Denmark and considered elsewhere e.g., California, USA
2000s	Research into environmentally friendly AF alternatives increases
2001	International Maritime Organization (IMO) adopts “AFS Convention” to prohibit the use of harmful organotins from AF coatings
2003	prohibition of further application of TBT
2008	prohibition of active TBT presence
2008	IMO “AFS Convention” entered-into-force

2021	IMO drafts an amendment to the AFS Convention to prohibit the use of cybutryne (industry name Irgarol-1051) in anti-fouling systems on ships from January 1 <sup>st</sup> , 2023
------	--

Since 2008, the International Maritime Organization (IMO) has banned the use of organotin-based anti-fouling coatings due to their detrimental effects on non-target marine organisms (IMO, 2001). As a result, the shipping industry has become heavily reliant on copper and zinc leeching mechanisms to protect against fouling organisms during long stationary docking periods (Dafforn et al., 2011). The two main types of biocide-based anti-fouling systems include Controlled Depletion Polymer (CDP) and Self Polishing Copolymer (SPC) coatings which vary by the mechanisms they use for leeching toxic chemicals into the ocean (Shipping et al., 2007).

Fouling release coatings are primarily silicone-based and utilize the sheer force of water to remove fouling organisms without leeching biocides into the environment (Zhang et al., 2014). These coatings have become increasingly popular due to their inherent fuel savings, as they maintain a lower average hull roughness throughout their lifetime. However, these coatings leech silicon oils on the interface between seawater over time, and the environmental impact of the silicone oil leachate is not well understood (Zhang et al., 2014). To avoid future detrimental effects of anti-fouling systems, marine coatings companies have shifted their focus to developing chemically inert hull coatings that are still able to provide the same performance benefits to shipowners (Shipping et al., 2007).

There is a growing need for further development of marine coating technologies within the maritime industry to improve the energy efficiency of ships. To match this need, there have been many recent advances in marine coating that are focused on improving anti-fouling performance such as amphiphilic nanostructured polymers (eg Sundaram et al., 2011), and biomimetic surfaces (eg Chen et al., 2021). However, the biocidal anti-fouling systems still dominate today's marine coatings market (Safinah Group, 2021). Table 2 provides a comparison of the main types of marine coatings used on today's global shipping fleet.

Table 2: Overview of the main marine coating types, adapted from Van Rompay (2012).

Marine Coating Type	Protection & Durability	Fuel Saving Properties	Maintenance & Repair	Environmental Concerns
<b>Typical anti-fouling system (SPC/CDP)</b>	Soft coating. Fairly easily damaged, especially with hull cleanings. 3-5 years before AF coating needs to be replaced. Full recoating down to bare steel 2 or 3 times in 25 years.	Unfouled hull roughness from AF coating gives 2-4% fuel penalty. Usually covered with slime = up to 20% fuel penalty. Effectively reduces higher fuel penalties (hard fouling). Coating degradation increases fuel penalty over time.	5-8 drydockings required for paint alone during ship's service life including 1-3 full blasting and repainting. Multiple coats and length curing times can mean 2-3 weeks in drydock for a full repaint.	Contaminates marine environment with toxic biocides, harming marine life, the food chain, and humans. Large release of biocides if cleaned in-water. High VOC content when applied. Limits fuel consumption and GHG emissions from effects of heavy fouling. Prevent some invasive species but further others.
<b>Typical fouling release (FR) system</b>	Soft coating. Easily damaged, with or without hull cleanings. 3-5 years before FR coat needs repair/reapplication. Full recoating required 1-3 times in 25 years.	Smoothest tested surface when unfouled. Usually sails with slime = up to 20% fuel penalty. Can foul badly if vessel has long layups. Coating degradation increases fuel penalty over time.	5-8 drydockings required for paint alone during ship's service life including 1-3 full blasting and repainting. Multiple coats and long curing times can mean 2-3 weeks in drydock for a full recoat.	Does not contain biocides but leaches potentially harmful silicone oils, alters enzymes in barnacle glue; some silicones are catalyzed by highly toxic dibutyltin dilaurate. Medium VOC content. Some reduction in fuel consumption/GHG. Can help limit the spread of invasive species.
<b>Hard / Icebreaking</b>	Hard coating, not easily damaged. Claims to last the lifetime of a vessel (25 years) with only minor touch-ups.	Highest unfouled roughness. Meant to be paired with routine hull cleanings to minimize hull fouling.	Applied once to a hull. Usually applied in 2 thick coats with 2 - 3 hours minimum and no maximum between coats.	Chemically inert, non-toxic. Low VOC. Hull cleaning in-port can prevent the spread of invasive species.

Table 2 demonstrates that each coating system has its inherent benefits and drawbacks depending on the category for comparison. The type of marine coating system is typically chosen based on the type of ship and its planned operational activity. This table also highlights the need for further technological advancements in the field of marine coatings, to minimize their impact on the environment. Life cycle design has been identified as method to produce such products, and life cycle assessment can be used as a research tool to make environmental comparisons to existing coating technologies.



**Inventory analysis:** This stage provides a description of each material and energy input flow within the product system, while highlighting any output emissions to the environment. This is the most important phase for understanding which phases of the product's life cycle will contribute to each environmental impact category.

**Impact assessment:** This stage takes the input details from the inventory analysis and provides the results of each environmental indicator based on their respective impact categories, such as global warming potential, acidification, eutrophication, marine toxicity, etc. Once the inventory results are assigned an impact category, the impacts are typically normalized grouped and weighted against each other or against other products.

**Interpretation:** This stage of a life cycle involves critical review of the data quality, sensitivity, and presentation of results. The results from the impact assessment are summarized and discussed to form conclusions and recommendations for future decision making with product design. The findings from an LCA can be utilized by the product's manufacturer to improve the product's environmental performance.

The abovementioned descriptions for each LCA stage are meant to serve as a general overview of the required methodological framework. Further requirements and guidelines for performing life cycle assessments are outlined in ISO 14044 (2006). Most notably, the performance of an LCA can assist in: improving environmental performance of products, informing decision-makers in industry, government or non-government organizations, selecting the appropriate environmental indicators and measurement techniques, and environmental product declarations (ISO 14044, 2006)

## **1.4 Research Motivation**

Graphite Innovation and Technologies (GIT) is a research and development company founded in 2017 and located in Dartmouth, N.S, Canada. The company's mission is to provide the shipping industry with sustainable coating technologies based on the use of nanomaterials such as graphene. GIT has researched and developed a new marine coating product, XGIT-Fuel™, to serve as an alternative to biocide-based anti-



fouling coatings. XGIT-Fuel is a nanostructured hybrid hard foul release coating whose goal is to reduce the frictional resistance of the hull while providing a surface that can be cleaned without damage or increased surface roughness.

GIT is looking to understand the environmental impact of XGIT-Fuel compared to existing commercial marine coatings that solve the same problem. Given this specific research objective, LCA was selected as an appropriate method for carrying out the product comparison.

## **1.5 Structure of this Thesis**

This thesis is a paper-based thesis containing three separate papers in Chapters 2, 3 and 4, followed by a concluding chapter that provides insight on the conclusions and limitations of the research as well as the recommendations for future work.

Chapter 2 is a fuel consumption and GHG analysis on four small inshore fishing vessels, known as “cape islanders”. The aim of this research was to quantify the impact of both biofouling and GIT’s newly applied hull coating on their fuel performance and speed.

Chapter 3 is a fully turbulent flow channel study on various marine coating types including XGIT-Fuel. The aim of this research was to determine the skin frictional resistance of coated flat plates in the turbulent boundary layer so that it can be used to make predictions on ship scale frictional resistance and powering.

Chapter 4 is a comparative LCA of a cuprous oxide based anti-fouling coating (BRA640), a PDMS based foul release coating (INT1100SR) and the new XGIT-Fuel coating. The aim of this research was to quantify the environmental impacts of each coating system from production, application and once applied to the hull of a ship and compare them using well established environmental indicators.

## **CHAPTER 2 FUEL & GHG ANALYSIS OF A SMALL FISHING FLEET**

### **2.1 Introduction**

Depending on the severity of the hull roughness due to biofouling, it can have a negative impact on a ship's fuel efficiency and resulting greenhouse gas (GHG) emissions (Schultz, 2007). To combat this problem, toxic and non-toxic marine coating systems have been employed by shipowners to protect their hulls from biofouling attachment (Anderson et al., 2003).

There have been numerous experimental lab-scale studies that have provided a methodology for predicting the effects of coating roughness and hull fouling effects on ship resistance and powering. The concept of full-scale ship trials to capture the effect of fouling on the drag of a ship's hull began with the studies of Lewthwaite et al. (1985) and Haslbeck & Bohlander (1992). Both the laboratory and full-scale tests indicate that fouling causes a significant increase in frictional resistance, but the magnitude of this resistance depends on the hull shape, the type of fouling and its percent coverage (Schultz, 2007).

In 2007, Schultz presented a range of fouling conditions in accordance with the Navy Systems Technical Manual (NSTM) fouling rating. Based on his previous research in Schultz (2004), he proposed that this range of fouling conditions behave similarly to the roughness functions of Schultz and Flack (2007) and Shockling et al. (2006). Schultz then assigned an equivalent sand grain roughness height for each fouling condition as well as an average coating roughness (Rt50) height which stemmed from his work in Schultz (2004). The roughness functions in Schultz (2007) were applied to the full-scale trial results of Woo et al., (1983) on the US Navy Oliver Hazard Perry class frigate (FFG-7) to test their validity. Shultz found that the predictions in increased shaft power requirement due to fouling were within 1.5% of the full-scale trial results (Schultz, 2007). These hull fouling conditions have been widely accepted and adapted by many authors (Demirel et al., 2019; Safinah Group, 2021; Song et al., 2020a; Swain and Lund, 2016) including a recent study by Oliveira and Granhag (2020).

Past work conducted by Yeginbayeva & Atlar (2018) studied the effects of mimicked hull roughness on a variety of coating types. The findings indicated that a marine coating's roughness alone can increase a KRISO containership's frictional resistance by up to 20% (Yeginbayeva and Atlar, 2018). In a recent work, Yeginbayeva et al. (2020) looked specifically at the effects of mimicked roughness and biofilms on the hydrodynamics of foul release coatings. A boundary layer similarity-law scaling method was used to predict the combined effects of coating roughness and biofilms on the frictional resistance and powering requirements of two large benchmark vessel types. The added power requirement was estimated to be up to 16% depending on the type of biofilm, thickness, and percent coverage (Yeginbayeva et al., 2020).

In a research article by Corbett and Winebrake (2011) a fluoropolymer foul release (FFR) coating system was treated as an environmental retrofit on multiple case vessels. The fuel oil consumption and associated CO<sub>2</sub> emissions of one of the vessels was modeled using a multiple linear regression (MLR) analysis (Corbett and Winebrake, 2011). As a result of the MLR, it was determined that the foul release retrofit achieved a statistically significant reduction in fuel consumption of approximately 10% (Corbett and Winebrake, 2011).

As part of a larger life cycle analysis, we are looking to understand the effects of hull coatings, specifically XGIT-Fuel, a hybrid foul release coating for which there is no available data in the literature. From analyzing studies such as Corbett and Winebrake (2011) and Blanco-Davis et al. (2014), it became clear that the fuel performance data from one or multiple vessels prior to retrofitting with XGIT-Fuel, and post-retrofit data was required. This opportunity presented itself when Transport Canada issued a study to assess the impact of GIT's product on the hulls of local in-shore fishing craft.

This information included in this chapter was acquired in partnership with GIT, Lloyd's Register, Glass Ocean Electric and Transport Canada. The analysis is conducted on four traditional 'Nova Scotia Cape Islander' vessels to understand how their hull

condition effects their fuel efficiency and GHG emissions. Despite drag penalties from hull form, this study identified the negative impact of fouling growth on fuel efficiency and highlighted the benefits of a clean and coated hull condition on the environment. An estimated emissions savings is also provided for fishing boat captains to make educated decisions on hull maintenance activities and choice in hull coatings. This work aims to serve as fundamental evidence that smaller vessel testing can identify statistically significant changes in fuel consumption solely due to changes in hull condition.

## 2.2 Materials & Methods

### 2.2.1 Vessel dimensions and specifications

This study was conducted on four ‘Nova Scotia Cape Islander’ vessels to understand how their hull condition affects their fuel efficiency and GHG emissions. These vessels have a unique hull design as they were specifically built to function as lobster fishing vessels with the need for a cabin space and a large carrying capacity. As a result, these vessels have high “length-to-beam” ratios and are not built to be hydrodynamic due to their bulky hull design. Despite their drag penalty from hull form, it is hypothesized that these vessel’s will be largely impacted from a fouled hull to a clean hull and potentially benefit from the application of a new hull coating (XGIT-Fuel) over their existing gelcoat barrier coating.

The engine specifications and vessel dimensions of the fishing vessels are provided in Table 3.

Table 3: Attributes of the four Cape Islander fishing vessels.

<b>Nova Scotia Cape Islanders</b>				
<b>Vessel Name</b>	Alpha	Bravo	Charlie	Delta
<b>Engine Layout</b>	In Line	In Line	In Line	In Line
<b>Engine Make</b>	Caterpillar	Detroit	John Deere	Caterpillar
<b>Engine Model</b>	3208, naturally aspirated, (no turbo)	417, super charged	6067FM, turbo charged	C7
<b>Number of Engines</b>	1	1	1	1
<b>Engine Stroke</b>	4	2	4	4
<b>Engine hp</b>	210	160	300	251
<b>Engine Type</b>	Motor Diesel	Motor Diesel	Motor Diesel	Motor Diesel

<b>Length (m)</b>	11.3	10.7	12.0	10.4
<b>Beam (m)</b>	4.9	4.0	6.7	5.5
<b>Operating Speed (kts)</b>	8.0	8.0	8.0	8.0
<b>Froude Number</b>	0.391	0.427	0.379	0.408

As these fishing vessels move through water, there are many factors that contribute to the total resistance force experienced by the hull (USNA, 2002). The main contributors to the total hull resistance “ $R_T$ ”, are the frictional and viscous pressure effects of water flowing over the hull “ $R_V$ ”, the added resistance due to creating and maintaining the bow and stern waves “ $R_W$ ”, and the resistance from air “ $R_{AA}$ ”, written in Equation 2.1 as:

$$R_T = R_V + R_W + R_{AA} \quad [2.1]$$

For a typical vessel, the viscous (frictional) resistance dominates at lower speeds and upon reaching higher speeds the wave making resistance increases exponentially (USNA, 2002). Table 3 shows the cruising/operating speed of all cape islanders was recorded as 8 knots. According to USNA (2002), the term “hull speed” calculated as the last fuel efficient speed for a ship and is given by a rule of thumb equation based on a ratio between the vessel speed and length. To demonstrate the relative total hull resistance acting on each vessel due to their operating speed of 8 knots, the formula was applied for each length and is shown in Figure 3 along with the most fuel-efficient speed-to-length ratio of 1.34.

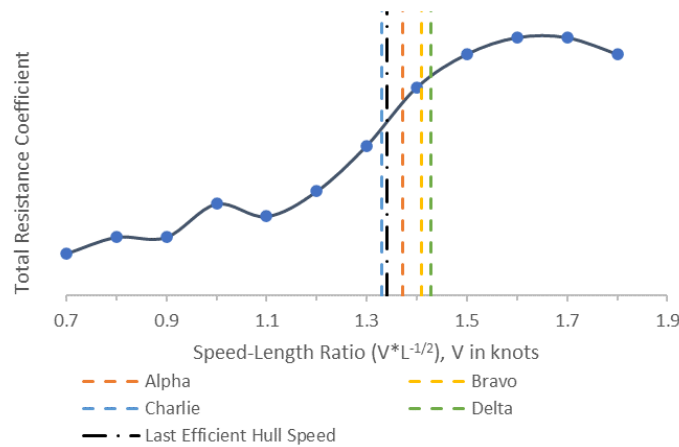


Figure 3: Typical relationship between total resistance coefficient and vessel speed, adopted from (USNA, 2002)

This figure demonstrates the concept that all four of these vessels are operating near or above their last fuel-efficient speed and are therefore subject to added wavemaking resistance (USNA, 2002).

### 2.2.2 Sea Trials

Four Cape Islanders fishing vessels (Alpha, Bravo, Charlie & Delta) were monitored throughout a fishing season and retrofitted with XGIT-Fuel. The goal was to quantify how the new coating and hull fouling affects their fuel efficiency. To analyze the impact of hull condition on the vessel’s fuel oil consumption, speed, fuel and power data was collected directly from the fishing vessels by performing sea trials according to ISO 15016:2015 Ships and marine technology — Guidelines for the assessment of speed and power performance by analysis of speed trial data (ISO 15016, 2015). The instrumentation used and recorded measurements are provided in Table 4 below.

Table 4: Instrumentation and parameters recorded during the sea trials.

Instrument/Sensor	Location on Vessel	Recorded Measurement	Units
Hemisphere A222 GNSS (X2)	Boat mast, Boat stern	Time	Sampling interval of 1 Hz (seconds)
		Latitude/Longitude	(coordinates)
		Heading	(degrees)
		Speed over Ground	(knots)
Anemometer AP-856A Pro Handheld	Anchored standby boat	Wind Speed & Direction	(m/s) N/E/S/W
Climate Buoy SMA-Halifax, (COVE, 2022)	Halifax (Herring Cove) (44.54611667 N - 63.53693333 W)	Current Speed & Direction	(m/s) N/E/S/W
RPM Sensor iR pickup system	Propeller shaft	Shaft RPM	(Revolutions per minute)
Fuel flow meters (X2)	Diesel engine supply line	Fuel Flow rate 1	(L/min)
	Diesel engine return line	Fuel Flow rate 2	(L/min)

The sea trials were conducted from October 2020 – October 2021 in Shad Bay, N.S. which is located as the southwest of Halifax municipality, as depicted in Figure 4 below.



Figure 4: Image of the sea trial location (denoted by the red star), obtained from *Mapcarta* (2022).

The sea trial site provided a protected water channel of several kilometers' length with a uniform depth of approximately 20 m and width of 500 m. The sea trials were not performed if the weather and sea state were thought to be detrimental to data collection. Figure 5 shows an example of a close to ideal sea state for the performance of speed trials.



Figure 5: Image of vessel Delta heading out for a sea trial on a calm day, typical of other testing conditions.

To capture the complete range of fuel performance, speed trials were conducted at various nominal speeds from 4 - 10 knots. The general breakdown for the tested hull conditions and nominal speed runs for each vessel are provided in Table 5.

Table 5: Sea trial hull conditions and nominal speed runs for all vessels.

Vessel Name	Hull Condition	Nominal Speed Runs (knots)
Alpha	Summer Fouled	4, 6, 7, 8*
	Winter Fouled	4, 5, 6, 7, 8, 9*
	XGIT-Fuel Coated	4, 5, 6, 7, 8, 9*
Bravo	Summer Fouled	4, 6, 7, 9*
	Winter Fouled	4, 5, 6, 7, 9*
	XGIT-Fuel Coated	4, 5, 6, 7, 9*
Charlie	Clean	4, 6, 7, 8
	Summer Fouled	4, 5, 6, 7, 8
	XGIT-Fuel Coated	4, 5, 6, 7, 8
Delta	Clean	4, 5, 6, 8, 10*
	XGIT-Fuel Coated	4, 5, 6, 8, 10*

\*Max throttle speed.

### 2.2.3 Fuel Oil Consumption Analysis

For Alpha & Bravo, the speed trials were performed in three different intervals to capture the summer fouled, winter fouled, and XGIT-Fuel coated hull conditions. The objective of this analysis is to determine the difference in the fuel oil consumption values of the fishing vessels at cruising speed solely due to the various hull conditions. From this fuel oil consumption data, the greenhouse gas emissions can be forecasted for various scenarios in a fishing vessel’s lifecycle. From these developed scenarios a general case for this size fishing vessel can be created and later compared against similar studies. This chapter’s findings should allow fishing vessel owners to make educated decisions when choosing fouling control solutions and hull maintenance strategies to best match their vessel’s operational profile. Two methodologies were chosen from literature to analyze and predict the relative change in fuel consumption at cruising speed depending on hull condition.

### 2.2.4 Analysis Method #1: One-Way ANOVA Normalized 8 knots

A vessel’s effective power “ $P_E$ ” is a measure of the required power to move the vessel’s hull at a given speed without propeller action (USNA, 2002). The effective power is absent of losses due to factors further up the drivetrain such as the gearbox, shafting and propeller



and does not include the interaction between the propeller and the hull (USNA, 2002). This power is equivalent to the product of the resistance of a vessel “ $R_T$ ” and its speed “ $V$ ” shown in Equation 2.2:

$$P_E = R_T V \quad [2.2]$$

A vessel’s total hull resistance is related to its coefficient of total resistance “ $C_T$ ” by Equation 2.3:

$$R_T = \frac{1}{2} \rho S C_T V^2 \quad [2.3]$$

Where “ $\rho$ ” is the sea water density, “ $S$ ” is the wetted hull surface area, and “ $V$ ” is the ship speed. Combining Equation 2.2 and 2.3 with the concept that a vessel’s fuel oil consumption “ $FOC$ ” is directly correlated with its effective power, gives the following relationship:

$$FOC \propto V^3$$

This relationship was used in a previous study by Corbett et al. to normalize a vessel’s fuel oil consumption based on speed for sake of comparison between two hull coating systems (Corbett and Winebrake, 2011). The chosen reference speed “ $V_{norm}$ ” was 8 knots for Alpha and Bravo, as it was the most common cruising speed logged by the boat captains and falls within their operating range. Equation 2.4 reflects the theoretical fuel consumption “ $FOC_{norm}$ ” that would have occurred at cruising speed:

$$FOC_{norm} = FOC_i \left( \frac{V_{norm}}{V_i} \right)^3 \quad [2.4]$$

Minitab® statistical software package was used to perform a one-way ANOVA test on the means of the cruising speed fuel consumption values for each hull condition. The Interval plots and confidence intervals are provided in the results and discussion for vessels Alpha and Bravo respectively.

#### **2.3.4 Analysis Method #2: All Speed Runs**

The second method of analysis was to plot the average fuel consumption for each speed run conducted at the varying hull conditions. An exponential fit was applied to each dataset

to capture the trend of fuel consumption vs. speed for the summer fouled, winter fouled, and XGIT-Fuel coated vessels. The exponential fit was chosen due to the physical significance it offers for the relationship between fuel consumption and speed, compared to a 2<sup>nd</sup> or 3<sup>rd</sup> order polynomial fit. A coefficient of determination was provided for each fit to show the level of correlation to the trend. For sake of comparison to the first analysis method used, an intersection line was drawn at a cruising speed of 8 knots. This allowed for the prediction of the fuel oil consumption for each hull condition the same speed for which analysis method 1 was conducted.

The percent difference in mean fuel consumption between the two analysis methods was then calculated and an average of the two values was taken to reduce the bias associated with each method. The average of the two methods was also applied to the percentage fuel savings from summer fouled to winter fouled and winter fouled to XGIT-Fuel coated hull conditions.

## **2.4 Results and Discussion**

Only the sea trial data obtained from the performed sea trials with vessels Alpha and Bravo is analyzed in this chapter since the fuel consumption datasets for vessels Charlie and Delta were not comparable. Vessel Charlie underwent a change in propeller pitch between the clean and XGIT-Coated trial which could have affected its resulting fuel efficiency. Vessel Delta's summer fouled dataset contained fuel consumptions values that did not correspond to the established relationship with its shaft RPM and thus were deemed invalid. However, a max throttle speed comparison is included in Section 3.4 to provide some indication as to how the change in hull condition affected the other two vessels (Charlie and Delta).

The fuel consumption datasets were truncated so that the same number of samples per heading direction at each speed run were included in our analysis. The complete datasets were compared against the truncated datasets for each hull condition and the difference in average fuel consumption for each speed was minimal. The summer fouled, winter fouled, and XGIT-Fuel coated hull condition datasets for Alpha and Bravo contained 3007 and

2246 cumulative data points respectively. The sampling frequency for the trials was one second and the average speed run length was three to four minutes.

### 2.4.1 Hull Biofouling Results

The hull fouling conditions were captured after the summer fouled and winter fouled sea trials were conducted on each vessel. The two vessels had not previously used an anti-fouling coating and solely relied on a gelcoat barrier coating. It is of note that one of Transport Canada’s goals with funding this work was to quantify the importance of hull maintenance and anti-fouling measures to gain fuel efficiency and reduce GHG emissions for Canada’s inshore fishing craft.

A version of the NSTM fouling ratings from 0-100 was used from Oliveira and Granhag (2020) and adopted for this study. The various fouling ratings correspond to commonly occurring soft and hard marine organisms and the descriptions of each condition and corresponding equivalent sand grain roughness heights ( $k_s$ ) are provided in Table 6 below.

Table 6: NSTM fouling ratings adopted from Oliveira and Granhag (2020) for this study.

<b>frNSTM</b>	<b>Type</b>	<b>Hull fouling condition</b>	<b><math>k_s</math> (<math>\mu\text{m}</math>)</b>
0	Undetectable	Foul-free surface.	47
10	Soft	Incipient slime, visible underlying paint/metal surface.	83
20	Soft	Advanced slime, obscured underlying paint/metal surface. Juvenile barnacles $\leq 1$ mm (this study).	146
30	Soft	Soft fouling (e.g., filaments) $<76$ mm in length and $<6.4$ mm in height.	257
40	Hard	Tubeworms $<6.4$ mm in height. Encrusting bryozoans and tunicates (this study).	452
50	Hard	Barnacles $<6.4$ mm in height. Encrusting bryozoans and tunicates (this study).	796
60	Hard	Combination of tubeworms and barnacles $<6.4$ mm in height. Encrusting bryozoans and densely packed tunicates (this study).	1403

70	Hard	Combination of tubeworms and barnacles > 6.4 mm in height.	2471
80	Hard	Tubeworms closely packed and upright from surface, or barnacles on top of each other, < 6.4 mm in height.	4353
90	Hard	Densely packed tubeworms or barnacles, > 6.4 mm in height; presence of mussels or oysters; or slime/grass overlay.	7668
100	Composite	All forms of fouling; soft animal fouling (tunicates) growing on various forms of hard fouling	13509

We found that most of the biofouling growth occurred over the summer months (May – September) as the temperature of the water was warmer and the two vessels were stationary for most of June through October which their “off-season”. The lobster fishing season for the two vessels occurs over the winter months (November – April) where the vessels heavily increase their activity, leaving less time idle for fouling growth to occur. An estimation of the change in NSTM fouling rating over time was generated based off of two documented fouling regions (Tjärnö & Kristineberg), adapted from Oliveira et al. (2021). The estimation for the summer fouled season was modelled based on Tjärnö (26psu), while the winter fouled season was modelled based on Kristineberg (23psu) due to their similar average sea water temperature (7-17°C) and salinity (20-30psu), respectively. The fouling trend for each adapted region is provided in Appendix A. The estimated change in fouling rating over time is shown in Figure 6 for vessels Alpha and Bravo, since only a snapshot of the hull condition was captured close to each trial date (provided in Appendix A).

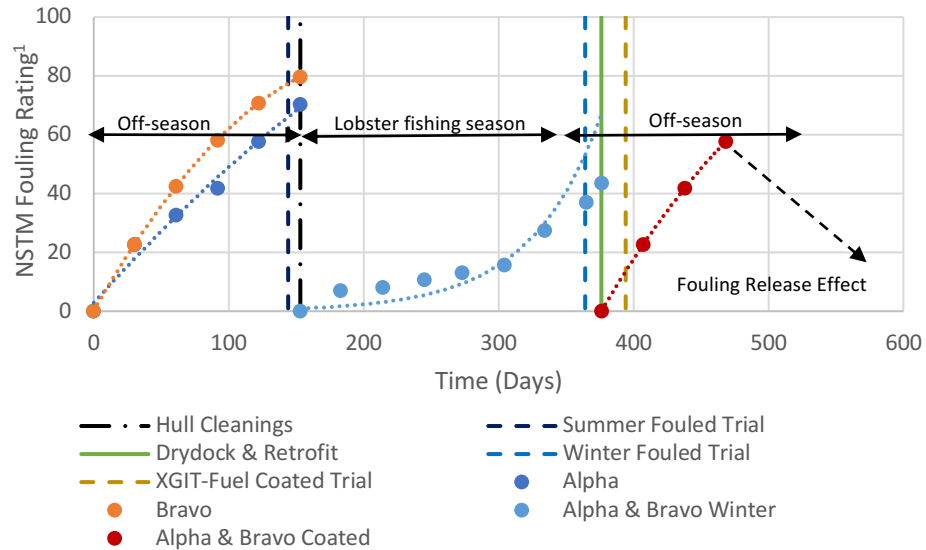


Figure 6: Estimated hull fouling rating over time based on environmental conditions and number of idle days.

The time axis begins in May, summer fouled trials were conducted in late October prior to the removal of both vessels for a hull cleaning. The winter fouled trials were conducted at the end of lobster fishing season in May, the boats were drydocked cleaned and retrofitted with XGIT-Fuel coating in June. Lastly the coated sea trials were conducted at the end of June. Once coated, underwater images of the hulls were captured in July and August which showed similar levels of growth to the previous summer due to extended idle periods of up to 15-20 days consecutively. However, underwater images of the hulls were captured the following winter (end of January) which showed both hulls were 90-100% clean of all fouling aside from what appears to be slime in some areas (underwater images shown in Appendix A). This provides evidence of a fouling release effect by the XGIT-Fuel coating combined with the effect of a decrease in seawater temperature. Moreover, vessels Alpha and Bravo were not removed for a hull cleaning as was done with the gelcoat barrier coating in the previous year.

Figure 7 demonstrates the operational profiles of Alpha and Bravo over a 12-month period and highlights the cumulative idle days of each vessel. Notice vessel Alpha was more active in the summer months and thus would be assumed to have had a lower hull fouling rating during the summer fouled speed trials.

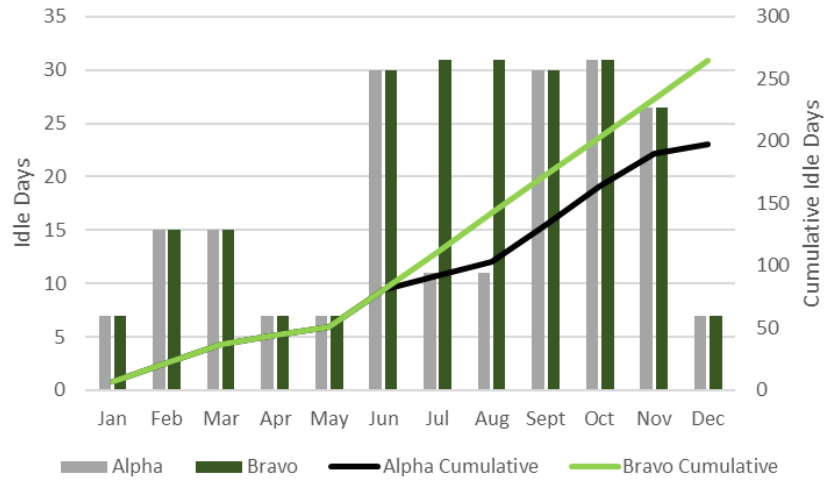


Figure 7: Idle time of vessels Alpha and Bravo over 12-months.

Each hull condition was examined, and the heights and coverages of the various fouling organisms were recorded using an electronic caliper. The results from the hull inspections of each vessel are presented in Table 7 below.

Table 7: Hull inspection results for each vessel including coating type and hull fouling coverage/condition.

Vessel name	Hull Condition	Total fouling coverage (%)	Slime (%)	Algae, encrusting bryozoans & tunicates (%)	Barnacles (%)	Hull fouling condition
Alpha	Summer Fouled Gelcoat	100	10	75	15	Heavy layer of algae and barnacles (~7mm in height)
Alpha	Winter Fouled Gelcoat	20	10	5	5	Thin layer of slime and barnacles (~2mm in height)
Bravo	Sumer Fouled Gelcoat	100	10	55	35	Heavy layer of algae and barnacles (~7mm in height)
Bravo	Winter Fouled Gelcoat	20	10	5	5	Thin layer of slime and barnacles (~2mm in height)
Charlie	Summer + Winter Fouled Gelcoat	100	10	80	10	Composite fouling, densely packed ~50mm tunicates growing with ~7mm barnacles

To evaluate the impact of hull roughness on skin friction drag, an equivalent sand grain roughness ( $k_s$ ) value was calculated for each hull condition. This was done using the percent coverage values of each fouling organism combined with the  $k_s$  values provided in

Table 6. The summer fouled hulls (NSTM rating 60-70) had much larger  $k_s$  values due to the height and diameter of the adhered barnacles. The winter fouled hulls (NSTM 30-40) had  $k_s$  values much closer to that of a freshly applied anti-fouling coating (NSTM 0) as the barnacles were juvenile in size. The results of the fouling evaluation for each hull condition are shown in Table 8.

Table 8: Resulting hull fouling NSTM ratings and corresponding  $k_s$  values for each vessel.

<b>Vessel name</b>	<b>Hull Condition</b>	<b>NSTM rating</b>	<b><math>k_s</math> (<math>\mu\text{m}</math>)*</b>
Alpha	Summer Fouled	50-70	1000
	Winter Fouled	30-40	300
	XGIT-Fuel Coated	0	50
Bravo	Summer Fouled	50-70	1000
	Winter Fouled	30-40	300
	XGIT-Fuel Coated	0	50
Charlie	Clean	0	50
	Summer + Winter Fouled	50-70	2000
	XGIT-Fuel Coated	0	50
Delta	Clean	0	50
	XGIT-Fuel Coated	0	50

\* $k_s$  values were estimated based on fouling percent coverage & NSTM rating.

The equivalent sand grain roughness values can be used as a rationale tool for any observed changes in fuel consumption due to hull condition. The equivalent sand grain roughness values represent the heights of the roughness elements that are protruding through the viscous sublayer, resulting in added frictional resistance for the Cape Islanders vessels (Yeginbayeva and Atlar, 2018).

### 2.4.2 Fuel Data Results from Analysis Method #1

Once the dataset for each hull condition was normalized to cruising speed, an interval plot was created to show the difference in mean fuel consumption at the 95% confidence interval. The interval plots for vessels Alpha and Bravo are shown in Figure 9 and Figure 8, respectively.

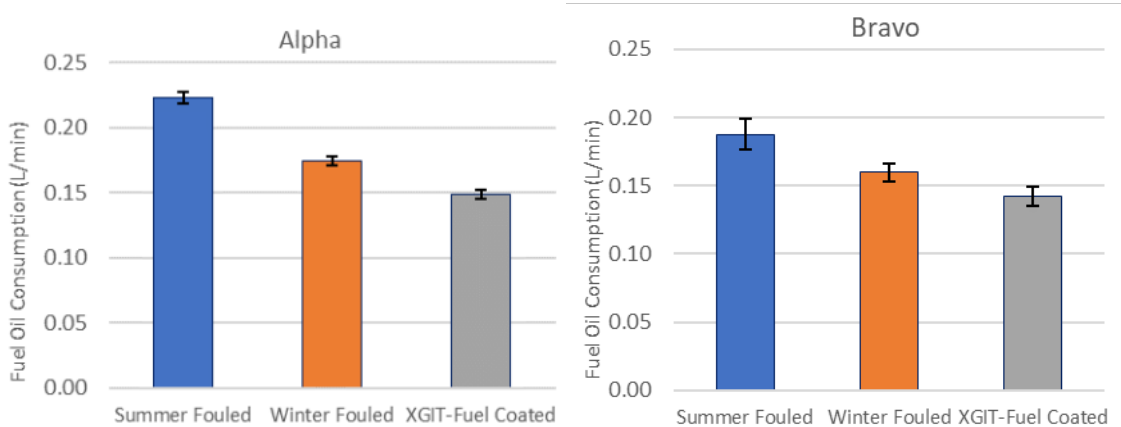


Figure 9: Alpha 8 knot Speed Adjusted Fuel Oil Consumption for Various Hull Conditions.

Figure 8: Bravo 8 knot Speed Adjusted Fuel Oil Consumption for Various Hull Conditions.

The null hypothesis that all means are equal for vessel Alpha was rejected at this confidence interval as the p-value was zero and the 95% confidence intervals of each mean value do not overlap. The null hypothesis was also rejected for vessel Bravo. Notice the individual standard deviations were larger for vessel Bravo across all hull conditions compared to vessel Alpha. The larger standard deviations could be due to multiple factors including engine type, power rating and weather conditions during the sea trials. The choice of 8 knots as the normalized speed will affect the resulting GHG emissions quantified in section 3.4 however it has no effect on the percent difference observed between the summer fouled, winter fouled, and XGIT-Fuel coated conditions.

Using this analysis method, the fuel savings achieved for Vessel Alpha from the summer fouled to winter fouled condition was 21.8% ( $\pm 3.6\%$ ) and the fuel savings achieved from winter fouled to XGIT-Fuel coated condition was 14.6% ( $\pm 3.0\%$ ). The fuel savings achieved for Vessel Bravo from the summer fouled to winter fouled was 14.7% ( $\pm 9.2\%$ ) and the fuel savings achieved from clean to FR coated condition was 11.1% ( $\pm 6.0\%$ ). The resulting fuel oil consumption values at cruising speed are presented in Table 9.



Table 9: Cruising speed FOC results from the interval plot of the average speed adjusted FOC.

Vessel Name	Hull Condition	8knot Average Speed-Adjusted FOC [L/min]
Alpha	Summer Fouled	0.2231 ± 0.004
	Winter Fouled	0.1746 ± 0.005
	XGIT-Fuel Coated	0.1490 ± 0.002
Bravo	Summer Fouled	0.1876 ± 0.012
	Winter Fouled	0.1600 ± 0.007
	XGIT-Fuel Coated	0.1422 ± 0.007

### 2.4.3 Fuel Data Results from Analysis Method #2

The results from the exponential fit analysis are shown in Figure 10 and Figure 11 with the dashed black line representing the intersection points at cruising speed (8 knots) for each hull condition. Using this analysis method, the fuel savings achieved for Vessel Alpha from the summer fouled to winter fouled condition was 26.9% (± 3.3%) and the fuel savings achieved from winter fouled to XGIT-Fuel coated condition was 16.8% (± 3.6%). The fuel savings achieved for Vessel Bravo from the summer fouled to winter fouled condition was 13.8% (± 10.8%) and the fuel savings achieved from winter fouled to XGIT-Fuel coated condition was 14.1% (± 9.7%).

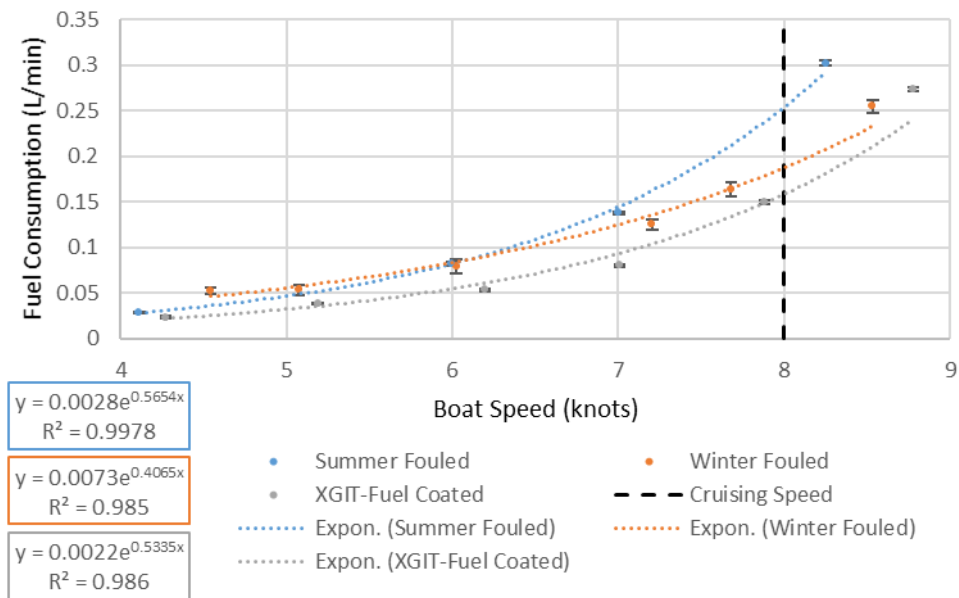


Figure 10: Exponential Fit for Alpha Fuel Oil Consumption vs. Speed

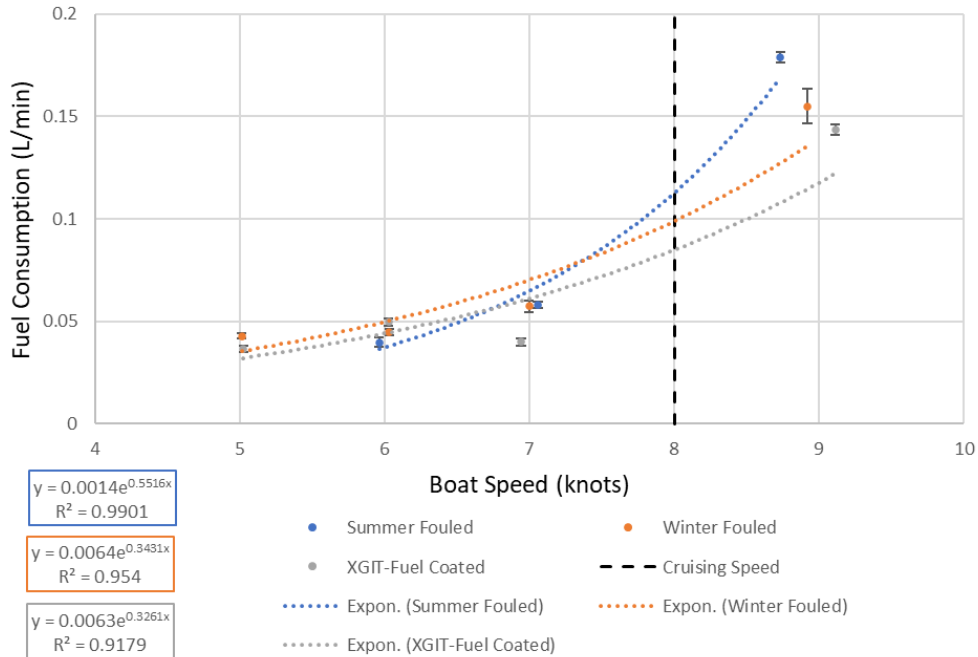


Figure 11: Exponential Fit for Bravo Fuel Oil Consumption vs. Speed

It was noted that the expected trend for the effect of hull condition on fuel consumption only starts to develop above 6 knots for both vessels. The Bravo vessel had its lowest fuel consumption at 5 knots which was deemed to be a result of “engine tuning”, causing the engine to perform the most efficiently at this speed. This was also the reason for omitting the 4-knot speed run from Figure 11, as it did not follow the exponential fit. At higher speeds there is a clear differentiation in fuel consumption between the hull conditions as expected. This finding could be attributed to a thinner viscous sublayer surrounding the hull as it gains velocity (Yeginbayeva and Atlar, 2018). A thinner viscous sublayer means the underlying roughness elements namely hull fouling and coating roughness, can increase the frictional resistance of the hull, thus increasing fuel consumption (Yeginbayeva and Atlar, 2018). The resulting fuel oil consumption values at cruising speed are presented in Table 10.

Table 10: Cruising speed FOC results from exponential fit.

Vessel Name	Hull Condition	FOC at Cruising Speed [L/min]
Alpha	Summer Fouled	0.2631 ± 0.002
	Winter Fouled	0.1954 ± 0.007
	XGIT-Fuel Coated	0.1727 ± 0.002

Bravo	Summer Fouled	0.1155 ± 0.004
	Winter Fouled	0.0996 ± 0.009
	XGIT-Fuel Coated	0.0856 ± 0.004

### 2.4.4 Max Throttle Speed Comparison for All Boats

During the conducted speed trials, a “max throttle” trial set was run for vessels Alpha, Bravo and Delta. This was done for each tested hull condition to identify a gain in max speed at the maximum shaft RPM because of reduced frictional resistance between summer fouled, winter fouled, clean and XGIT-Fuel coated hull conditions. Figure 12 shows the averaged max speed gain from both headings for each vessel.

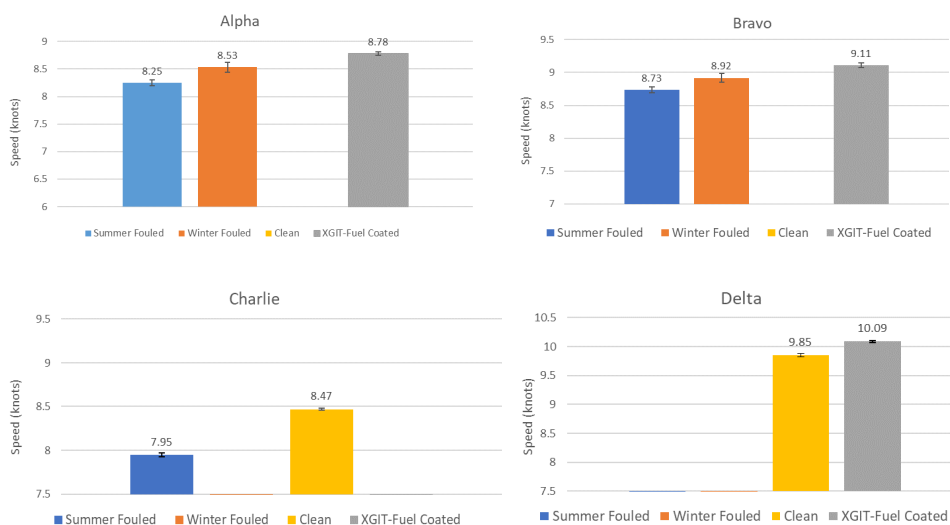


Figure 12: Max throttle speed comparison for all boats in various hull conditions.

Note Charlie’s max speed values for the clean XGIT-Fuel coated hull conditions were extrapolated from the shaft RPM vs. speed plot provided in the Appendix A. Notably, all vessels exhibited a max speed increase from a reduction in frictional resistance due to improvement in hull condition. Vessel Alpha gained approximately 0.28 knots from summer to winter fouled and 0.25 knots from winter fouled to XGIT-Fuel coated. Vessel Bravo gained approximately 0.19 knots from summer to winter fouled and 0.19 knots from winter fouled to XGIT-Coated. For these two vessels specifically, the improvement from a clean hull to the XGIT-Coated hull is confounded in the observed difference between winter fouled and XGIT-Fuel coated and is therefore cannot be distinguished with the data collected. Vessel Charlie gained approximately 0.52 knots from dirty to clean but underwent a change in propeller pitch before its XGIT-Fuel coated

trials, therefore its max speed could not be accurately compared against the other two hull conditions. Vessel Delta gained approximately 0.24 knots from clean to XGIT-Fuel coated which also implies a frictional resistance reduction in the coated condition. The standard error for each max speed ranged between 0.01 – 0.04 knots due to varying weather conditions between trials.

## 2.5 Sources of Error

There are multiple factors that could have affected the speed and fuel consumption values collected during the performed sea trials. Weather parameters including wave height, wind speed and direction, air and water surface temperature are known factors that can contribute to increased vessel resistance through water (Lindholdt et al., 2015). As previously discussed, each speed trial was performed in opposing directions to minimize the influence of wind and waves and current speed on the collected results. However, the change in vessel draft due to load (added weight of fuel and passengers) and changes in sea water density are two factors that were not held constant and there their impacts should be investigated. With reference to Figure 5, the summer fouled trials for vessels Alpha and Bravo were performed in October while the winter fouled, and XGIT-coated trials were performed in early and late June. According to the weather data from COVE (2022), the sea water temperature changed from approximately 7°C to 17°C between the date range. Annex E of ISO 15016 (2015) provides a methodology for accounting for the additional resistance due the change in sea water properties “ $R_{AS}$ ” from their reference value at 15°C (ISO 15016, 2015). If we take 17°C as the reference value for the XGIT-Coated trials in this case, we can calculate the added resistance due to viscosity and density changes using Equations 2.5-2.8.

$$R_{AS} = R_{TO} \left( \frac{\rho_S}{\rho_{S0}} - 1 \right) - R_F \left( \frac{C_{F0}}{C_F} - 1 \right) \quad [2.5]$$

$$C_F = \frac{0.075}{\left( \log \left( \frac{\rho V_S L}{\mu} \right) - 2 \right)^2} \quad [2.6]$$

$$R_F = \frac{1}{2} \rho_S S V_S^2 C_F \quad [2.7]$$

$$R_{T0} = \frac{1}{2} \rho_{S0} S V_S^2 C_{T0} \quad [2.8]$$

Where “ $C_F$ ” is the frictional coefficients for the measured sea water temperature, viscosity, and density, “ $S$ ” is the wetted hull surface area, “ $V_S$ ” is the speed of the vessel, “ $\mu$ ” is the calculated viscosity, and  $\rho_S$  is the calculated water density for a measured salinity and temperature. The coefficient of friction term accounts for the extra hull resistance due to a 30% change in viscosity from 0.001130 Pa s to 0.01483 Pa s. This increase in viscosity would serve to increase the boundary-layer thickness and decrease the velocity gradient at the hull’s surface, as a result of a less favorable pressure gradient.

- Sea water (35% salinity) at 17°C from ITTC (2011): Density = 1025.56 kg/m<sup>3</sup>, Viscosity = 0.001130 Pa s
- Sea water (35% salinity) at 7°C from ITTC (2011): Density = 1027.47 kg/m<sup>3</sup>, Viscosity = 0.001483 Pa s

$$R_{AS} = 6,754 N \left( \frac{1,027.47}{1,025.56} - 1 \right) - 1,468 N \left( \frac{0.0241}{0.0252} - 1 \right) = 74.1 N$$

$$R_{AS} = 12.6N(\text{due to } \Delta\text{density}) + 61.5N(\text{due to } \Delta\text{viscosity}) = 74.1 N$$

$$\frac{R_{AS}}{R_{T0}} \approx 1.10\%$$

Therefore, the change in sea water density and viscosity due to a 10-degree temperature difference contributed to a 1.1% change in the total hull resistance between the summer and winter fouled trials conducted in 7°C sea water and the XGIT-Fuel coated trials in 17°C sea water. The above relationship implies that colder sea water (higher density and viscosity) results in a greater hull resistance. Other factors that could have impacted the displacement of the vessel (thus hull resistance) include the weight of equipment and crew members on board during the trials and the volume of fuel. The number of crew members remained relatively constant between trials ( $\pm 2$  crew or 136kg) as well as the volume of diesel fuel loaded ( $\pm 25$  gal or 80kg). Annex H of ISO 15016 (2015) provides a relationship between power and displacement to account for such

changes but these calculations were not included in this study due to the lack of shaft power data.

## 2.6 Avoided Green House Gas Emissions

For this study, global warming equivalents for 100 years of climate damage ( $GWP_{100}$ ) were used to quantify the impact of diesel fuel combustion from the fishing vessels. The greenhouse gas particles considered include carbon dioxide ( $CO_2$ ), methane ( $CH_4$ ), nitrogen dioxide ( $N_2O$ ) and a form of particulate matter known as black carbon (BC). Each of these pollutants has an associated emission factor and global warming potential shown in Table 11.

Table 11: List of GHG pollutants from the combustion of marine diesel oil according to the Fourth IMO GHG Study (2020).

GHG Pollutants	Emission Factor kg/MT fuel	Global warming potential (100-yr GWP)
$CO_2$	3,206	1
$CH_4$	0.05	25
$N_2O$	0.18	298
BC	0.38	680
<b>Total <math>GWP_{100}</math> Impact: 3,519 kg <math>CO_2e</math>/MT fuel</b>		

To analyze the potential emissions savings, an average value of the fuel oil consumption results from Sections 3.2 and 3.3 was used. The relative savings of each hull condition at cruising speed are presented in Table 12.

Table 12: Relative fuel and GHG emissions savings based on hull condition.

Vessel Name	Hull Condition Scenario	Relative Fuel Savings	FOC Reduction (MT/yr.)	GHG Emissions Savings (MT $CO_2e$ /yr.)
Alpha	Summer vs. Winter	24.5% ± 3.5%	4.03 ± 0.5	14.2 ± 2.0
	Winter vs. XGIT-Fuel	15.7% ± 3.3%	1.96 ± 0.4	6.9 ± 1.5
Bravo	Summer vs. Winter	14.4% ± 10.0%	1.13 ± 0.8	4.0 ± 2.8

	Winter vs. XGIT-Fuel	12.3% ± 7.8%	0.83 ± 0.5	2.9 ± 1.9
--	----------------------	-----------------	------------	-----------

The change in collective GHG emissions of Alpha and Bravo due to hull condition are shown in Figure 13 below.

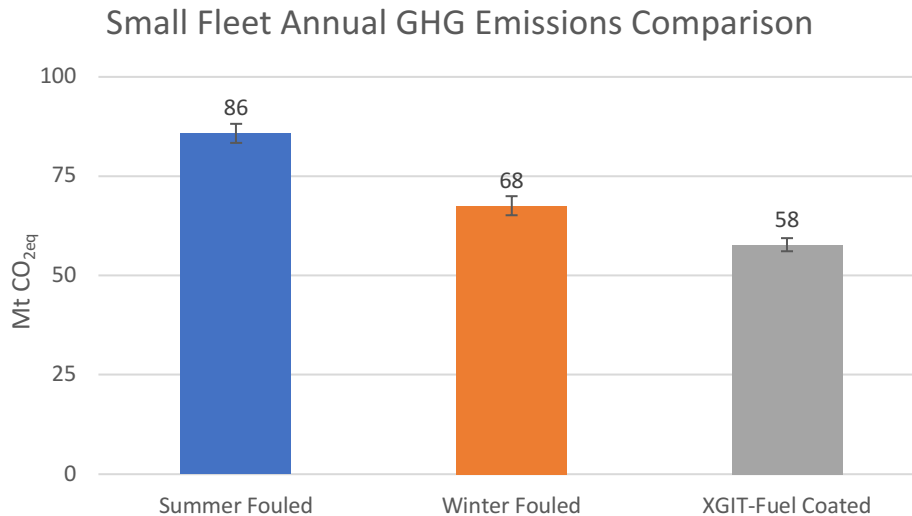


Figure 13: Visual representation of collective GHG emissions for each hull condition.

From the first year of this study, we saw the fishing boats are subject to both winter and summer fouling growth seasons when they are coated with an inert coating (gelcoat). The rate of this growth is approximated in Figure 6 for each season as well as a prediction for how the XGIT-Fuel coated hulls will behave in the summer and winter seasons based-off underwater images of the hulls. Clearly the XGIT-Fuel coating was unable to negate static fouling growth during the summer season as vessels Alpha and Bravo were static (idle) for periods of 15-20 days at a time. However, once the vessels began their lobster fishing season over the winter months, the vessels appeared to be clean of fouling in the underwater images that were captured. To compare a full-year operation with and without the XGIT-Fuel coating would require further study, however a prediction on its long-term performance can be made as follows. If these vessels follow the summer fouling season of growth when retrofitted with XGIT-Fuel but maintain a clean hull during the winter lobster fishing season; they could collectively save the added fuel penalty due to the winter season of fouling, which lasts for 6 months of the year.

To put this study's findings in perspective, there are 18,142 fishing vessels of lengths 6m-18m that currently operate in Canada ("OECD.Stat," 2018). If we assume that 50% of these vessels are currently using fouling control methods such as a polishing anti-fouling coating, that leaves 9,071 vessels that remain subject to the detrimental effects of biofouling at the commercial fishing level. Assuming the remaining vessels were to be retrofitted with XGIT-Fuel, the fleet could save up to 89,000 metric tons of CO<sub>2eq</sub>. This is equivalent to 0.22% of the global fishing fleet's CO<sub>2e</sub> emissions as the fleet contributes 40.7 million MT CO<sub>2e</sub> annually, according to the Fourth IMO GHG Study (International Maritime Organization, 2021). These fleet calculations cannot be viewed as absolute but are purely a means of demonstrating the environmental importance of maintaining a smooth clean hull condition versus a winter fouled condition.

From the added resistance diagrams in Demirel et al. (2019), the ship model of an IMOCA Open 60 class yacht was chosen as a candidate for comparison due to its relative size and speed compared to the cape islander vessels. The IMOCA vessel operates at 15 knots and had a predicted increase in effective power of 38% - 57% due to small and medium calcareous fouling versus a typical applied anti-fouling coating (Demirel et al., 2019). This vessel is 20m in length which is longer than a cape islander and may have a relatively higher component of frictional drag due to its hull shape (USNA, 2002). This provides a comparison for the values obtained in this study, a 25% - 36% increase in fuel consumption due to the development of fouling growth. Assuming the change fuel consumption of the cape islanders is a direct result of the increase in effective power (outlined in Equation 2.4), the findings are somewhat consistent with what was reported for the IMOCA vessel with small calcareous fouling or weed.

The question then becomes, what is the true improvement in fuel efficiency for the as applied XGIT-Fuel coating compared to the previous gelcoat barrier coating. Clearly there is some benefit to a smoother hull surface, as vessel Delta displayed an increase in max speed gain of 0.24 knots ( $\pm 0.03$  knots). We know that a max speed gain equates to a fuel consumption reduction at constant speed from the vessel's speed trial results. Therefore, we can conclude that there was an improvement in overall efficiency from the retrofit with XGIT-Fuel. It will now be interesting to determine how the coating



performs over time in terms of frictional resistance, static fouling growth, and cleanability (via movement and hull cleanings).

Other environmental factors such as acidification and photochemical ozone creation from diesel combustion emissions have not been considered in this chapter to avoid repetition in Chapter 4. Small vessel owners such as fishing boat captains should also consider the environmental impact of their choice in anti-fouling coating, especially those containing biocidal components such as copper. The environmental impact of increased shipping emissions and choice in coating system will be explored in Chapter 4, as these impacts scale proportionally with ship size and operational activity.

## **2.7 Limitations and Recommendations for Future Work**

The analysis of the sea trial data was performed on the back of the work of a Transport Canada study on the GHG emissions of a small in-shore fishing fleet. Therefore, our ability to control the number of vessels, variations in hull condition and sea trial data collected were somewhat limited to the pre-defined project timeline and scope. Each vessel was unique in terms of its propulsion system, design specifications, operational activity, etc., which added another degree of difficulty when it comes to creating a general case for a typical cape islander. However, this also represents reality since both the national and global fishing fleets have these same variations. In an ideal case, multiple sister boats would be used as test candidates to isolate the effect of a hull coating on their fuel performance and powering requirement.

Follow-on sea trials are recommended for the continued anti-fouling performance monitoring of the XGIT-Fuel coating. These trials could be performed 6 months later, once the coated vessels have been through a fouling season (winter). This would also help identify if the coating is preventing marine growth through its fouling release mechanism. If the coatings are fouled, their fuel consumption results can be compared to those obtained from the previous year to determine if there is any variability in their fuel performance. Another recommendation for future work would be to perform ASTM D3623, a standard method for testing the anti-fouling performance of coated panels in

shallow water environments (ASTM, 2020). The static panel testing could be performed in conjunction with sea trials to monitor the static and dynamic fouling ratings of both control and XGIT-Fuel coated panels over time. Ideally, this test would be performed in the same marine environment as the stationary fishing vessels throughout both summer and winter fouling seasons. Results from this test regimen could be utilized as valuable inputs for a comparative life cycle analysis between the gelcoat barrier coating and the XGIT-Fuel coating on the hull of a cape islander vessel.

## **2.8 Conclusions**

The relationship of fuel consumption versus speed data for three hull conditions on two fishing vessels was analyzed. A reduced fuel consumption in the range of 14.4% - 24.5% from the summer fouled to winter fouled hull condition was observed. Moreover, a 12.3% - 15.7% reduction was observed when the hulls went from being winter fouled to coated in the new XGIT-Fuel coating. When we compared the speed gain at max throttle, vessels Alpha, Bravo and Charlie exhibited improvements from dirty to clean/coated and vessel Delta showed an increase in speed from clean to coated with XGIT-Fuel. The fuel consumption vs. speed results from the fouled conditions provide a strong indication that fishing vessel owners should adopt an anti-fouling strategy to avoid excess fuel costs and GHG emissions.

This study has shown that in the absence of biocides, regularly scheduled hull maintenance is a key factor in improving the performance of these vessels. If the Canadian fishing fleet were to be retrofitted with XGIT-Fuel, a hybrid foul release coating, there is potential for substantial greenhouse gas emission reductions. The level of this reduction will depend on vessel size, engine performance, fouling conditions, and operational activity. To understand the long-term impact of XGIT-Fuel on the fuel efficiency of these fishing boats, a set of follow-on sea trials was suggested. Continuous monitoring of the XGIT-Fuel coating fouling rating over time when applied to a vessel's hull, will serve as a valuable input for its life cycle assessment.

## **CHAPTER 3    FRICTIONAL DRAG MEASUREMENTS IN A FULLY TURBULENT FLOW CHANNEL**

### **3.1 Introduction**

Throughout history, there have been several experimental setups for determining the fluid drag characteristics of coated surfaces. Lindholdt et al. (2015) presents a comprehensive overview of these experimental methods which include: rotating disks, rotating cylinders, towing tanks, water tunnels, static and dynamic panel exposure tests on a moving vessel, pipe flow, and optical methods such as Laser Doppler Velocimetry (LDV). Each of these methods have their advantages and disadvantages when it comes to determining a marine coating's drag performance, outlined in detail in Lindholdt et al., (2015).

In 2001, frictional drag measurements of a foul release and a tin-free SPC were conducted at the University of Newcastle Upon Tyne towing tank facility (Anderson et al., 2003). The study found that the foul release coating exhibited between a 2% - 23% lower drag compared to the tin-free SPC coating (depending on the quality of coating application). Follow-on rotor experiments with rotating cylinders also identified a 3.6% lower drag for the sprayed foul release coating and 2.2% lower when rollered, compared to the sprayed tin-free SPC coating (Anderson et al., 2003). This study identified the possibility to achieve various levels of frictional drag depending on the type of marine coating and employed method of application. This study also describes the concept of a "roughness function" as the downward shift in the log law region of the velocity profile, which demonstrates a difference in local frictional resistance between a rough surface and an uncoated smooth reference surface. This concept will be explained in further detail in Sections 2 and 3.3.

Following this study, Schultz and Myers (2003) compared three different methods for determining the roughness function of a rough surface using epoxy and sand paper grits at the United States Naval Academy Hydromechanics Laboratory. The study found that the velocity profile method, towed plate method, and rotating cylinder method all

showed good agreement for both the epoxy and sand paper surfaces despite differences in the Reynolds number range examined (Schultz and Myers, 2003). This study references two universal roughness functions to describe the behavior of rough surfaces; the Colebrook-type roughness function for engineered surfaces, and the Nikuradse-type roughness function for sand-grain surfaces (Schultz and Myers, 2003). These two universal functions serve to describe the behavior of rough surfaces in the smooth, transitionally rough, and fully rough flow regimes (Schultz and Myers, 2003).

Once the roughness function methodology was verified, further studies were carried out on marine coatings (Schultz, 2004), and marine coatings covered in biofilms (Schultz et al., 2015; Walker et al., 2014) to determine their impacts on frictional resistance at high Reynolds numbers. The studies found that foul release coatings typically performed better in terms of frictional resistance than anti-fouling coatings. The increase in frictional resistance at ship speed was determined through Granville's boundary layer similarity-law scaling technique (Granville, 1958). This technique allowed for the prediction of ship scale frictional resistance and powering from all types of experimentally rough surfaces including marine coated surfaces and biofouled surfaces in Demirel, 2015; Demirel et al., 2019; Song et al., 2020a; Yeginbayeva et al., 2020; etc.

According to the (ITTC, 2011b), it was recommended that researchers should generate an extensive database of the roughness function for various anti-fouling coatings and biofouling. Consequently, the roughness function of a surface must be known to properly predict the roughness effect that the surface will have on a ship's frictional resistance (Demirel, 2015). Through personal communication with Prof. Yigit Kemal Demirel of the University of Strathclyde, a research collaboration was formed with Dalhousie University. The goal of this combined research effort, was to determine the roughness functions and drag performances of multiple marine coating types in the as-applied condition, including GIT's newly developed coating XGIT-Fuel.

The goal of the chapter is to capture the roughness function of XGIT-Fuel, along with various other marine coating types that are commonly used in the shipping industry. The resulting effects on a ship's frictional resistance can then be used as inputs for a comparative LCA.

## 3.2 Materials & Methods

### 3.2.1 Experimental Apparatus

The University of Strathclyde's (UoS) Fully Turbulent Flow Channel (FTFC) was used to conduct a series of measurements for various types of fouling control coatings in the freshly applied condition. The FTFC is a closed-circuit flow channel that can accommodate two opposing panels in its test section located downstream of a single 22kW Grundfos centrifugal pump (Marino et al., 2019). The FTFC was specifically designed by the Department of Naval Architecture Ocean & Marine Engineering (NAOME), to assess the frictional resistance performance of marine coatings. For more information on the design, operation and calibration of this channel, the reader is advised to use Marino et al. (2019) as a reference paper. An image of the experimental apparatus for the skin friction measurements of the marine coated panels is shown in Figure 14.



Figure 14: The FTFC facility and experimental apparatus taken by Roberto Ravenna (PhD. candidate) at the University of Strathclyde.

### 3.2.2 Test Panel Design & Preparation

High density polyethylene was used as the material to manufacture six test panels according to the design test section dimensions within the FTFC. Six marine coating types were selected for testing including the XGIT coating for to collect input data for its life cycle assessment. The test panel design for testing in the FTFC is shown in Figure 15.

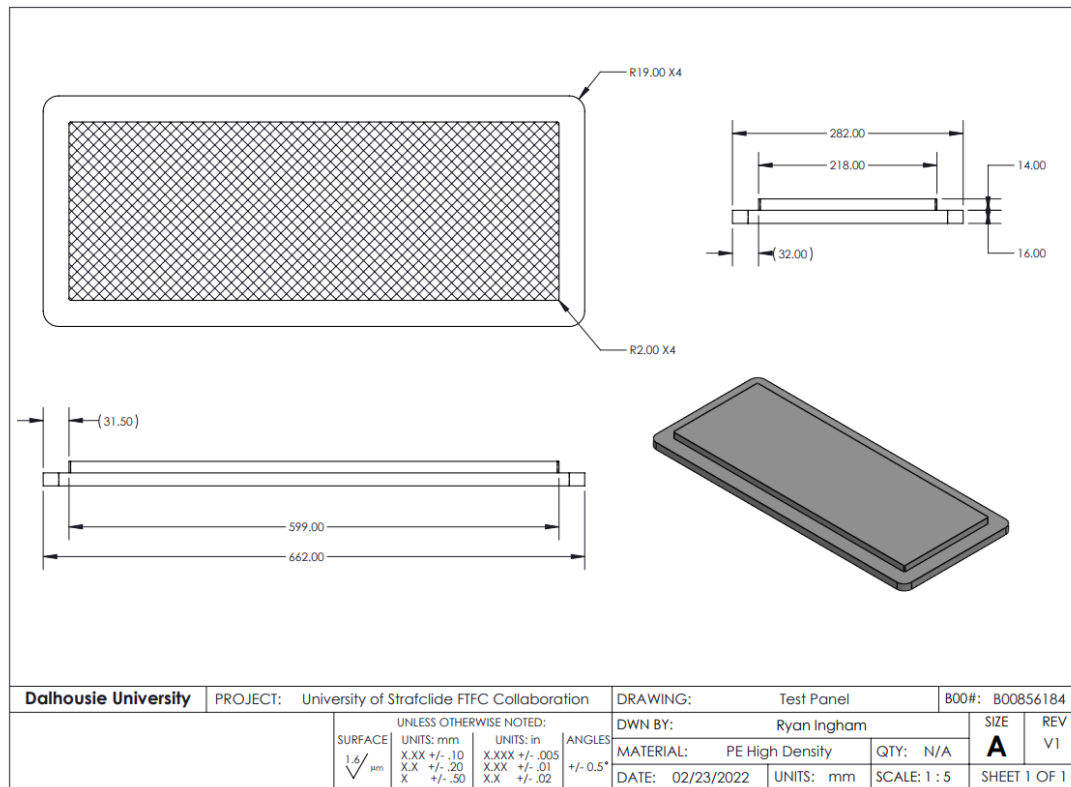


Figure 15: Solid Works drawing of the high-density polyethylene panels design for the FTFC test section.

Prior to coating application, each panel was lightly sanded with 220 grit sandpaper using an orbital sander to promote adhesion and to eliminate the waviness of the panel surface from machining. Once smooth, each marine coating system was applied by a qualified coating applicator and the underlayers (primer and tie coat if necessary) were also applied to simulate the scheme that is applied to a ship's hull. An example of the uncoated sanded HDPE panel and subsequent application of coating layers is shown in Figure 16.



Figure 16: HDPE panels after surface preparation and coating application

The coated panels were tested along with an uncoated acrylic control panel, which was included in the test matrix by the FTFC technicians to simulate a hydraulically smooth surface. The ideal method of application for each coating is airless spray as it creates the smoothest finish and is the method used for application to a vessel during newbuild or maintenance and repair. However, not all coatings were able to be applied using this method, as they required special application measures (glass flake) or resulted in contamination of spraying equipment (silicone). A breakdown of the name of each marine coating applied and method of application is provided in Table 13.

Table 13: Overview of each test panel set, marine coating systems applied, coating types and method of application.

Panel Set Name	Panel Material	Marine Coating System Applied	Coating Type (Topcoat, Underlayers)	Method of Application (Topcoat, Underlayers)
Reference	Acrylic	None (Smooth)	N/A	N/A
FR01	High Density Polyethylene	Intersleek 1100SR - Blue	Fluoropolymer/silicone foul release, elastomeric tie coat, anticorrosive primer	Roller, Roller, Airless spray
FR02	High Density Polyethylene	XGIT-Fuel	Hard foul release, anticorrosive primer	Airless spray, Airless spray
BL01	High Density Polyethylene	Gelcoat	Vinyl ester resin barrier	Airless spray
IB01	High Density Polyethylene	Ecospeed	Inert, glass flake ice breaking	Brush

AF01	High Density Polyethylene	Interspeed BRA640	Controlled depletion polymer anti-fouling, anticorrosive primer	Airless spray, Airless spray
------	---------------------------	-------------------	---	------------------------------

### 3.3.3 Panel Surface Roughness Profiles

The surface profiles of each of the test surfaces were measured with a VTSYIQI surface roughness gauge (Figure 17) by capturing various surface texture parameters. The arithmetic mean roughness “Ra” is used to evaluate the average roughness amplitude over a given sampling length known as the cutoff length (ISO/TC 213, 2021). Other surface parameters including maximum height of the profile “Rz”, root mean square deviation “Rq” and the height between the highest peak and the deepest valley “Rt” were also captured over the same cutoff length (ISO/TC 213, 2021). There is a list of recommended cutoff lengths in the 1998 ISO standard that includes 8, 2.5, 0.8, 0.25 and 0.08mm to measure the microroughness of a given surface according to Howell and Behrends (2006). The VTSYIQI surface roughness gauge (shown in Figure 17) provided three option of 0.25, 0.80 and 2.5mm for cutoff lengths depending on the relative scale of the roughness height parameters (Ra & Rz) for each surface profile. The choice of cutoff length for each surface was evaluated in accordance with JIS B0601-1994 referenced in section 10.1.2 of the user’s manual for a standard surface roughness tester (Mitutoyo Corporation, 2016).



Figure 17: VTSYIQI surface roughness gauge used for panel roughness measurements (Ra, Rz, Rq, Rt).

A cutoff length of 0.25mm was used for the silicone foul release coating (FR01), 0.80mm was used for the hard foul release, gelcoat and controlled depletion polymer and 2.50mm was used for the icebreaking coating. The sanded high density polyethylene surface was also measured for reference and to observe how the roughness profile of the surface changed after coating application. The measurement error according to the device



manufacturer is  $\pm 15\%$  with a variability in measurement of  $<12\%$ . Note that other stylus-based micro roughness measurement devices have had issues measuring soft (silicone-based) foul release coatings due to the properties of silicone (Howell and Behrends, 2006). This device uses a contacting pin with a 10 $\mu\text{m}$  could have caused issues with the accuracy of the measured surface roughness of FR01. An average of five individual roughness measurements on various surface areas was taken for each panel (combined ten measurements per panel set). The average results from each coated panel set are shown in Table 14.

Table 14: Average surface roughness parameters for each test surface from profilometer.

Test Surfaces	Cut-off length (mm)	Ra	Rz	Rq	Rt
Sanded HDPE (220 grit)	2.50	2.64	12.99	3.27	16.91
FR01	0.25	0.042	0.310	0.063	0.535
FR02	0.80	0.159	1.075	0.212	1.669
AF01	0.80	0.680	3.384	0.850	4.744
BL01	0.80	1.248	6.773	1.590	9.253
IB01	2.50	4.351	17.276	5.482	27.022

Due to the sheer size of the high-density polyethylene panels, they could not be measured under a laser confocal microscope to serve as a comparison between measurement methods. The concept of the importance of cut-off length as well the choice of a roughness parameter to use for calculating the roughness functions will be discussed in Section 3.4.

### 3.3.4 FTFC Pressure Drop Measurements

The FTFC contains six pressure taps each at a set distance of 120mm apart from each other in the direction of flow. The pressure drop measurements are made along the test panels by connecting two of the six pressure taps to a differential pressure transducer manufactured by “Aplisens”, with a range of 0-400 mbar (Marino et al., 2019). The FTFC circuit contains a total of three differential pressure transducers which connect to a chosen pressure tap configuration via plastic hoses (Marino et al., 2019). An image of the pressure tap distribution and measuring section are shown in Figure 18 below (with tap configuration 1-6 hooked up for measurement) (Marino et al., 2019).

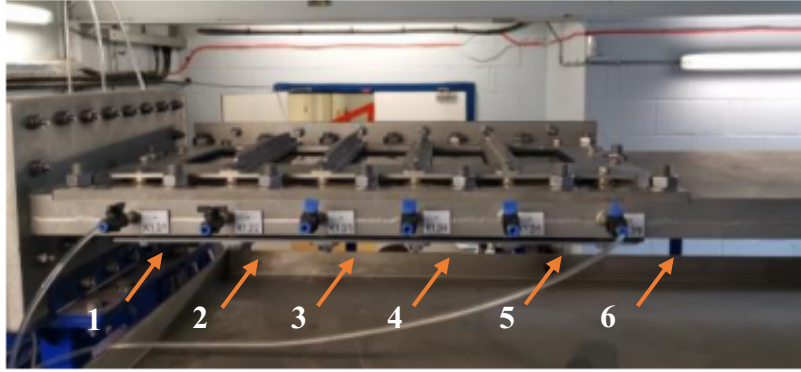


Figure 18: Visual of the pressure tap distribution along the test section of the FTFC.

Pressure taps 2-5 were chosen for pressure drop measurements by the FTFC operators during the calibration of the channel to avoid pressure waves and noise disturbances at the ends of the measuring section. Taps 2-5 also provided the lowest uncertainty in pressure drop values at the mid-range pump frequency (16 Hz) (Marino et al., 2019). The uncertainty for this tap configuration ranged from 1.48% - 1.23% at the lowest and highest pump frequency respectfully (Marino et al., 2019). For further details on why this configuration was chosen, see Section 2 of Marino et al. (2019).

For the pressure drop measurement on each set of test panels, the full range of pump frequencies were tested (5Hz – 40Hz) to give a total of 36 different mean bulk velocity values (approx. 1.5m/s – 13.5m/s). The mean bulk velocities were calculated based on the data received from a magnetic flow meter which was placed at the lower end of the FTFC (Marino et al., 2019). The variation in mean bulk velocity across the smooth reference panels for a given pump frequency is shown in Figure 19 below.

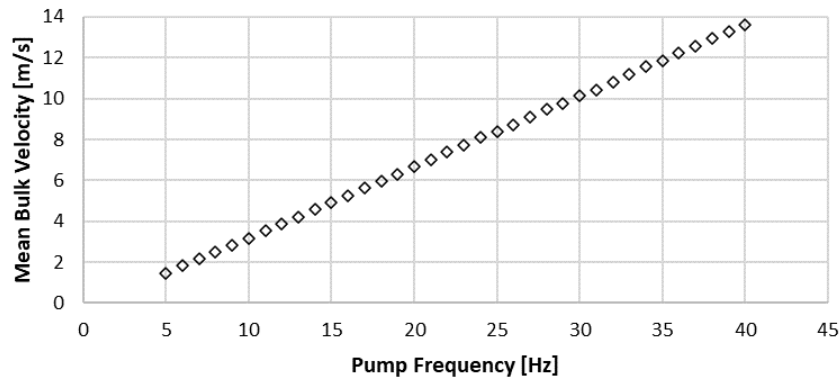


Figure 19: Centrifugal pump frequencies and corresponding mean bulk velocities at the test section of the FTFC with the hydraulically smooth acrylic reference (uncoated) panel.

The frictional resistance of the test panels is evaluated by the pressure differential of the two taps in relation to their longitudinal distance apart (dp/dx). The wall shear stress of each panel set can be calculated as

$$\tau_w = -\frac{D_h}{4} \frac{dp}{dx} \quad [3.1]$$

based on the hydraulic diameter ( $D_h$ ) of the channel and the resulting longitudinal pressure drop (dp/dx). The skin friction coefficient can then be calculated as

$$c_f = \frac{\tau_w}{\frac{1}{2} \rho U_m^2} \quad [3.2]$$

where  $\rho$  is the fluid density (fresh water @ ~16°C) and  $U_m$  is the mean bulk velocity of water flow in the channel test section (Marino et al., 2019). The mean bulk velocity of water was measured with a magnetic flowmeter and the channel-based Reynold's number ( $Re_M$ ) can be used to characterize each flow speed as

$$Re_M = \frac{U_m h}{\nu} \quad [3.3]$$

where  $h$  is the channel height and  $\nu$  is the kinematic viscosity of water. To represent the hydrodynamic drag performance of each marine coating, a unique "roughness function"  $\Delta U^+$ , is determined. The roughness function of surface can be directly related to the surface roughness parameters such as total roughness height, average height, skewness, waviness etc. For this study, the indirect method for fully developed pipe flow proposed by (Granville, 1987) is used to calculate the roughness function  $\Delta U^+$  and roughness Reynold's number  $k^+$  for each coating as follows

$$\Delta U^+ = \sqrt{\frac{2}{c_{f,s}}} - \sqrt{\frac{2}{c_{f,r}}} \quad [3.4]$$

$$k^+ = \frac{1}{\sqrt{2}} Re_{M,r} \sqrt{c_{f,r}} \frac{k}{D_h} \quad [3.5]$$

where the "r" and "s" subscripts denote rough and smooth surfaces respectfully and "k" is the roughness length scale (determined in Section 3.4). For this calculation,

$c_{f,s}$  and  $c_{f,r}$  must be evaluated at the same value of  $Re_M\sqrt{c_f}$  for fully developed pipe flow according to Granville (1987).

### 3.3.5 Experimental Uncertainty

The standard errors for the coefficient of friction were calculated based on four to six replicate runs of the FR01 panel at the minimum and maximum flow velocities respectively. The precision uncertainty in the skin friction coefficient was calculated at a 95% confidence interval by multiplying the standard error by the two-tailed t values ( $t=3.182, 2.571$ ) for three to five degrees of freedom, according to (Coleman and Steele, 1995). The accuracy of the differential pressure sensor is  $\pm 0.075\%$  and the accuracy of the magnetic flow meter was  $\pm 0.2\%$  according to the manufacturer's specifications. The total bias limit and precision limit for the coefficient of friction were combined using Equation [3.6] to give a total uncertainty of  $\pm 0.74\%$  at the lowest  $Re_M$  and  $\pm 0.47\%$  at the highest  $Re_M$ .

$$(U_A)^2 = (B_A)^2 + (P_A)^2 \quad [3.6]$$

where  $B_A$  is the bias uncertainty limit,  $P_A$  is the precision uncertainty limit and  $U_A$  is the total uncertainty. The  $P_A$  is caused by random errors in the repeatability of the experimental measurements and is calculated for "n" replicate runs as follows:

$$P_A = t_{0.95,n-1} * \frac{SDev}{\sqrt{n}} \quad [3.7]$$

$$\text{where } SDev = \left[ \frac{\sum_{i=1}^n (A_k - A_{average})^2}{n-1} \right]^{\frac{1}{2}} \quad [3.8]$$

The  $B_A$  is caused systematic errors due the uncertainty in the measurement devices and can calculated as follows:

$$B_A = \frac{\partial A}{\partial x} B_x + \frac{\partial A}{\partial y} B_y + \frac{\partial A}{\partial z} B_z + \dots \quad [3.9]$$

$$\text{where } A = f(x, y, z, \dots) \quad [3.10]$$

The uncertainty in the roughness function ( $\Delta U^+$ ) was calculated using typical error propagation techniques to give an overall uncertainty in  $\Delta U^+$  of  $\pm 14.4\%$  or 0.04

(whichever is larger) at the lowest  $Re_M \pm 6.5\%$  or 0.04 (whichever is larger) at the highest  $Re_M$ . For comparison, the high Reynold's number turbulent flow facility at the US Naval Academy achieved a relatively similar level of uncertainty with their skin friction data being  $\pm 1.2\%$  at  $Re_M$  between 40,000-300,000 (Schultz et al., 2015).

### 3.4 Results and Discussion

#### 3.4.1 Wall shear stress comparison

The FTFC was specifically designed to assess the performance of marine coatings and other surface patterns in full-scale conditions by achieving the same wall shear stress (WSS) value as that of a flat plate of ship length travelling at cruising speed. To demonstrate the range of WSS values that were simulated in the FTFC, a plot of WSS vs. flow speed for each panel set is shown and compared to the 1957 ITTC skin friction formulation for a 200m long flat plate in Figure 20.

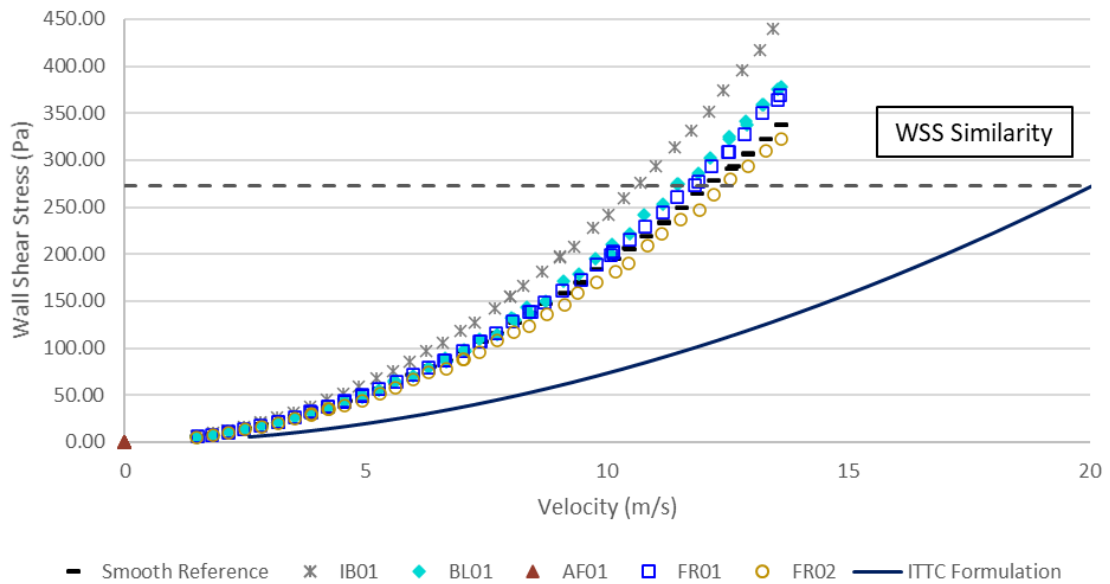


Figure 20: WSS achieved in FTFC compared to a 200m long flat plate using the ITTC formulation.

As shown in Figure 20, the 273 Pa wall shear stress of a flat plate at a speed of 20m/s (full scale ship speed) can be achieved in the FTFC at a considerably lower flow speed (10.7-12.5m/s) (Marino et al., 2019). The FTFC also enables the measurement of

much higher flow speeds and WSS values that would not be otherwise achievable in a towing tank with flat steel or aluminum plates (max towing speed of  $\sim 4$  m/s).

The above flow speed comparison illustrates that the panels were tested in an environment that is representative of full-scale flow conditions and captures the range of experienced frictional resistance by a 200m flat plate of ship length. In essence, it allows the results from the FTFC to be correlated to the turbulent boundary layer formed on a ship's hull at cruising speed.

### **3.4.2 Skin friction coefficients**

Figure 21 shows the skin friction coefficient ( $c_f$ ) of each test surface plotted against the Reynold's number  $Re_M$  compared the hydraulically smooth acrylic panel and reference data taken from Schultz and Flack (2013). All the surfaces had skin friction coefficient values beneath the smooth friction line at low Reynolds numbers except for the IB01 surface. Indeed, the AF01 displayed strange flow behavior below values of  $Re < 100,000$ , which could not be explained by its surface condition or roughness parameters. All the surfaces had skin friction coefficient values above the smooth friction line at higher Re values ( $Re > 200,000$ ) except for the FR02 surface. The FR01 and BL01 surfaces had skin friction curves that followed the behavior of the smooth acrylic reference panel up until 200,000 Re where the surfaces showed an increase in skin friction drag compared to the reference surface. FR02 was the only surface to maintain a lower skin friction coefficient than the smooth reference surface over the entire Reynolds number range ( $30,000 < Re < 300,000$ ).

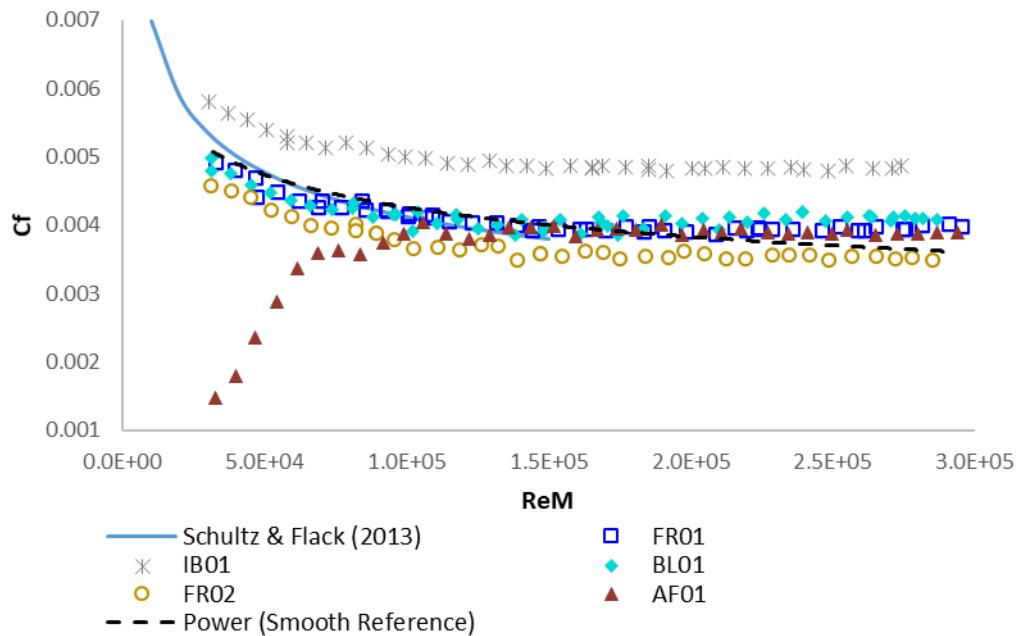


Figure 21: Skin friction coefficients vs. Reynold's number ( $Re_M$ ) for all marine coating surfaces.

Each panel set separated from the hydraulically smooth condition at slightly different values of Reynold's numbers. The IB01 coating separated immediately, showing the effects of its applied surface roughness with a skin friction value 34.0% greater than the smooth condition at the highest Reynold's number. Due to the noisy flow behavior of the AF01 coating, only the skin friction drag observed at  $Re > 140,000$  (20Hz pump frequency) was used for comparison between coating types. The change in skin friction coefficient compared to the reference panel for flow speeds of 6.66 – 13.62 m/s (5Hz intervals) are given in Table 15.

Table 15: Relative change in  $C_f$  values of the test panels with respect to the Reference Panel.

Change in $C_f$ (%) with respect to the Reference Panel						
Pump Freq (Hz)	Flow Speed (m/s)	IB01	BL01	FR01	FR02	AF01
20	6.66	25.12%	-1.08%	0.62%	-10.26%	1.64%
25	8.41	25.44%	-0.62%	0.52%	-9.60%	1.69%
30	10.15	26.81%	3.58%	3.00%	-7.78%	2.23%
35	11.87	28.20%	8.10%	4.66%	-7.17%	3.42%
40	13.62	33.95%	12.69%	9.26%	-4.20%	6.74%
<b>Average</b>		<b>27.9%</b>	<b>4.5%</b>	<b>3.6%</b>	<b>-7.8%</b>	<b>3.1%</b>

When comparing the skin friction data results to the surface roughness data, they are not directly correlated. This finding was also observed by Demirel (2015) when comparing measured macro roughness ( $R_{t50}$ ) values to the frictional resistance results from marine coated flat plates in a towing tank experiment. The AF01, FR01 and BL01 coatings all had an average increase in skin friction between 3.1-4.5% from the smooth reference panel. The IB01 coating had an average increase in skin friction of 27.9% while the FR02 panel had an average decrease in skin friction of 7.8%. This illustrates the impact of application method as well as each coating's ability (as applied) to behave like a smooth surface under high flow conditions.

There were various application methods used for each surface depending on the nature and properties of each coating and the equipment that was available. For instance, the icebreaking coating (IB01) had to be applied by brush as it was too viscous to be applied by airless spray and it had an undesirably short window for normal application. The brushed method led to a thicker film thickness than the other coatings and created an exaggerated waviness in the coating's surface finish. BL01 was applied by high viscosity low pressure spray and a smooth finish was achieved.

The silicone foul release system (FR01) was applied by a combination of airless spray and roller methods. The anticorrosive primer layer was sprayed followed by the tie coat and topcoat which were applied by roller due to issues of cross contamination. The roller application led to small, isolated blistering in the coating's surface which could have affected the resulting flow behavior in the FTFC. However, these imperfections were not captured in the measured roughness data as the isolated locations were not quantifiable in terms of a roughness value. Candries and Atlar (2005) found that applying a foul release coating by roller can increase the frictional resistance by approximately 2.5% during a turbulent boundary layer experiment.

The hard foul release coating (FR02) and controlled depletion polymer (AF01) systems were both applied by airless spray over top of an airless sprayed anticorrosive primer which created an ultra-smooth finish. It was noted that the FR02 panel had



significantly lower skin friction data than the AF01 (11.9%) despite the same application method. This difference in skin friction behavior is partially reflected in the measured surface roughness parameters but could also indicate an enhanced hydrophobicity effect of the hard foul release coating (FR02) which delayed the flow separation beyond the highest flow speed achieved in the FTFC. There is previous evidence of the ability of hydrophobic surfaces to delay the onset of flow separation and thus skin friction drag from circular cylindrical surfaces (You and Moin, 2007).

It is also important to note that these surfaces were applied in a largely isolated environment which is not representative of the conditions of a real-world coating application in a dockyard. A dockyard environment can be subject to a variety of external factors, including high winds, temperature, and pre-existing hull roughness (macro roughness). The coating surfaces presented in this study and those compared in other studies, especially the coatings that were airless sprayed (FR02 & AF01) should, therefore, be taken as a better finish than one that would be achieved on the surface of a ship in drydock (Walker et al., 2014; Schultz et al., 2015).

### 3.4.3 Determination of the Roughness Functions

The roughness function values ( $\Delta U^+$ ) and roughness Reynolds numbers ( $k^+$ ) were determined for each surface using Equations [3.4] & [3.5] respectively. To evaluate

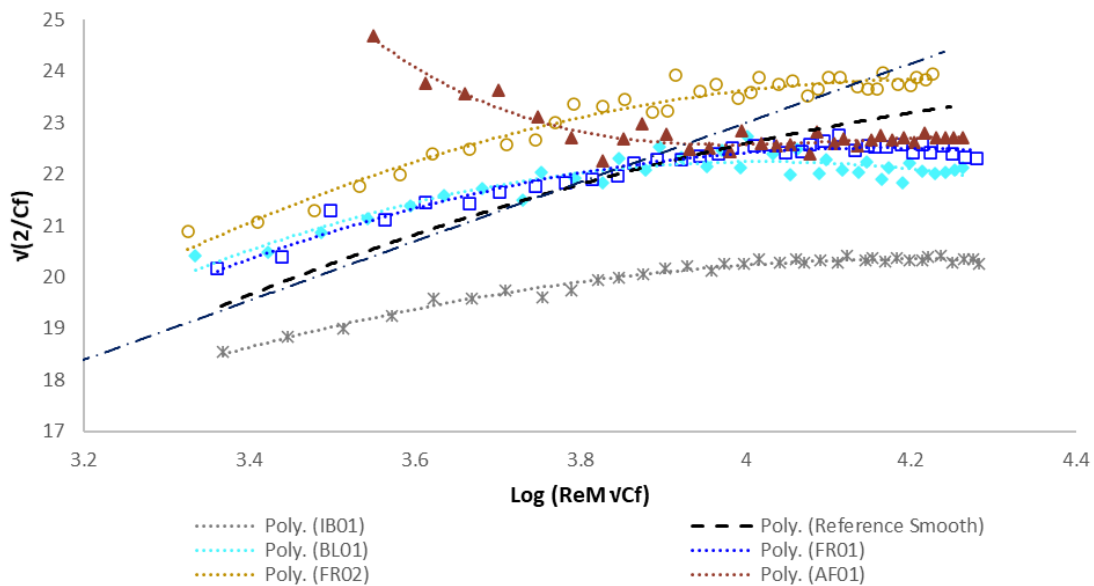


Figure 22: Plot of  $\sqrt{2/C_f}$  vs.  $\text{Log}(Re_M \sqrt{C_f})$  for each set of coated panels.

Equation [3.4], a plot of  $\sqrt{2/C_f}$  vs.  $\text{Log Re}_M\sqrt{C_f}$  was generated for each set of skin friction data and fitted with 2<sup>nd</sup> or 3<sup>rd</sup> polynomial fits as shown in Figure 22. Using polynomial fits allowed for the difference between the smooth (acrylic reference) and rough coefficients of friction to be evaluated at the same value of  $\text{Log Re}_M\sqrt{C_f}$  with a high level of validity in the coefficient of determination ( $R^2 > 0.85$ ). This indirect method of roughness function determination for rough pipe flow was first shown by Granville (1987) and originally advocated by Robertson et al. (1968). Granville (1987) also shows the commonalities between this method and three drag characterization methods for arbitrarily rough surfaces on flat plates which have been employed for towing tank experiments (Demirel, 2015).

The smooth data taken from Schultz and Flack (2013) was also shown as a reference line to demonstrate how closely the acrylic reference panel matched the smooth-wall fully developed channel flow observed in the facility at the United States Naval Academy using a TSI FSA3500 two-component LDV (Schultz and Flack, 2013).

Up until this point, the discussion has been on the skin friction data of each coated panel set in the FTFC. What is needed is the effect on performance these coated surfaces have when applied to the hull of a ship. The previously determined skin friction coefficients are not directly indicative of the drag and powering penalties that would be experienced by a ship (Schultz et al., 2015). This is where the concept of the roughness function is most useful, as it allows this data to be related to the flow at ship-scale. Typically, the roughness function represents a downward shift in the mean velocity profile (positive  $\Delta U^+$  values) as a result of increased surface roughness compared to the smooth wall regime (Schultz et al., 2015). However, this study also showed that the FR02 coating caused an upward shift in the mean velocity profile of the turbulent boundary layer which manifests itself as a decrease in frictional resistance (Demirel, 2015). This upward shift is compared to that of a hydraulically smooth acrylic surface which results in negative  $\Delta U^+$  values. Various other “next generation” marine coating surfaces have shown such behavior in other frictional drag experiments. A study conducted by Atlar et al. (2013) tested advanced poly (dimethyl siloxane) (PDMS) surfaces with randomly

dispersed amphiphilic copolymers that showed a 2.1-4.4% decreases in their coefficients of friction compared to the smooth reference surface (aluminum). (Demirel, 2015) towing tank study also found that a silicone foul release system (FoulXSpel 1) and a hybrid system (F0034) exemplified negative  $\Delta U^+$  values at various flow speeds. Figure 23 helps illustrate the concept of the roughness function for a rougher surface like IB01 and an ultra-smooth surface like FR02.

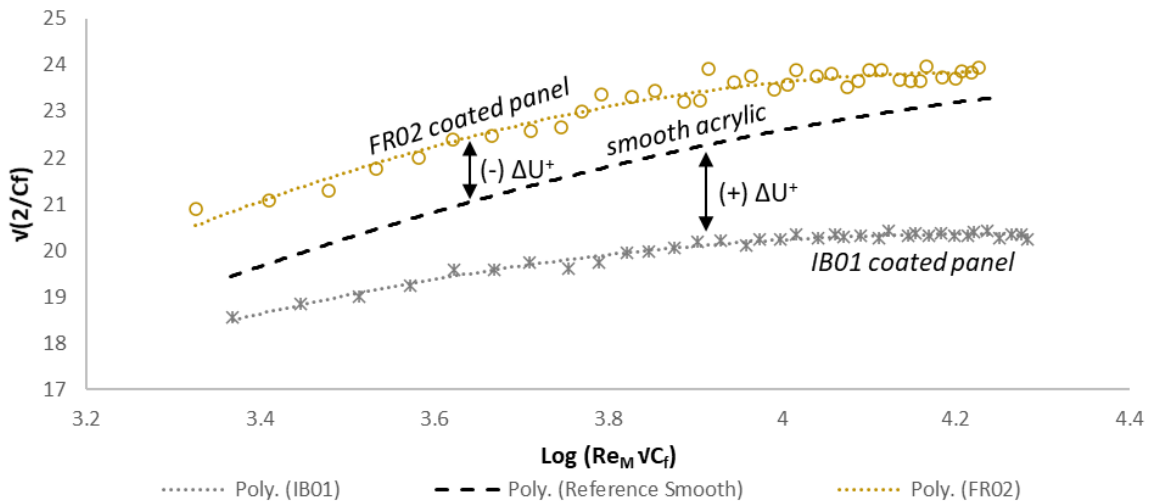


Figure 23: Exaggerated difference between the roughness functions of the smoothest and roughest coated panels.

Using Equations [3.4] and [3.5] combined with the polynomial curves in Figure 23, a table of roughness function values and roughness Reynolds numbers is shown in Table 16.

Table 16:  $\Delta U^+$  and  $k^+$  values for each coated panel set.

Pump Freq	IB01		BL01		FR01		FR02		AF01	
	$\Delta U^+$	$k^+$	$\Delta U^+$	$k^+$	$\Delta U^+$	$k^+$	$\Delta U^+$	$k^+$	$\Delta U^+$	$k^+$
5	0.90	11.16	-1.19	3.54	-0.76	0.22	-1.71	0.62	-61.20	0.89
10	1.59	22.31	-0.58	7.08	-0.26	0.44	-1.46	1.23	-2.87	3.45
15	2.02	33.60	0.10	11.00	0.03	0.66	-1.59	1.83	-0.34	5.64
20	2.25	45.01	0.29	14.67	0.07	0.88	-1.63	2.43	-0.08	7.57
25	2.55	56.33	0.79	18.52	0.38	1.11	-1.24	3.06	0.19	9.50
30	2.71	68.04	0.99	22.44	0.51	1.33	-0.96	3.71	0.46	11.45
35	2.85	79.48	0.98	25.80	0.66	1.55	-0.86	4.33	0.59	13.40
40	3.13	91.48	1.22	29.99	1.06	1.80	-0.69	4.97	0.63	15.36

The AF01, BL01, and FR01 coatings in this study also exemplified efficient drag properties (negative  $\Delta U^+$  values) at lower flow speeds. This can be explained by the low surface roughness achieved by professional application in a controlled environment.

The preferred way of showing the roughness function of each marine coating is to plot it versus the roughness-based Reynold's number ( $k^+$ ) which was defined in Equation [3.4]. This value is based off the roughness length scale ( $k$ ) which is chosen either as a single surface roughness parameter or multiple parameters in combination to characterize a given surface (Yeginbayeva and Atlar, 2018). The roughness function plot ( $\Delta U^+$  vs.  $k^+$ ) allows the investigator to search for a relationship between the surface characteristics and its hydrodynamic performance (Yeginbayeva and Atlar, 2018). The roughness functions using  $R_t$  as the roughness length scale are provided for each test surface in Figure 24.

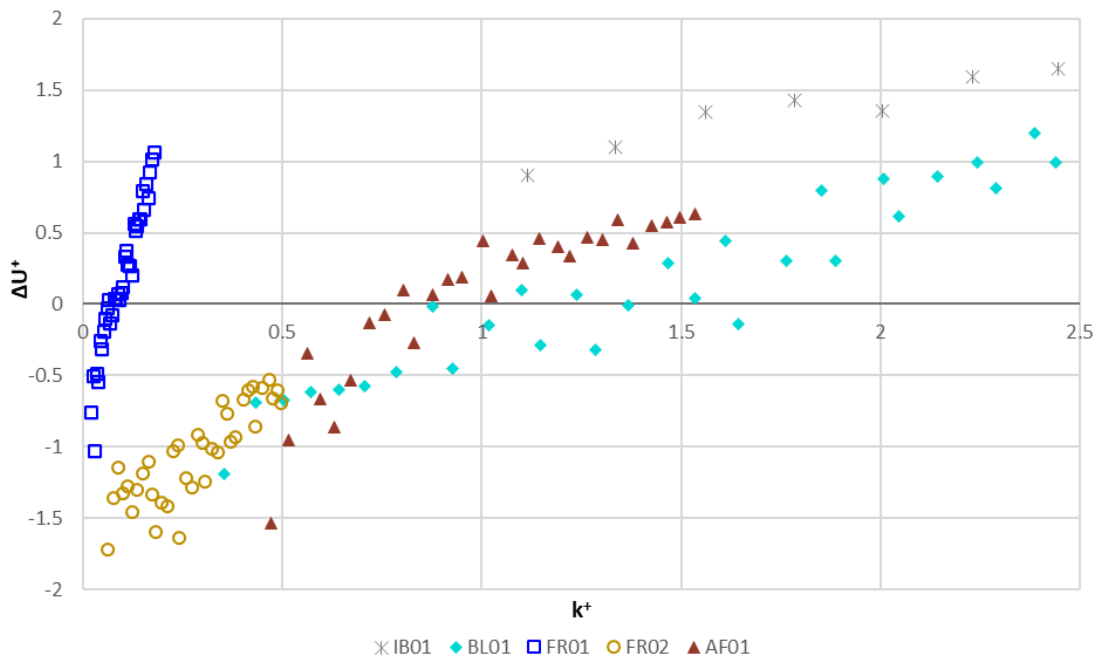


Figure 24: Roughness functions for all coated panel surfaces using  $R_t$  as the roughness length scale.

The increase in  $\Delta U^+$  with roughness functions for the silicone foul release coating (FR01) seem to increase significantly in  $\Delta U^+$  which is a common theme observed in the roughness functions of other silicone-based coatings (Walker et al., 2014). Indeed, the FR02 function remained negative with increasing  $k^+$  but does show a gradual increase in  $\Delta U^+$ , which could indicate it will behave like a hydraulically smooth surface ( $\Delta U^+ = 0$ ) at

even higher roughness Reynold's numbers. The AF01 and BL01 both had increasing trends in the positive  $\Delta U^+$  region which is evidence of their applied surface roughness elements protruding into the turbulent boundary layer. Lastly, the IB01 function was consistently increasing in  $\Delta U^+$  well above the x axis which can be partially attributed to the application by brush, which created a level of waviness in the surface. These results also back up the notion that the largest “hydraulically-relevant” roughness elements determine the point at which roughness effects will occur (Walker et al., 2014).

To model the frictional resistance and powering penalty due to the roughness of the applied marine coatings; the roughness function data of each surface will be used in a flat-plate similarity-law scaling procedure known as the “Granville Method”.

### 3.4.4 Granville Similarity Law Scaling Procedure

An in-house code was developed to conduct Granville's similarity law scaling procedure based on the roughness function data obtained in this study (Section 3.4). The process for this scale up method is explained in detail in but has been slightly adapted for the indirect pipe flow methodology used in this FTFC study (personal communication, Demirel, 2015; Song et al., 2021). This adapted Granville scale-up method is outlined in four steps below:

**Step #1:** Solve the Schoenherr smooth friction line equation to determine a best fit equation for  $C_{F \text{ smooth}}$  vs.  $Re$  as follows:

$$0.242C_f = \text{Log}(Re * C_f) \quad [3.6]$$

**Step #2:** Shift the  $C_{F \text{ smooth}}$  curve by  $\Delta U^+ \kappa * [\ln(10)]^{-1}$  to create a  $C_{F \text{ rough}}$  curve for a given surface by selecting a  $\Delta U^+$ ,  $k^+$  pair.

**Step #3:** Draw a curve of constant  $L_{\text{plate}}^+$  by solving the implicit form of the following equation:

$$Re = \frac{L_{\text{plate}}^+}{\sqrt{\frac{C_f}{2}} * \left(1 - \frac{1}{\kappa} * \sqrt{\frac{C_f}{2}}\right)} \quad [3.7]$$

Where  $L_{plate}^+$  is a non-dimensional length of the plate defined by:

$$L_{plate}^+ = L_{plate} * \frac{k^+}{\nu} \quad [3.8]$$

**Step #4:** Shift the  $L_{plate}^+$  line by a distance of  $\log(L_{ship}/L_{plate})$  in the  $\log(Re)$  direction, creating a new line of  $L_{ship}^+$ . The intersection point between the  $C_{F\ rough}$  curve and the line of  $L_{ship}^+$  gives the  $C_F$  value at ship scale, as shown in Figure 25.

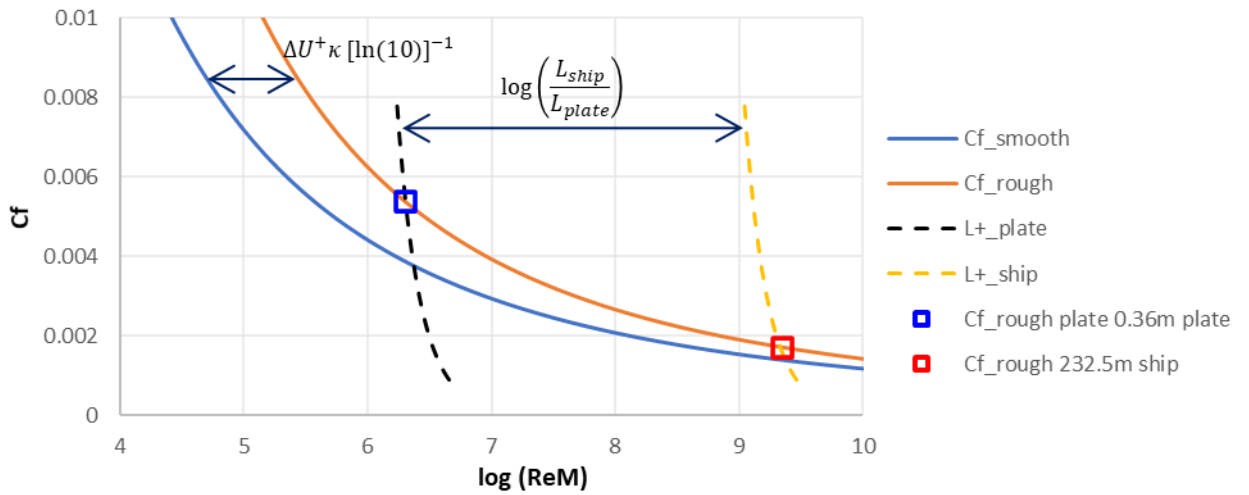


Figure 25: Outline of the Granville similarity law scaling procedure.

The relative difference between the ship's  $C_{F\ rough}$  value and the  $C_{F\ smooth}$  value at the same Reynold's number is the added resistance coefficient ( $\Delta C_F$ ) of the ship's underwater hull due to the roughness of the surface condition. When completing the Granville scale-up procedure, a ship length and speed must also be chosen so that the ship scale Reynolds number is known. The Korea Research Institute for Ships and Ocean Engineering (KRISO) created a model container ship with a bulbous bow and stern called the KRISO Container Ship (KCS). The KCS has been tested in various towing tank studies to obtain its frictional and residuary resistance components which were then validated using CFD (Song et al., 2021b, 2021a, 2020a). This case vessel was chosen for this study so it could be compared to other marine coating types that have had their roughness functions used for similar purposes. The design parameters for the KCS

including the input parameters, length of waterline and design speed, are shown in Table 17.

Table 17: Design parameters for the KRISO Container Ship (KCS), adapted from (Song et al., 2021a).

Design parameter	Value
Length between perpendiculars (m)	230
Length of waterline (m)	232.5
Beam at waterline (m)	32.2
Depth (m)	19.0
Design draft (m)	10.8
Wetted surface area (m <sup>2</sup> )	9,424
Block coefficient	0.6505
Design speed (knot)	24
Froude number	0.26

The full-scale predictions for the KCS hull form were predicted for two different service speeds, its cruising speed of 24 knots and a representative slow-steaming speed of 19 knots. These two speeds were also chosen by Demirel (2015) and Yeginbayeva and Atlar (2018) to investigate the effects of coatings and a range of biofouling conditions on ship resistance. There are a few areas for direct comparison between this study and that of (Yeginbayeva and Atlar, 2018), as two of the same silicone foul release and controlled depletion polymer coatings were tested and scale-up accordingly. The Granville procedure results are presented in terms of added frictional resistance ( $\Delta C_F$ ), followed by the percent increase in frictional drag ( $\Delta C_F$ ) and effective power increase ( $\% \Delta P_E$ ) for the KCS at speeds of 19 and 24 knots, shown in Table 18.

Table 18: Granville scale-up results using the previously determined roughness functions compared to those found in literature.

Test Surface	Speed (knots)	$\Delta C_F$	$\% \Delta C_F$	$\% \Delta P_E$
FR01	19	0.000022	1.6%	1.2%
	24	0.000045	3.3%	2.2%
FR02	19	-0.000065	-4.6%	-3.5%
	24	-0.000049	-3.6%	-2.4%
IB01	19	0.000227	16.1%	12.2%
	24	0.000240	17.5%	11.6%
BL01	19	0.000044	3.1%	2.4%

	24	0.000070	5.1%	3.4%
<b>AF01</b>	19	0.000012	0.8%	0.6%
	24	0.000029	2.1%	1.4%
<b>Typical applied AF (Demirel, 2015)</b>	19	0.000088	6.3%	4.7%
	24	0.000121	9.0%	5.8%
<b>Avg FR as applied (Yeginbayeva &amp; Atlar, 2018)</b>	19	0.000023	1.6%	1.3%
	24	0.000037	2.6%	1.8%
<b>Avg LPP as applied (Yeginbayeva &amp; Atlar, 2018)</b>	19	0.000066	4.5%	3.5%
	24	0.000081	5.7%	3.9%
<b>Avg CDP as applied (Yeginbayeva &amp; Atlar, 2018)</b>	19	0.000102	7.0%	5.5%
	24	0.000126	8.8%	6.1%

The results from the Granville method are somewhat in agreement with the findings from other studies for similar coating types, which demonstrates validity in the current results despite differences in surface preparation, coating application methods and surface roughness equipment. The “as applied” coatings in Yeginbayeva and Atlar (2018) were Intersleek 1100SR (FR), Intercept 8000 (LPP), and Interspeed 6400 (CDP) which are all products of International Paint Ltd. (Yeginbayeva and Atlar, 2018). These marine coatings were applied in their full schemes by air spray by professional applicators in a controlled environment (Yeginbayeva and Atlar, 2018). Comparing the results for the same coating in two different turbulent flow channel experiments (FR01 & FR as applied), we see that the predicted change in frictional resistance and effective power are effectively the same at 19 knots (1.6% increase in  $C_F$ ) and slightly different at 24 knots (3.3% vs 2.6% increase in  $C_F$ ). The observed difference at high speed could be due to the change in application method for the topcoat (roller vs. spray). Another comparison can be made between the two CDP coatings, the AF01 showed a smaller increase in frictional resistance than the as applied CDP at both speeds. The CDP data might be more representative of a typical anti-fouling coating as it lies closer in value to the “Typical AF” coating reported by Demirel (2015). It should be noted that the CDP coating does not show strange drag behavior in the lower flow speed range like the AF01 panel showed in this study.



In a recent conference paper by Zhang et al. (2021), the effect of four types of anti-fouling coatings on ship resistance were modelled and simulated using a Computational Fluid Dynamics (CFD) model software called NUMECA Fine<sup>TM</sup>/Marine. The University of Strathclyde’s turbulent flow channel was also utilized to determine the roughness function of each coating in the applied condition. The modelled coatings included two biocidal self-polishing coatings (SPC-1 and SPC-2), a foul release coating (FRC) and a hard coating (HC). The model was run using the roughness function data for each coating on a Korean Very Large Crude Carrier (KVLCC2) which has an overall length of 326m and a design speed of 15.5 knots (7.97 m/s). For sake of comparison, the Granville similarity law scaling was also conducted for FR01, FR02 and AF01 using data obtained from Song et al. (2020b) for the  $C_{T, smooth}$  and  $C_{F, smooth}$  values of the KVLCC2. The compiled results are shown in Table 19.

Table 19: Granville scale-up results for the KVLCC2 compared to CFD simulated results (Zhang et al., 2021).

Test Surface	Speed (knots)	$\Delta C_F$	$\% \Delta C_F$	$\% \Delta P_E$
<b>FR01</b>	15.5	0.000007	0.5%	0.4%
<b>FR02</b>	15.5	-0.000075	-5.1%	-4.1%
<b>AF01</b>	15.5	0.000000	0.0%	0.0%
<b>SPC-1*</b>	15.5	-0.000034	-2.3%	-1.9%
<b>SPC-2*</b>	15.5	0.000063	4.3%	3.5%
<b>FRC*</b>	15.5	-0.000031	-2.1%	-1.7%
<b>HC*</b>	15.5	0.000139	9.4%	7.7%

\*Data was obtained from (Zhang et al., 2021).

When comparing the results for the KLVCC2 case vessel compared to the values in Table 18 for the KCS, the relative change in added frictional resistance is less for the KLVCC2. This is due to the lower design speed of the KVLCC2, where most of the marine coatings tested are still behaving like a hydraulically smooth surface. It has been shown that water friction can account for 85% of a hull’s total resistance at low speed (Froude numbers < 0.12) (USNA, 2002). It was also noted that the frictional resistance makes up a larger fraction of the total resistance for the KVLCC2 as it has a lower Froude number (0.142) versus that of the KCS (0.26). Therefore, for each percent

increase in frictional resistance due to coating roughness, there is a greater increase in the effective power required to propel this case vessel compared to the KCS.

From Table 19 we can see that the SPC-1 coating had a relative frictional resistance reduction of 2.3% over the AF01 panel and the FRC coating had a relative frictional resistance reduction of 2.6% over the FR01 panel. These coatings were not expected to have identical performances although they are the same fundamental product types, they come from different coating manufacturers and were applied under different circumstances. Interestingly the FR02 coated panel had the best performance with a relative frictional resistance reduction of 2.8% and 3.0% compared to the SPC-1 and FRC coatings respectively.

The surface roughness, method of application and other surface characteristics including coating type can influence the magnitude of the frictional resistance reduction for the KCS from -3.6% – 17.8% and -5.1% – 9.4% for the KVLCC2 (at cruising speeds of 24 knots and 15.5 knots respectively). This change in frictional resistance was then translated into a change in the total hull resistance or effective power of each vessel based on their design parameters. The KCS vessel could undergo a -2.4% – 11.6% change in effective power while the KVLCC2 vessel could undergo a -4.1% – 7.7% change in effective power compared to that of a hydraulically smooth surface.

Demirel (2015) developed an in-house code that produced added resistance diagrams for a range of representative coating and biofouling conditions, namely (as applied AF coating, deteriorated coating or light slime, heavy slime, small calcareous fouling or weed, medium calcareous fouling and heavy calcareous fouling). These diagrams were meant to be used to estimate the resulting fuel penalties of a ship with a particular homogeneous hull condition which could then be used as a tool for life cycle cost estimation (Demirel, 2015). This concept was replicated for the coatings in this study as the goal is to use these results to model the as applied coating condition for the “in-service” period stage of a marine coating’s life cycle. The resulting added resistance diagram for the coating of study (FR02) is provided in Figure 26 while the diagrams for the other coatings are provided in Appendix B.

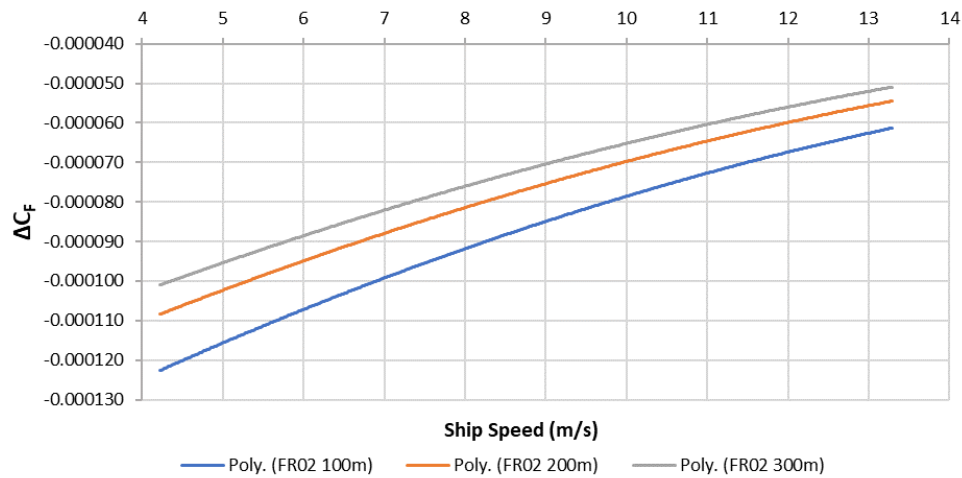


Figure 26: Added resistance diagram for FR02 for 100m, 200m and 300m ship lengths.

### 3.5 Conclusions and Recommendations for Future Work

Among the six marine coatings that were tested in the FTFC, the FR02 coating (XGIT-Fuel), displayed the best hydrodynamic performance across the entire Reynold’s number range. This coating also displayed lower frictional resistance than the smooth acrylic reference panel (7.8% decrease). The frictional resistance results for the FTFC were used to determine roughness functions for each coated surface and subsequently scaled up to ship length using the Granville similarity law scaling procedure. The results from the Granville and CFD simulations indicate that it is possible to achieve an effective power reduction for a vessel that is freshly out of drydock with a newly applied marine coating. The marine coatings tested in the FTFC were used to model the “as-applied” condition for a KRISO containership. Depending on the skin friction drag of each coating the vessel could undergo a change in effective power of -2.4% – 11.6% at cruising speed compared to its hydraulically smooth hull condition.

The limitations of this study include the use of smaller cut-off lengths for surface roughness data collection due to the lack of necessary equipment. This restricted the

ability to compare the measured surface roughness of coating systems in other studies which used larger cut-off lengths of 25 and 50mm.

Another limitation of this study was the use of various application methods across marine coating types as previously discussed. This chapter shows how the Granville similarity law is a useful tool for LCA calculations. There is a large opportunity for growth in this area of research, as this study represents a small fraction of the number of coating products and surface roughness conditions found in industry. Through a research collaboration with the University of Strathclyde, it was determined that the coatings should undergo further testing to understand their hydrodynamic performance under the effects of biofilm growth. The developed roughness functions for each coating can also be inputted into the wall function of a CFD software such as NUMECA Fine<sup>TM</sup>/Marine and compare the results to those obtained from the Granville scale up procedure.

Further investigation should be conducted on predicting the performance of these marine coatings once they've been exposed to dynamically grown biofilms. This will give a better indication to shipowners as to what powering penalty they should expect from these coatings after 2-3 years in active service. Applying a mimicked hull roughness to the panels prior to coating application could also serve as a better method to predicting the frictional resistance behavior of the as-applied condition to an existing rough ship hull.

We can also look at the result of an increase in max speed of  $2.4\% \pm 0.6\%$  from Chapter 2 which compared a Cape Islander vessel coated with clean gelcoat to XGIT-Fuel. We can then perform a Granville scale-up procedure on this fishing vessel for both coating systems and compare the results accordingly. The difference in frictional resistance from the gelcoat (BL01) to XGIT-Fuel was found to be 3.9% (0.000090), translates to a 1.6% decrease in effective power at a cruising speed of 8 knots (assuming frictional resistance makes up 40% of the total resistance). This is in the relative range of what would be expected since the 2.4% max speed increase could indicate an effective power reduction of 5-9% between each coated hull in their tested condition.

The findings from this chapter will be used in the following comparative LCA case study (Chapter 4) for the as applied coating condition in the “in-service” phase of the life cycle.

## CHAPTER 4 LIFE CYCLE ASSESSMENT OF MARINE COATINGS

### 4.1 Introduction

Global shipping activity is currently responsible for approximately 3% of global GHG emissions ( $\text{CO}_{2\text{eq}}$ ) which translates to 1 billion tons emitted per year (Olmer et al., 2017). The combustion of heavy fuel oil and other bunker fuels widely used in the shipping industry, are responsible for a range of different environmental pressures, affecting air quality, human health, and the ocean environment (Ytreberg et al., 2021). Improving the energy efficiency of ships, thus reducing their fuel consumption and emissions; can benefit both the environment and the shipowner/operator from a cost perspective. Marine coatings are utilized by the marine industry as a means of preventing biofouling which in worst cases can increase shipping emissions by greater than 100% due to added frictional resistance of the ship (Swain et al., 2007).

Copper ablative anti-fouling (AF) coatings make up 96% of the coatings applied to naval vessels (Swain et al., 2022) and greater than 90% of the coatings on commercial vessels (Oliveira and Granhag, 2020). This coating type offers a somewhat effective solution to preventing biofouling while causing another environmental problem with the anthropogenic emission of copper as a biocide. In a study conducted by Ytreberg et al. (2021) in the Baltic Sea region, copper discharge from anti-fouling (along with other booster biocides) were found to represent roughly 94% of the damage costs (545 million $\text{€}_{2010}$ ) of marine ecotoxicity due to shipping activity. To combat this issue, marine coating manufacturers have developed new coating technologies that do not rely on biocides for their anti-fouling mechanism. These coating are known as “fouling release” and rely on the sheer force of water flowing over the ship’s hull paired with reduced fouling adhesion to prevent the negative impacts of biofouling (Lejars et al., 2012). These fouling release coatings are typically based on silicone or more specifically poly(dimethylsiloxane) which can provide a smoother coating finish with amphiphilic surface properties (Lejars et al., 2012).

As discussed in Chapter 3, both copper-based anti-fouling and silicone fouling release coatings have had extensive studies on their as-applied drag performance, anti-fouling performance, and cleanability (Hearin et al., 2015; Oliveira and Granhag, 2020; Swain et al., 2022, 2007; Tribou and Swain, 2015; Walker et al., 2014, etc). GIT wants to understand the environmental performance of their new coating XGIT-Fuel when compared to existing coating technologies. Since GIT is in a unique position to update their formulations before they reach the commercial market, I suggested the investigation of their product's lifecycle to determine its environmental impact and quantify it by using the standard principles and reporting framework of life cycle assessment (LCA). LCA was chosen as a useful tool for combining the available historical data with the research results from Chapters 2 and 3 and using it to compare the most widely used coating systems to the new XGIT-Fuel coating. The cost of each marine coating system was not seen as a viable factor for comparison as ship owners were found to be more interested in the performance benefits and durability rather than the up-front cost for coating application in drydock (personal communication with GIT).

The first documented application of LCA for the purpose of marine coating comparison was a case study of a fouling release retrofit application on a ferry-type ship performed by Blanco-Davis et al. (2014). The goal of the study was to assess the retrofit's potential environmental impacts by employing the LCA methodology (Blanco-Davis et al., 2014). A secondary goal was to demonstrate how LCA could be used as a decision-making tool for both shipowners and shipyards to improve the efficiency and environmental impact of their operations (Blanco-Davis et al., 2014). The study compared the benchmark scenario where the ferry hull was coated with a conventional anti-fouling coating to the alternative scenario where it was retrofitted at the midpoint of its 25-year lifetime (Blanco-Davis et al., 2014). As a result of the midpoint retrofit to the FRC coating, a 7.65% drop in CO<sub>2</sub> emissions was observed because of reduced engine load. It was noted that the reported environmental score is not directly comparable to other vessel types such as a containership due to variations in vessel activity and hull form (Blanco-Davis et al., 2014).

In a recent paper by Uzun et al. (2019) a time-dependent biofouling growth model was suggested for predicting the effects of biofouling on a ship's frictional resistance and powering requirement. The biofouling model accounted for seawater surface temperature, water salinity and various other input parameters which can affect the rate of biofouling accumulation (Uzun et al., 2019a). This model was then used to simulate the added resistance of a crude oil carrier over three years of operation and validated against the vessel's actual operational power data. Once validated, an LCA was performed using the time-dependent growth model to account for the increase in CO<sub>2eq</sub> emissions during the operation phase (Uzun et al., 2019b).

A recent article by Augusto Paz-Villarraga and Fillmann, (2021) found that cuprous oxide was the main biocidal component used in over 76% of anti-fouling coatings that were included in the study. It was found in over 700 different coating formulations, followed by copper pyrithione, zinc pyrithione, and zineb as the next most common toxic substances (traditionally used simultaneously with cuprous oxide) (Augusto Paz-Villarraga and Fillmann, 2021). This finding verifies the importance of conducting a life cycle assessment on a copper-based anti-fouling coating. Studies by Rossini et al. (2019) and Ayer et al. (2016) have both conducted LCAs on copper-based marine coatings and will be useful for comparison to the findings herein.

After a review of the literature, it became evident there is a lack of life cycle assessment (LCA) studies on marine coatings, particularly for their use in the commercial shipping industry. This chapter aims to address the knowledge gap in this research area by providing a framework and methodology for LCA of various marine coating types when applied to a ship's hull. The methodology of this LCA will follow the principles and framework outlined in ISO 14040 (2006) while incorporating the LCA requirements and guidelines provided in ISO 14044 (2006). The goal of this chapter is to present the findings from a comparative LCA for three marine coating systems applied to the hull of a newly built (newbuild) 3600 TEU containership. The aim is for the LCA methodology presented herein,



## 4.2 LCA Methodology

### 4.2.1 Goal and scope definition

This LCA aims to compare the environmental impact of a novel marine coating (XGIT-Fuel) to that of two commercial marine coating types, namely a biocide-based anti-fouling coating and a fluoropolymer fouling release coating, by using LCA methodology. The scope of this LCA contains three phases for comparing the marine coating systems: i) raw material production, ii) application at newbuild, and iii) in-service operation of the case vessel (treating the coating and case vessel as one system).

The end goal of this comparative LCA is to quantify the environmental impacts of the three coating systems in terms of global warming impact (GWP), acidification of air (AP), photochemical ozone creation (POCP) and marine aquatic ecotoxicity potential (MAETP). These four environmental indicators are reported using the “CML-IA baseline” life cycle impact assessment method. This impact assessment method was chosen since it contains the relevant impact categories required and provides an opportunity for direct comparison with an LCA study on marine coatings by Rossini et al. (2019). The environmental impact potentials of each modeled coating system are described in detail below:

- Global warming potential (GWP100) quantifies the negative effects due to the release of greenhouse gases over a period of 100 years, using a unit of kgCO<sub>2</sub> equivalents (kgCO<sub>2eq</sub>).
- Acidification potential (AP) of land and water with a unit of kg SO<sub>2</sub> equivalents (kgSO<sub>2eq</sub>). It evaluates the effects of released acidifying substances over eternity.
- Photochemical oxidation (POCP) for air emissions with a unit of kg C<sub>2</sub>H<sub>4</sub> equivalents. Photochemical oxidation involves the creation of ground-level ozone through the reaction of nitrogen oxides (NO<sub>x</sub>) and volatile organic compounds (VOCs) in sunlight.

- Marine aquatic ecotoxicity potential (MAETP), which involves the impacts of toxic substances (biocides) on marine ecosystems with a unit kg dichlorobenzene (1,4 DCB) equivalents.

#### **4.2.2 LCA boundary and model assumptions**

The comparative LCA will be conducted using the 232.5m long KRISO container ship model detailed in Chapter 3. To model the life cycle of a coating system applied to this vessel over a complete drydock cycle, several modelling assumptions must be made and explicitly stated to be in accordance with (ISO 14040, 2006; ISO 14044, 2006).

##### LCA Modelling Assumptions:

- Three marine coating systems will be modelled on a case vessel, a novel marine coating XGIT-Fuel, a biocide-based anti-fouling coating Interspeed 640 (BRA640) and a fluoropolynated silicone foul release coating Intersleek 1100SR (INT1100SR).
- The loss of paint during coating application is assumed to be 30% for each layer applied at newbuild. This is used as a standard loss for industrial applicators due to environmental conditions and overspray on complex structures (International Paint Ltd., 2011).
- The case vessel will be the full-scale KRISO containership hull design (as modelled in Chapter 3). Its in-service operation will be represented by a mid-sized (3600 TEU) container ship due to their identical carrying capacities, as per Shin et al. (2019). According to the global fleet average, this sized-vessel spends approximately 75% of its time at sea (25% in port) and consumes 12,700 metric tons (MT) of fuel per year in its main engine (International Maritime Organization, 2021).

- Heavy fuel oil (HFO) was selected as the fuel type as it made up 79% of the global fleet's total fuel consumption by energy content in 2018 (International Maritime Organization, 2021).
- A 5-year operation was selected as it reflects the typical length of one complete drydock cycle for this vessel class.
- The KRISO containership design speed is 24 knots, and its slow steaming speed is 19 knots. The slow steaming speed was considered to be the “at sea” speed as it was the most realistic scenario when compared to the global average speed for this vessel class (14.7 knots) (International Maritime Organization, 2021).
- Using vessel tracking software, the recent routing activity of a small fleet of 3600 TEU containerships was analyzed to determine an average operational profile (VesselFinder, 2022). The dataset included the number of port calls per year, distance travelled, average/max speed and time spent in port. From the data collected, it was deduced that the average time spent idle (consecutively) was one day in port for every three days at sea. In reality, the time spent in between ports will vary depending on factors such as port location, shipping traffic, weather, etc.
- For vessel idle periods, a time-dependent biofouling model was used to reflect the change in the hull fouling rating, frictional resistance, and thus effective power penalty of the vessel over time. The effective power requirement was assumed to be directly proportional to the vessel's heavy fuel oil consumption, as per (Demirel et al., 2017; Uzun et al., 2019a)

The LCA phases with their respective input and output flows as well as the system boundary are shown in Figure 27.

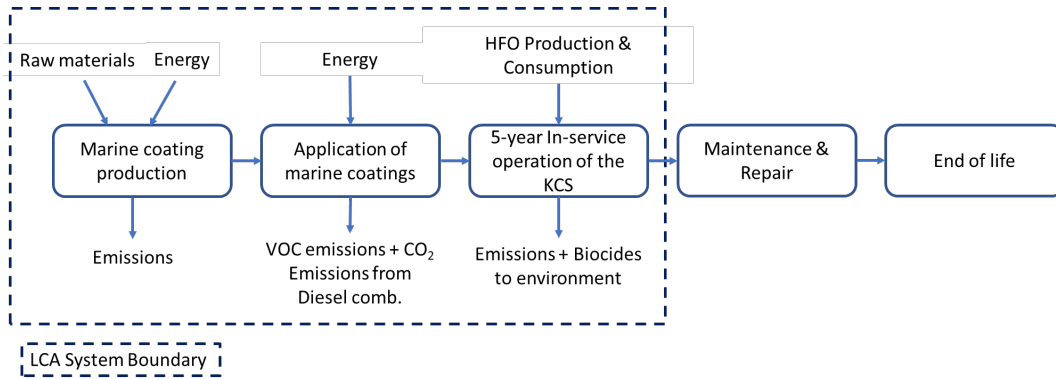


Figure 27: LCA phases and system boundary included for comparison

The system boundary was drawn around the first three phases of the life cycle, marine coating production, application, and in-service operation of the containership. The expected lifetime of the modelled commercial coating systems ranges from 5-10 years, depending on vessel operations, anti-fouling mechanism and environmental conditions (AkzoNobel Sustainability, 2017). An extended lifetime past 5 years typically relies on touch-ups and repairs conducted in drydocking intervals (AkzoNobel Sustainability, 2017). Since there is no existing data 5-year data for XGIT-Fuel, the “maintenance and repair” phase is excluded from this LCA. The end-of-life phase was also excluded since the emissions from transportation of the coatings to a landfill facility and leftover paint incineration with heat recovery would be comparable between all coating systems, thus not critical to include in this comparison.

## 4.3 Life Cycle Inventory

### 4.3.1 Marine Coating Production

The production of each marine coating type was modelled with the openLCA 1.10.3 software, using the Ecoinvent 3.5 database (Ecoinvent Centre, 2018). This database was utilized to model the production of the raw material components of each coating. These components are typically sourced from the individual paint companies, but this information was found to be highly confidential for intellectual property reasons. Therefore, this phase of the LCA was limited in scope to comparing the raw materials of each product as reported in their respective material safety data sheets. The main Ecoinvent flow category used was the “Manufacture of basic chemicals” (ISIC#2011)

which did not contain the data for some hazardous raw materials, further limiting the comparison in this phase. The average of the range was taken for each hazardous raw material as listed on the material safety data sheets provided by GIT upon request and obtained from International Paint’s website (International Paint Ltd., n.d.). The corresponding raw material tables for each coating product are provided in Appendix C. An example table that was generated from the openLCA data for the BRA640 coating is provided in Table 20.

Table 20: OpenLCA inventory for BRA640 hazardous raw material components.

<b>Raw Material Component</b>	<b>Raw Material (kg)</b>	<b>Avg. Weight Fraction (%)</b>
Copper oxide	4018.5	41.97%
zinc oxide	1675.6	17.50%
xylene	957.5	12.50%
1-butanol	239.4	2.50%
ethyl benzene	239.4	2.50%
<b>Total</b>	<b>7,369.7</b>	<b>77.0%</b>

The life cycle inventory process was also followed for INT1100SR and XGIT-Fuel according to their hazardous raw material components. These life cycle inventories do not represent the true value of the environmental impact from raw material production. The purpose of this inventory was to purely evaluate the relative magnitude of the impact and compare it to the other two phases included in the LCA. An example of the life cycle inventory for the hazardous raw materials in BRA640 is shown in Figure 28 below.

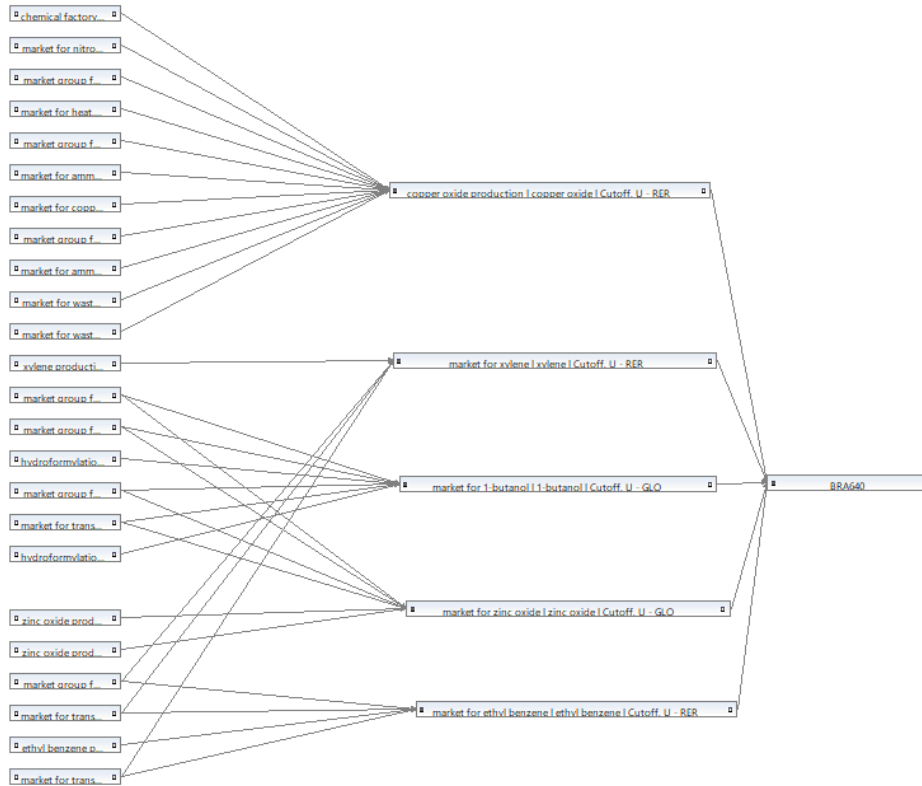


Figure 28: OpenLCA Unit Process Flow Diagram for production of BRA640.

Each hazardous raw material was allocated by weight in terms of its contribution to the production of 1kg of coating and the process was scaled up to meet the mass requirements accordingly. In terms of the energy requirement to produce each a marine coating, a value of 7.5kWh/L of anti-fouling coating determined from Rossini et al. (2019) was used as an input for all three systems.

#### 4.3.2 Application of Marine Coatings

The coating application of each system was accounted for using the hull coating schemes provided in Figure 29. The recommended dry film thickness (DFT) for each layer of applied coating was determined according to the manufacturer’s technical data sheets. XGIT-Fuel and INT1100SR both recommend one topcoat of DFT of 200µm while BRA640 recommends two (or three) coats each at 100µm respectively. INT1100SR and BRA640 both require a “tie coating” to allow for proper adhesion to the underlying anticorrosive primer layer (Intershield 300 HS). These tie coatings include

“Intersleek 737” which is a silicone elastomer and “Intergard 263” which is an epoxy tie coating. Since all three schemes require two primer coats of Intershield 300HS, this product was not included in the life cycle inventory. Note the tie coatings (INT737 & ING263) were not included as inputs for the production phase due to lack of available input data in the Ecoinvent database.

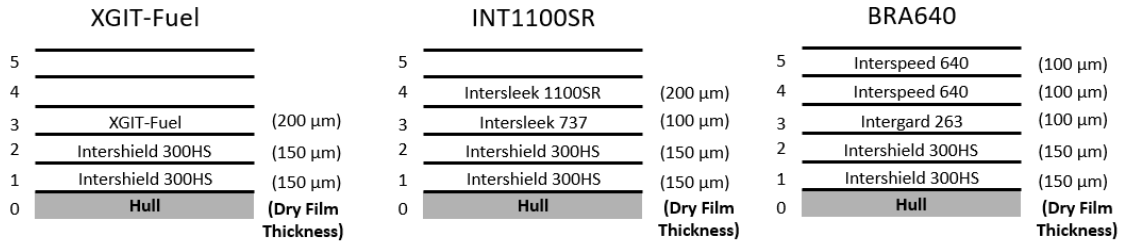


Figure 29: Hull coating schemes with the number of layers and required dry film thickness on the newbuild case vessel.

The underwater hull surface area of the case vessel was assumed to match the size of the KRISO containership hull design, 9,424m<sup>2</sup> (Song et al., 2021a). The product specification details for each coating layer were used to calculate the practical coverage values and thus the amount of paint required to cover the underwater hull area of the case vessel in liters and in kilograms (using density). An example of the practical coverage calculation is shown in Equation [4.1]:

$$Practical\ Coverage\ (m^2/L) = \frac{Volume\ Solids\ (\%)}{DFT\ (\mu m)} * 10 * (100 - \%Loss) \quad [4.1]$$

The amount of volatile organic compounds (VOCs) were also a notable emission in this phase as these compounds are emitted to the environment during the application process (AkzoNobel Sustainability, 2017). The amount of VOC content is related to the volume solids of the coating through the evaporation of solvents (Kim et al., 2014). The emission of these compounds to air is known to have impacts on human health and photochemical ozone creation and are thus strictly regulated in marine paint compositions (400-700 g/L depending on the legislation body and coating type) (UK Statutory Instruments, 2012; US EPA, 2017). Some compounds such as methyl formate, methyl acetate and acetone have been exempted from the list of restricted VOCs as they were

found to have a negligible impact on the environment (US EPA, 2018). Table 21 provides a summary of the coverage, quantity, and VOC calculations for each product (including the respective tie coating layers). The data for XGIT-Fuel was provided by GIT upon request and data for the other products was taken from the International Paint website which provides technical data sheets for each product (International Paint Ltd., n.d.).

Table 21: Product specifications including dry film thickness, VOC content, coverages, and amounts to coat the hull of the newbuild case vessel.

Coating Specification	XGIT-Fuel	INT1100SR	BRA640 (per coat)	INT737	ING263
Volume Solids (%)	84.0	72.0	62.0	57.0	57.0
Dry Film Thickness (µm)	200	200	100	100	100
Theoretical Coverage (m <sup>2</sup> /L)	4.13	3.54	6.10	5.61	5.61
Practical Coverage (m <sup>2</sup> /L)	2.89	2.48	4.27	3.93	3.93
Amount for KCS (L)	3256.7	3799.5	2206.2	2399.7	2399.7
Weight for KCS (kg)	4168.6	4087.6	4787.4	3388.4	2920.4
VOC content (g/L)	24.0	240.0	385.0	377.0	445.0
VOC for KCS (kg)	78.2	911.9	849.4	904.7	1067.9

When a vessel is newly built, the coatings are usually applied to building blocks at various stages throughout the construction process (AkzoNobel Sustainability, 2017). Due to the lack of available drydock operational data, an assumption from AkzoNobel Sustainability (2017) was used to represent the resulting energy input for spray application. This LCA study assumed a work force of four applicators each equipped with an airless spray gun and cherry picker for coating application (AkzoNobel Sustainability, 2017). The spray pump compressor (pump ratio 68:1, input pressure of 80psi) and cherry picker consumed diesel fuel at a combined total of 16L/hour (AkzoNobel Sustainability, 2017). The coating process with this work force and equipment was assumed to cover 150m<sup>2</sup>/man/hour through personal communication with Irving Shipbuilding (professional paint applicators).

#### 4.3.3 In-Service Operation of the KRISO containership

The time-dependent biofouling model was built using the large static panel data from the long-term Port Canaveral, Florida study on BRA640 and INT1100SR (Swain et



al., 2022). Results from a short-term static anti-fouling test campaign on XGIT-Fuel were also provided by the coating manufacturer. This test campaign was performed by the Centre for Corrosion and Biofouling Control over a period of 11 weeks (Aug & Sept 2021) in Port Canaveral, Florida. From the obtained preliminary results, XGIT-Fuel demonstrated a similar static anti-fouling performance to INT1100SR in terms of both surface coverage and cleanability (once removed). Due to the lack of long-term static anti-fouling performance, it was assumed for the purpose of this LCA, to behave identically to INT1100SR in terms of static fouling development during the modelled idle days in Port Canaveral.

The selection of Port Canaveral, Florida to represent the biofouling growth conditions during idle periods was viewed as a worst-case scenario assumption for this comparison. The explanation for this assumption is two-fold:

1) This port’s ocean environment is subject to “high fouling pressure” due to the year-round high sea water temperature (~15-30°C) and salinity (~26-36psu) shown in Figure 30.

2) The BRA640 and INT1100SR coated panels were subject to an extended period (33-54 months) of static fouling growth with no intermittent movement other than the natural effects of wind and waves (Swain et al., 2022).

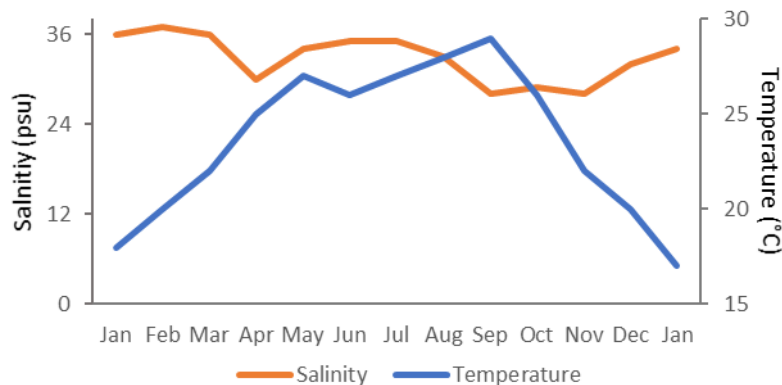


Figure 30: Annual surface water temperature and salinity for Port Canaveral, Florida testing site (adapted from (Swain et al., 2022))

One set of panels were subject to cleaning when a fouling rating (FR) of 40-50 was reached over a percentage of the panel surface, explained in Swain et al. (2022). This cleaning occurred seven times for BRA640 over 54 months and twice for INT1100SR over 33 months (Swain et al., 2022). The other set of panels were “groomed” weekly with nylon bristles and were able to keep the coatings clean apart from tenacious biofilm growth (Swain et al., 2022). Neither test condition was able to best represent the dynamic flow (shear) conditions that would be present on the hull of the KRISO container ship at a speed of 19 knots.

Due to the varying performances of each coating depending on the type of anti-fouling performance test conducted, a sensitivity analysis was performed. This analysis aims to determine the effect of foul release performance of the INT1100SR, and XGIT-Fuel coatings compared to BRA640 which has no foul release capabilities. To perform this analysis, two in-service scenarios were considered, detailed below:

- **In-Service Scenario #1:** This scenario best represents the growth rate that the foul release coatings would experience if they did not provide any foul release mechanism while applied to the ship’s hull. Each coating system was modelled in the “as-applied” condition and was then subject to the fouling growth rates experience by the ungroomed static panels in (Swain et al., 2022). These growth rates were modelled on a per-month basis to be consistent with the reported growth data. This scenario captured both the summer and winter season period of consecutive fouling growth as the total number of idle days experienced by the vessel reached 427 days over the 5-year period.
- **In Service Scenario #2:** This scenario represents best represents the growth rate that the foul release coatings would experience if they were subject to weekly grooming (this was assumed to simulate the concept of intermittent dynamic flow periods). The BRA640 coating was modelled identically to Scenario #1 to be consistent with its coating type. This coating also underwent a hull cleaning when its fouling rating reached FR-40 over 20% of the surface (27.5% increase in

effective power) as per the US Navy criteria (Naval Sea Systems Command, 2006). Once cleaned, it was assumed that the coating returned to its as applied condition which disregards the potential effects of increased coating roughness due to cleaning that was observed on the cleaned BRA640 coating in Swain et al. (2022).

The methodology used to translate the fouling growth rates and surface coverage values into an added frictional resistance and effective power is well documented in Oliveira et al.(2021) and Uzun et al. (2019). However, the frictional resistance and effective powering requirements for the KRISO containership for each fouling rating (FR 0 -100) have already been calculated by Demirel (2015) using the data from Schultz (2007) for the representative biofouling roughness heights. The resulting change in effective power of the KSC due to each fouling condition at 19 knots is provided in Figure 31.

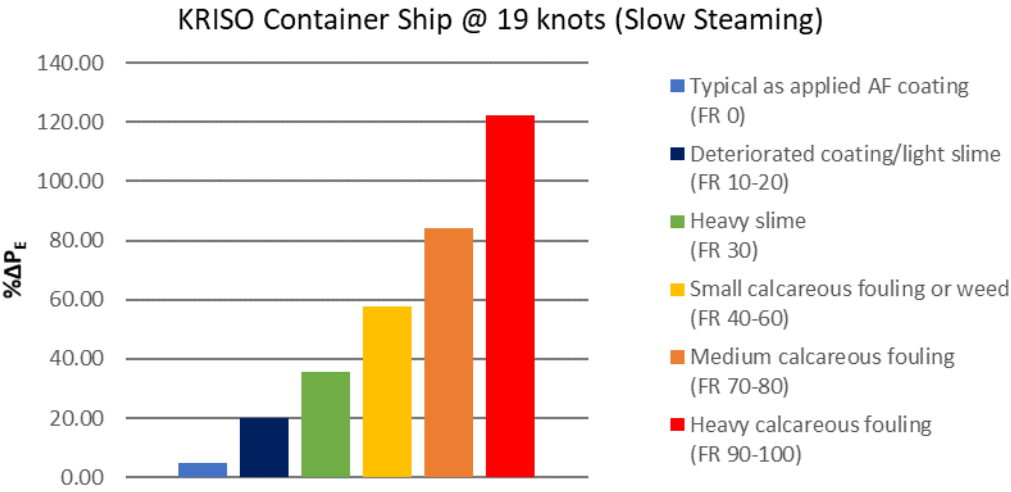


Figure 31: Data adapted from (Demirel, 2015) for the % effective power increase for KRISO container ship at 19knots.

The growth of fouling organisms in Swain et al. (2022) included biofilms, bryozoans, tubeworms, tunicates and barnacles (only on BRA640). Since there were no fouling heights reported in the study it was assumed that the biofilms were FR20 (light slime), and all other forms of growth were FR40-60 (small calcareous fouling or weed). The resulting effective power values for the respective fouling ratings were taken from

Figure 31 and applied to both in-service scenarios (with and without foul release performance) to create Figure 32 and Figure 33, respectively. The case vessel operational data was mapped by using the above-mentioned assumptions for active days and days in-port (3:1 ratio) with effective power requirement reporting on a per month basis. The two predictive scenarios model the complete 5-year drydock cycle, totaling 1398 active days and 427 idle days (modelled consecutively).

The baseline fuel consumption of the case vessel was linearly correlated to the effective power increase of the BRA640 coated hull over time. The BRA640 coating was chosen as the baseline for the fuel consumption model as it was noted in Swain et al. (2022) to have the highest fouling penalty, and copper ablative coatings are the most widely used in the shipping industry (Oliveira and Granhag, 2020). The baseline fuel consumption for both in-service scenarios was determined to be 37.0 MT/day for the BRA640 coating. The resulting effective power increase for each fouled hull condition was calculated in Equation [4.2]:

$$\% \Delta P_E = \sum_{i=1}^n FR_i * SC_i \quad [4.2]$$

Where  $FR_i$  is the drag penalty due to the fouling rating according to Figure 31, and “ $SC_i$ ” is the surface coverage of the fouling rating which was linearly interpolated from Swain et al. (2022).

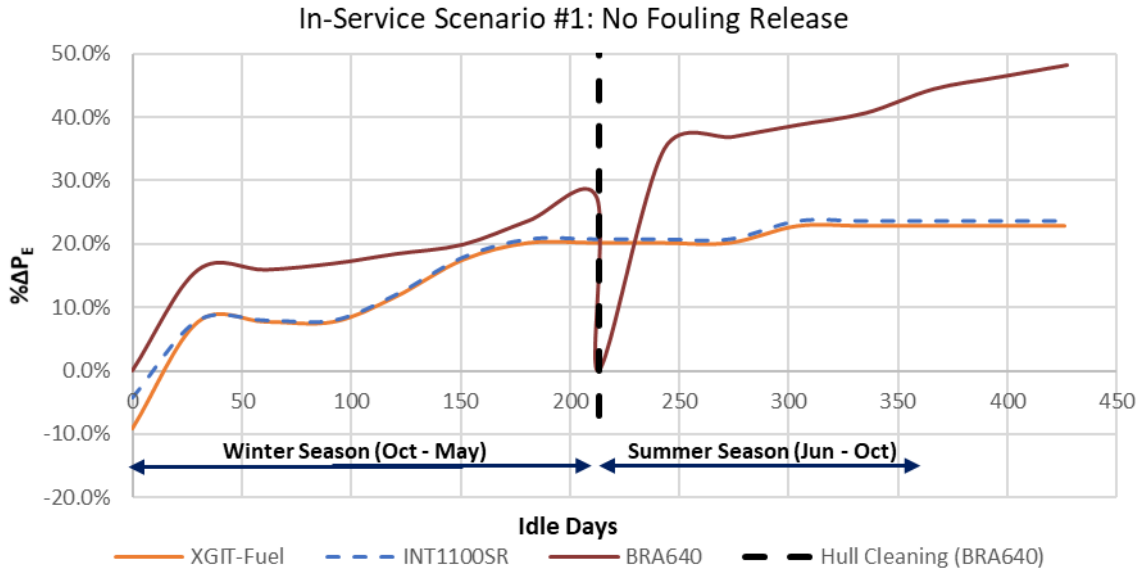


Figure 32: In-service biofouling growth scenario #1 using static panel data with minimal fouling release performance for an active vessel.

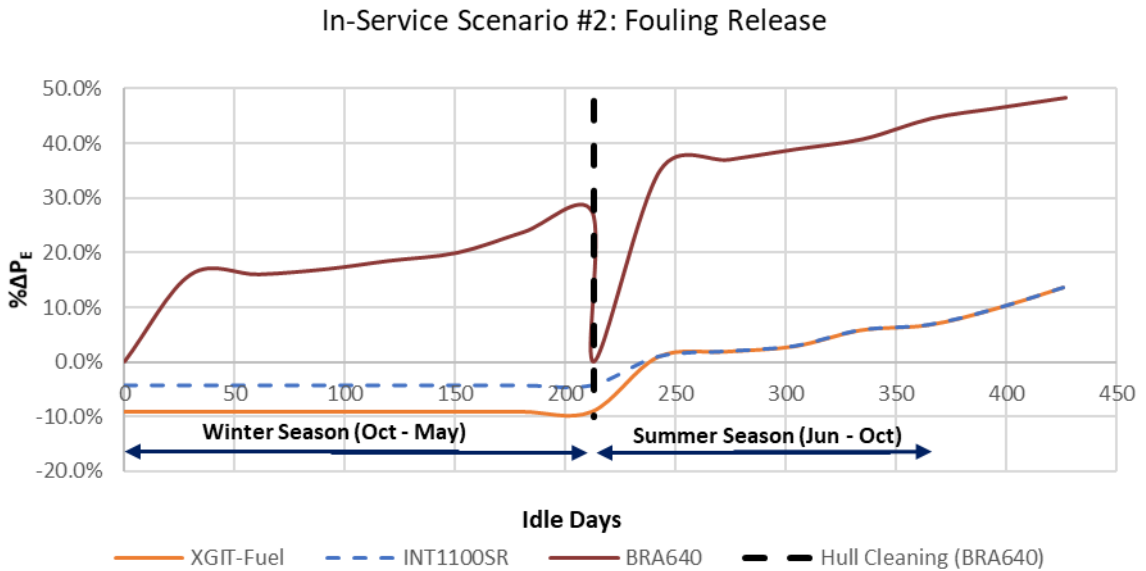


Figure 33: In-service biofouling growth scenario #2 using weekly groomed panel data to represent fouling release performance for an active vessel

Note that in Scenario #1 XGIT-Fuel and INT1100SR only maintain their as-applied condition for 30 consecutive idle days due to high fouling pressure in a static ocean environment. In Scenario #2, both foul release coatings are assumed to maintain their as-applied condition for 213 idle days (translates to 2.3 years active). For validation,

a case study from AkzoNobel contains underwater pictures of a “Very Large Crude Container ship” coated with INT1100SR after 20 months of in-service and the coating appears to remain in the as-applied condition (AkzoNobel, 2017). After the 2.3 year mark, it assumes that the foul release coatings begin to develop a tenacious biofilm just as was observed weekly groomed panels INT100SR panels in (Swain et al., 2022). The resulting fuel consumption during active days was then modelled using Equation [4.3] for each in-service scenario:

$$FC_i = FC_{baseline} * (100 + \% \Delta P_E) * t_{days} \quad [4.3]$$

The BRA640 coating uses copper as a biocide (cuprous oxide is the active ingredient) to deter marine growth (Swain, 1999). For this LCA, the copper emission was considered as a continuous point source discharge from the vessel to the ocean. The minimum release rate for a copper-based anti-fouling coating to prevent fouling growth has been quoted to be 10-20  $\mu\text{g}/\text{cm}^2/\text{day}$ . To determine the average release rate and total mass of copper emitted from the BRA640 coating scheme when applied to the case vessel, a mass balance calculation method (Equation [4.4]) was adopted from ISO 10890 (2010):

$$m_{rel} = \frac{L_a * a * w_a * \rho * DFT}{\% Volume Solids} \quad [4.4]$$

$$m_{rel} = \frac{100 * 0.89 * 41.79 * 2.17 * 203.2}{62.00\%} \approx 26,451 [\mu\text{gCu}/\text{cm}^2]$$

Where “ $m_{rel}$ ” is the estimated total mass of biocide released per unit area of coating film over the 5-year lifetime of the coating; “ $L_a$ ” is the percentage of biocide released from the film; “ $a$ ” is the mass fraction of biocide (copper) in the active ingredient; “ $w_a$ ” is the mass fraction of the active ingredient in the coating; “ $\rho$ ” is the density of the coating as manufactured and “ $DFT$ ” is the dry film thickness of two coats for the lifetime of the coating. The resulting average release rate per day “ $m_{rel\ rate}$ ”, and total mass of copper emitted to the environment over the 5-year period “ $M_{hull}$ ”, can be calculated as follows:

$$m_{rel\ rate} = 26,251 / (365 * 5) \approx 14.5 \mu\text{gCu}/\text{cm}^2/\text{day}$$

$$M_{hull} = \frac{14.5 * 365 * 5 * 9,424\text{m}^2 * 10,000 \frac{\text{cm}^2}{\text{m}^2}}{1 * 10^9 \frac{\mu\text{g}}{\text{kg}}} = 2,492.8\text{kgCu} \pm 42.0\text{kgCu}$$

The uncertainty of  $\pm 4.2\text{kg}$  stems from the uncertainty in the manufacturer’s declaration for the volume solids content of the coating ( $62\% \pm 2\%$ ). Comparing the calculated average releases rate to those found in literature, the results for BRA640 range from 2.2 – 48.6  $\mu\text{gCu}/\text{cm}^2/\text{day}$  depending on the calculation method and number of days averaged (Takahashi, 2009). The actual release rate can vary depending on factors such as immersion time, ship activity and environmental properties (Finnie, 2007; Swain et al., 2022). The total amount of copper released should be taken as the worst-case scenario, as it assumes the copper content from both layers of BRA640 are completely released to the environment after 5-years on the hull of the case vessel.

## 4.4 Life Cycle Impact Assessment

### 4.4.1 Results for Marine Coating Production & Application

Figure 35 and Figure 34 show the results from each impact category for the marine coating production and application phases respectively. For the production phase, the XGIT-Fuel coating was found to have the lowest impact in all environmental categories when compared to the other two coating systems. Each coating production process was assessed in openLCA, and the flow system was comprised of hazardous raw material input flows and electricity as an energy input flow for the mixing process.

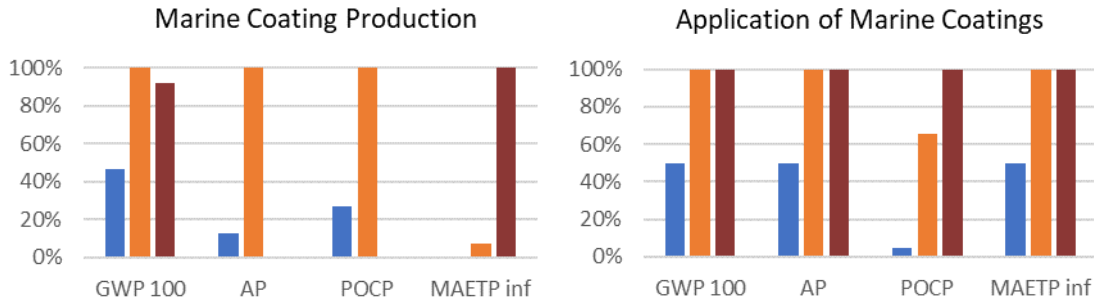


Figure 35: Relative environmental impact categories for marine coating production.

Figure 34: Relative environmental impact categories for application of marine coatings.

The global warming potential (GWP) of INT1100SR was the highest in value followed by BRA640 and XGIT-Fuel respectively. The relatively high GWP value for INT1100SR can be explained by the included production of a functionalized raw material, being poly(dimethylsiloxane). This raw material contributed to 78% of the overall GWP from production through its linked processes such as using silicon and methyl chloride to produce dimethyldichlorosilane. The GWP value for BRA640 was also noticeably high due to the emission intensive process of copper oxide production. The copper ore refining processes were also found to have a large impact on the other impact categories as was noted by Rossini et al. (2019). However, due to a lack in data quality of the Ecoinvent database, the AP and POCP impact categories could not be included for the BRA640 coating (further explained in Section 5). XGIT-Fuel had the lowest GWP value since less coating was required to cover the hull when compared to the other two systems. Furthermore, the included components (methyl acetate, benzyl alcohol and graphite) do not come from emission intensive processes, based on the data obtained from the Ecoinvent database. It should be noted that the manufacturing processes for commercial scale production of these hazardous raw materials can vary depending on location and end-use, as such the Ecoinvent database serves as approximation for these uncertainties.

For sake of comparison to Rossini et al. (2019), the GWP values per m<sup>2</sup> of applied coating were calculated for each coating system and are shown in Table 22. This comparison shows that the modelled GWP estimates for the three coating systems analyzed are in the same order of magnitude as those obtained from other confidential paint manufacturers in Rossini et al. (2019).

Table 22: GWP comparison per m<sup>2</sup> surface area with biocide-based anti-fouling coatings found in literature.

Coating System	GWP (kgCO <sub>2e</sub> /m <sup>2</sup> )
XGIT-Fuel	3.10
Intersleek 1100SR	6.66



Interspeed 640	6.12
Copper Anti-fouling*	2.76
Zinc Anti-fouling*	5.94

\*Data obtained from Rossini et al. (2019) for a copper (I) oxide (cuprous oxide) anti-fouling coating (25-50% by weight) and a zinc oxide anti-fouling coating (25-50% by weight) for comparison.

Another environmental impact category of interest to the shipping industry, more specifically the paint applicators, is the PCOP or VOC emissions from the coatings during spray application. The VOC content for each coating layer was considered for the application of all three systems and the VOC emissions contribution to the POCP was >95% in the application phase. Notably, XGIT-Fuel had the lowest impact value since it uses methyl acetate as a solvent which is a VOC exempt substance (US EPA, 2018). INT1100SR and BRA640 use xylene and ethyl benzene as solvents, which are both listed as VOCs by the US EPA and contribute to greater POCP values. Human health particulate (air) is another impact category that is directly affected by VOC emissions but is not included in this assessment to limit redundancy.

As predicted, the results from both phases were much smaller in magnitude compared to the environmental impact of the in-service phase scenarios. For instance, the combined impact from each environmental category account for less than 1% of the impact associated with the in-service operation of the case vessel.

#### **4.4.2 Results for In-Service Scenarios #1 & #2**

Figure 36 and Figure 37 show the results from the in-service scenarios, with BRA640 leading all impact categories as the baseline for comparison. Indeed, the environmental impacts of the in-service scenarios are directly related to the amount of heavy fuel oil consumed by the 3600 TEU containership over the 5-year period (and the underlying HFO production process). The only exception to the above statement is the MAETP potential for the BRA640 system as it includes the mass of copper discharged from the hull over the 5-year lifecycle (calculated in Section 3.3).

As a result of In-service Scenario #1, the fouling release coatings (XGIT-Fuel and INT1100SR) avoided 7.2% - 6.9% of the GWP, AP, and POCP values emitted by the

BRA640 system and avoided 10.1% - 10.7% of the MAETP value respectively. For In-service Scenario #2, XGIT-Fuel and INT1100SR avoided 21.9% - 19.9% of the GWP, AP and POCP values emitted by the BRA640 system and avoided 24.6% - 22.6% of the MAETP value respectively. It should be noted that these in-service scenarios are theoretical and do not represent the actuality of the operation of this containership vessel. Actual fuel consumption data (noon-data) from a container vessel paired with data from on-board instrumentation such as an automatic identification (AIS) system is recommended to validate the fouling growth rates and associated fuel penalty models assumed in both in-service scenarios. The uncertainties in the LCA will be further discussed and assessed in Section 5 (Interpretation phase).

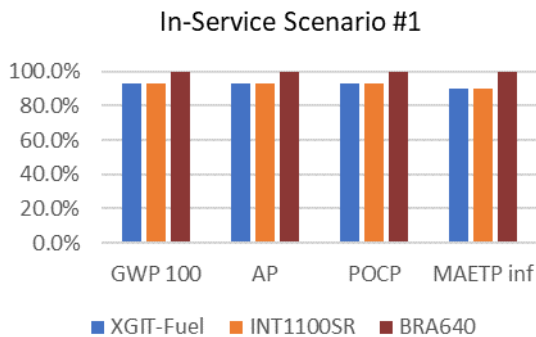


Figure 36: Relative environmental impact categories for In-Service Scenario #1 (BRA640 is the baseline for comparison).

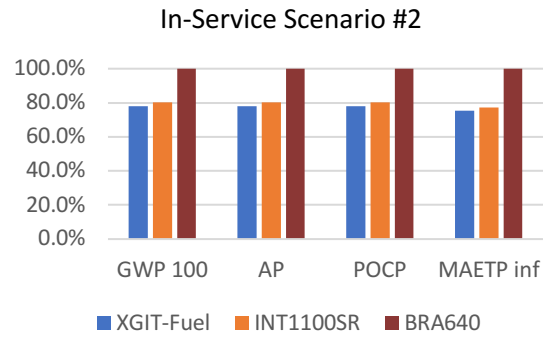


Figure 37: Relative environmental impact categories for In-Service Scenario #2 (BRA640 is the baseline for comparison).

It should be stated that each in-service scenario contains an inherent uncertainty value with the powering requirement for the “as-applied” condition for each coating type. These values were taken from the results of Chapter 3 and thus have corresponding uncertainty values from their determined roughness function values ( $\Delta U^+$ ) at 19 knots. This uncertainty in each coating was propagated through the in-service scenarios and resulted in a total uncertainty value of  $\pm 0.02\%$  ( $\pm 88-91$  MT HFO) in Scenario #1 and  $\pm 0.2\%$  ( $\pm 252-278$  MT HFO) in Scenario #2. As mentioned in Chapters 1 and 2, GWP and the reduction of global CO<sub>2</sub> emissions from shipping traffic is at the forefront of environmental issues for the industry. Shipping companies are constantly searching for solutions to reduce their environmental impact and meet upcoming regulations set by the International Maritime Organization (IMO). To illustrate the potential role of marine

coating choice on vessel efficiency, an avoided GHG emissions plot is presented in Figure 38.

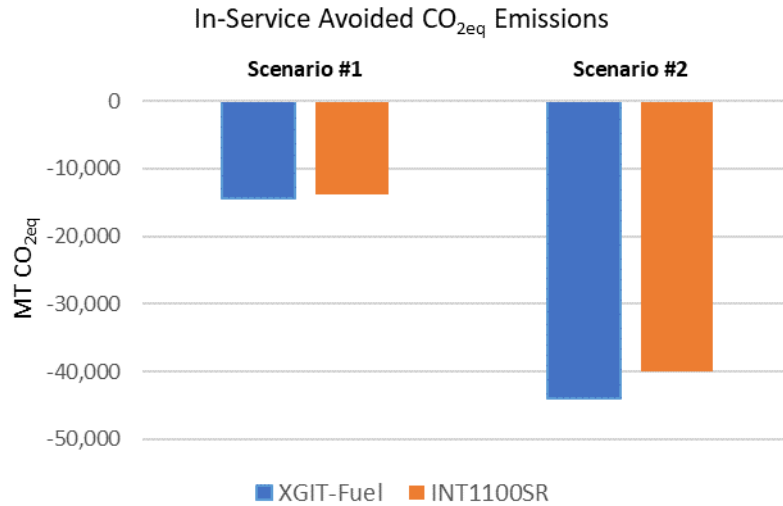


Figure 38: Avoided GHG emissions for each In-Service Scenario using BRA640 as the baseline.

A summary of the individual impact(s) from each LCA phase as well as the total impact value for GWP, AP, POCP, and MAETP is tabulated for all three systems in Table 23. The data quality and uncertainty in the result from each phase will be discussed in Section 5.

Table 23: LCA results for each coating system in both in-service scenarios (in terms of Global Warming Potential (GWP<sub>100</sub>), Acidification Potential (AP), Photochemical Oxidation Creation Potential (POCP), and Marine Aquatic Ecotoxicity Potential (MAETP<sub>inf</sub>).

XGIT-Fuel	Category	Unit	Production	Application	In-Service	Total
In-Service Scenario #1	GWP <sub>100</sub>	kg CO <sub>2</sub> eq	2.92E+04	7.45E+02	2.05E+08	2.05E+08
	AP	kg SO <sub>2</sub> eq	2.86E+01	1.92E+01	5.27E+06	5.27E+06
	POCP	kg C <sub>2</sub> H <sub>4</sub> eq	3.44E+00	1.23E+01	1.69E+05	1.69E+05
	MAETP <sub>inf</sub>	kg 1,4- DB eq	4.42E+06	3.54E+04	9.73E+09	9.73E+09
In-Service Scenario #2	GWP <sub>100</sub>	kg CO <sub>2</sub> eq	2.92E+04	7.45E+02	1.73E+08	1.73E+08
	AP	kg SO <sub>2</sub> eq	2.86E+01	1.92E+01	4.45E+06	4.45E+06
	POCP	kg C <sub>2</sub> H <sub>4</sub> eq	3.44E+00	1.23E+01	1.43E+05	1.43E+05
	MAETP <sub>inf</sub>	kg 1,4- DB eq	4.42E+06	3.54E+04	8.22E+09	8.23E+09
INT1100SR	Category	Unit	Production	Application	In-Service	Total
In-Service Scenario #1	GWP <sub>100</sub>	kg CO <sub>2</sub> eq	6.28E+04	1.49E+03	2.06E+08	2.06E+08
	AP	kg SO <sub>2</sub> eq	2.26E+02	3.83E+01	5.30E+06	5.30E+06

	POCP	kg C <sub>2</sub> H <sub>4</sub> eq	1.26E+01	2.74E+02	1.70E+05	1.70E+05
	MAETP <sub>inf</sub>	kg 1,4- DB eq	5.69E+07	7.08E+04	9.79E+09	9.85E+09
<b>In-Service Scenario #2</b>	GWP <sub>100</sub>	kg CO <sub>2</sub> eq	6.28E+04	1.49E+03	1.78E+08	1.78E+08
	AP	kg SO <sub>2</sub> eq	2.26E+02	3.83E+01	4.57E+06	4.57E+06
	POCP	kg C <sub>2</sub> H <sub>4</sub> eq	1.26E+01	2.74E+02	1.46E+05	1.47E+05
	MAETP <sub>inf</sub>	kg 1,4- DB eq	5.69E+07	7.08E+04	8.43E+09	8.49E+09
<b>BRA640</b>	<b>Category</b>	<b>Unit</b>	<b>Production</b>	<b>Application</b>	<b>In-Service</b>	<b>Total</b>
<b>In-Service Scenario #1/#2</b>	GWP <sub>100</sub>	kg CO <sub>2</sub> eq	5.76E+04	1.49E+03	2.22E+08	2.22E+08
	AP	kg SO <sub>2</sub> eq	0.00E+00	3.83E+01	5.70E+06	5.70E+06
	POCP	kg C <sub>2</sub> H <sub>4</sub> eq	0.00E+00	4.16E+02	1.83E+05	1.83E+05
	MAETP <sub>inf</sub>	kg 1,4- DB eq	8.14E+08	7.08E+04	1.09E+10	1.17E+10

## 4.5 Life Cycle Interpretation

In terms of data quality, the Ecoinvent database was investigated and put through a data quality rating system for all input flows associated with the production phase of each coating. The rating system uses four indicators, reliability of the data, completeness of the data, temporal correlation (how recent it was collected), and further technical correlation (is the data related to the paints and coatings industry). Each indicator was given a score out of 5 in openLCA, with 1 being the best and 5 being the worst score. As noted above, two environmental indicators for the BRA640 coating system were deemed unreliable because of this rating system. The results from the data quality investigation are provided in Table 24 below.

Table 24: LCA data quality rating system for the Ecoinvent database using four indicators (Reliability, Completeness, Temporal Correlation, and Further Technological Correlation)

Marine Coating	Impact Category	Reliability	Completeness	Temporal correlation	Further technological correlation
<b>XGIT-Fuel</b>	<b>GWP<sub>100</sub></b>	2/5 – “Verified data partly based on assumptions or non-verified data based on measurements”	3/5 – “Representative data from only some sites (<< 50%) relevant for the market considered or > 50% of sites but from shorter periods”	5/5 – “Age of data unknown or more than 15 years of difference to the time period of the data set”	2/5 – “Data from processes and materials under study (i.e., identical technology) but from different enterprises”
	<b>AP</b>	3/5 – “Non-verified data	3/5 – “Representative data	5/5 – “Age of data	3/5 – “Data from processes

		partly based on qualified estimates”	from only some sites (<< 50%) relevant for the market considered or > 50% of sites but from shorter periods”	unknown or more than 15 years of difference to the time period of the data set”	and materials under study but from different technology”
	<b>POCP</b>	3/5 – “Non-verified data partly based on qualified estimates”	4/5 – “Representative data from only one site relevant for the market considered or some sites but from shorter periods”	5/5 – “Age of data unknown or more than 15 years of difference to the time period of the data set”	3/5 – “Data from processes and materials under study but from different technology”
	<b>MAETP<sub>inf</sub></b>	2/5 – “Verified data partly based on assumptions or non-verified data based on measurements”	2/5 – “Representative data from > 50% of the sites relevant for the market considered, over an adequate period to even out normal fluctuations”	4/5 – “Less than 15 years of difference to the time period of the data set”	1/5 – “Data from enterprises, processes and materials under study”
<b>INT1100SR</b>	<b>GWP<sub>100</sub></b>	2/5 – “Verified data partly based on assumptions or non-verified data based on measurements”	2/5 – “Representative data from > 50% of the sites relevant for the market considered, over an adequate period to even out normal fluctuations”	4/5 – Less than 15 years of difference to the time of the data set	2/5 – “Data from processes and materials under study (i.e., identical technology) but from different enterprises”
	<b>AP</b>	2/5 – “Verified data partly based on assumptions or non-verified data based on measurements”	2/5 – “Representative data from > 50% of the sites relevant for the market considered, over an adequate period to even out normal fluctuations”	5/5 – “Age of data unknown or more than 15 years of difference to the time period of the data set”	1/5 – “Data from enterprises, processes and materials under study”
	<b>POCP</b>	2/5 – “Verified data partly based on assumptions or non-verified data based on measurements”	2/5 – “Representative data from > 50% of the sites relevant for the market considered, over an adequate period to even out normal fluctuations”	4/5 – Less than 15 years of difference to the time of the data set	2/5 – “Data from processes and materials under study (i.e., identical technology) but from different enterprises”
	<b>MAETP<sub>inf</sub></b>	2/5 – “Verified data partly based on assumptions or non-verified data based on measurements”	2/5 – “Representative data from > 50% of the sites relevant for the market considered, over an adequate	4/5 – Less than 15 years of difference to the time period of the data set	1/5 – “Data from enterprises, processes and materials under study”

			period to even out normal fluctuations”		
<b>BRA640</b>	<b>GWP<sub>100</sub></b>	3/5 – “Non-verified data partly based on qualified estimates”	2/5 – “Representative data from > 50% of the sites relevant for the market considered, over an adequate period to even out normal fluctuations”	4/5 – “Less than 15 years of difference to the time period of the data set”	2/5 – “Data from processes and materials under study (i.e., identical technology) but from different enterprises”
	<b>AP (not included due to data quality)</b>	5/5 – “Non-qualified estimates”	4/5 – “Representative data from only one site relevant for the market considered or some sites but from shorter periods”	3/5 – “Less than 10 years of difference to the time period of the data set”	3/5 – “Data from processes and materials under study but from different technology”
	<b>POCP (not included due to data quality)</b>	5/5 – “Non-qualified estimates”	4/5 – “Representative data from only one site relevant for the market considered or some sites but from shorter periods”	5/5 – “Age of data unknown or more than 15 years of difference to the time period of the data set”	3/5 – “Data from processes and materials under study but from different technology”
	<b>MAETP<sub>inf</sub></b>	1/5 – “Verified data based on measurements”	1/5 – “Representative data from all sites relevant for the market considered, over and adequate period to even out normal fluctuation”	4/5 – “Less than 15 years of difference to the time period of the data set”	1/5 – “Data from enterprises, processes and materials under study”

For the application phase, data was obtained through personal communication with Irving Shipbuilding for the workforce and equipment required to paint a vessel of this size. The author is aware that these times reported can vary depending on the size of dockyard, equipment, and level of expertise in coating application. Secondly, the assumed values from AkzoNobel (2017) were specific to their case study and are not necessarily transferrable to all shipyard locations. However, these assumptions for coating application were found to have a minimal impact on the overall conclusion of the study.

Both in-service scenarios have assumptions and limitations that stemmed from a lack of data and the difficulty associated with modelling biofouling growth rates on the hull of an active vessel. The author believes that the most representative in-service

scenario would be based on both static and dynamic panel data rather than groomed panel data. This would reduce the uncertainty associated with the required ship speed to remove certain fouling organisms from the ship's hull. There are also niche areas on the hull that are not subject to high shear and therefore tend to foul much more aggressively than the main sections (vertical sides and flat bottom). Unlike the time-dependent fouling growth model presented in Uzun et al., 2019b for SPC coatings, this model presents data for a copper ablative and two foul release coatings for a high fouling pressure environment. It is of note that the time-dependent drag performances of all three coating systems will vary significantly depending on the fouling pressure, vessel activity and ship type.

It has been well-demonstrated that the largest hull roughness elements (coating roughness or fouling organisms) dominate the effects of frictional resistance (Schultz et al., 2015). Swain et al. (2022) determined that with a proactive non-invasive hull grooming scheme, the hydrodynamically smooth condition (fouling-free) can be maintained throughout the entire drydock cycle for the INT1100SR and BRA640 coatings. Moreover, the INT1100SR and XGIT-Fuel coatings have both demonstrated further reductions in frictional resistance compared to a hydraulically smooth surface. From a global perspective we can look at the total number of 3600 TEU container vessels (815) and run them through this LCA model with the INT1100SR and XGIT-Fuel coatings. If we assume they fall into Scenario #1, they could collectively save 11.3-12.4 million tons of CO<sub>2eq</sub> or save 32.5-25.8 million tons of CO<sub>2eq</sub> in Scenario #2 over a 5-year drydock cycle. This calculation is purely an illustration of the scale of the problem (fouling) as well as the potential positive environmental impact of a suitable marine coating.

#### **4.5.1 Other LCA Limitations**

Another limitation to the study is the assumption that the foul release coatings with partial coverage of biofilm will behave like a uniformly covered biofilm/slime surface. There has been research conducted to capture the frictional resistance of certain types of biofilm (micro fouling) in fully turbulent flow conditions by Schultz et al.

(2015). As a suggested next step, a research collaboration with the University of Strathclyde could analyze the flow behavior of dynamically grown biofilms on the surface of the coatings analyzed in this study, namely XGIT-Fuel. The author has also learned of a marine antifoulant model to predict environmental concentrations known as “MAMPEC”. This software could be useful for modelling the environmental impacts of biocides release rates under various environmental conditions and could serve as a more comprehensive analysis tool for this purpose rather than using LCA.

The developed methodology in this comparative LCA analysis can contribute to improving the environmental performance of anti-fouling coatings by highlighting the negative impacts on shipowners and the environment. This research should be of value to marine coating producers, LCA practitioners, shipping companies and environmental regulators. This comparative LCA of XGIT-Fuel demonstrates that it can have superior environmental performance to ablative anti-fouling coatings used on over 90% of ships in the industry in the GWP, AP, POCP and MAETP impact categories. The results for the production, application, and biocide release of the ablative anti-fouling coating (BRA640) in this chapter agree with other LCA studies conducted by Ayer et al., (2016), Blanco-Davis et al., (2014), Lin and Usino (2014) and Rossini et al. (2019).



## **CHAPTER 5 CONCLUSIONS, LIMITATIONS AND RECOMMENDATIONS FOR FUTURE WORK**

In Chapter 2, a small-scale fishing boat study was conducted to determine the potential fuel savings of the XGIT-Fuel coating against a pre-existing gelcoat barrier coating and two levels of fouling growth. The study was successful in identifying a relationship between the hull condition of the vessels, their fuel efficiency, and their max throttle speed gain. The study was limited in scope to a small fleet of four fishing boats, for which none were identical in size and propulsion. As a recommendation, sea trials should be conducted on a much larger vessel to determine if the fuel savings reported herein are repeatable.

The roughness functions of various marine coating types including XGIT-Fuel were successfully determined in Chapter 3. XGIT-Fuel had the lowest frictional resistance of all the marine coating measured in the fully turbulent flow channel including the smooth acrylic reference surface. This data was used in Granville's similarity law scaling procedure to determine the resulting effect on the frictional resistance at ship scale. For a 232.5m KRISO containership, XGIT-Fuel was found to reduce its frictional resistance by 4.6% at 19knots and 3.6% at 24 knots compared to a hydrodynamically smooth surface, which resulted in effective power reductions of 3.5% and 2.4% respectively. Future research is needed to determine the drag performance of XGIT-Fuel with dynamically grown biofilms, which can be accomplished through an extended test campaign at the University of Strathclyde

A comparative LCA was conducted on the production, application, and in-service phases of BRA640, INT1100SR, and XGIT-Fuel applied to the hull of a 3,600 TEU containership. Two in-service scenarios were used to compare the operation phase of the containership applied with each marine coating system. Since the BRA640 was found to have the worst drag performance over time, it was used as the baseline system for comparison. The BRA640 system also had the largest in all environmental impact categories due to the largest shipping emissions during the in-service phase, and the

release of cuprous oxide to the marine environment through its anti-fouling mechanism. The methodology used for this comparative LCA should be reviewed by other LCA practitioners, ship owners, and marine coating manufacturers to confirm that the assumptions and data quality align with industry standards. The interpretation phase of this LCA should be used as resource, to guide sustainable product design for future marine coating technologies.

## Appendix A: Supplementary Sea Trial Data

### Tjärnö & Kristineberg Regional Fouling Ratings

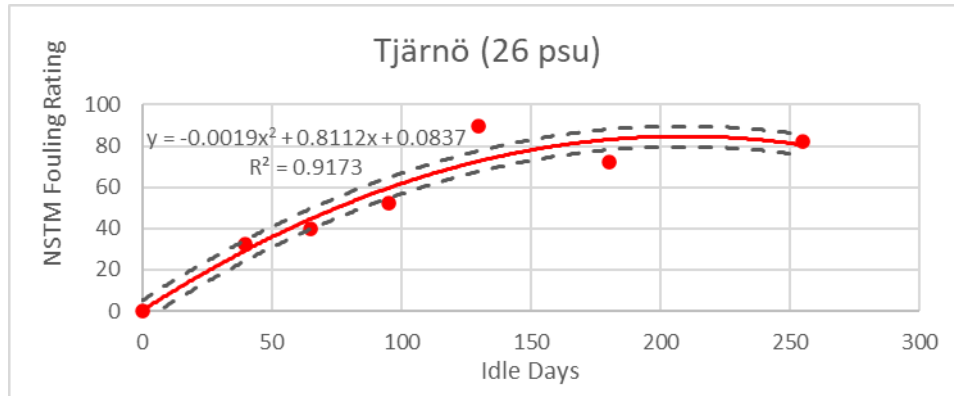


Figure 39: Tjärnö fouling region adapted from Oliveira et al. (2021).

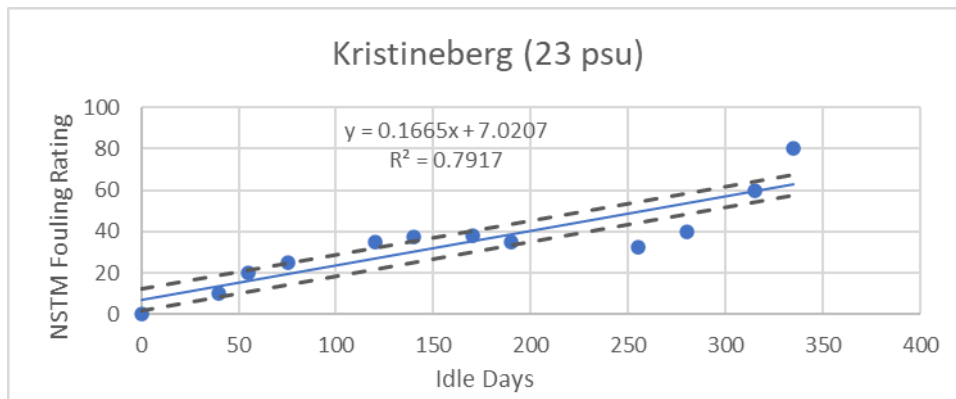


Figure 40: Kristineberg fouling region adapted from Oliveira et al. (2021).

Shaft RPM vs. Speed for All Vessels

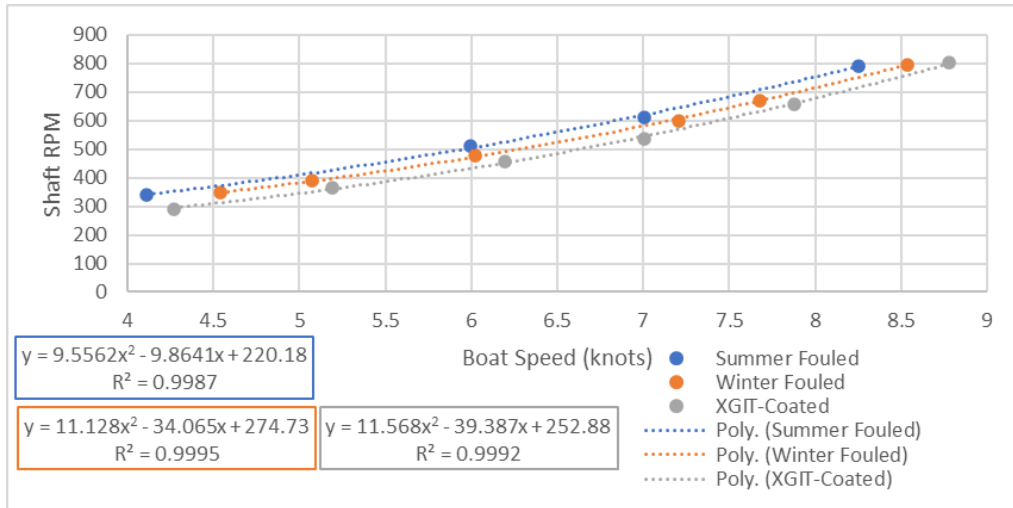


Figure 41: Shaft RPM vs. Speed for Vessel Alpha

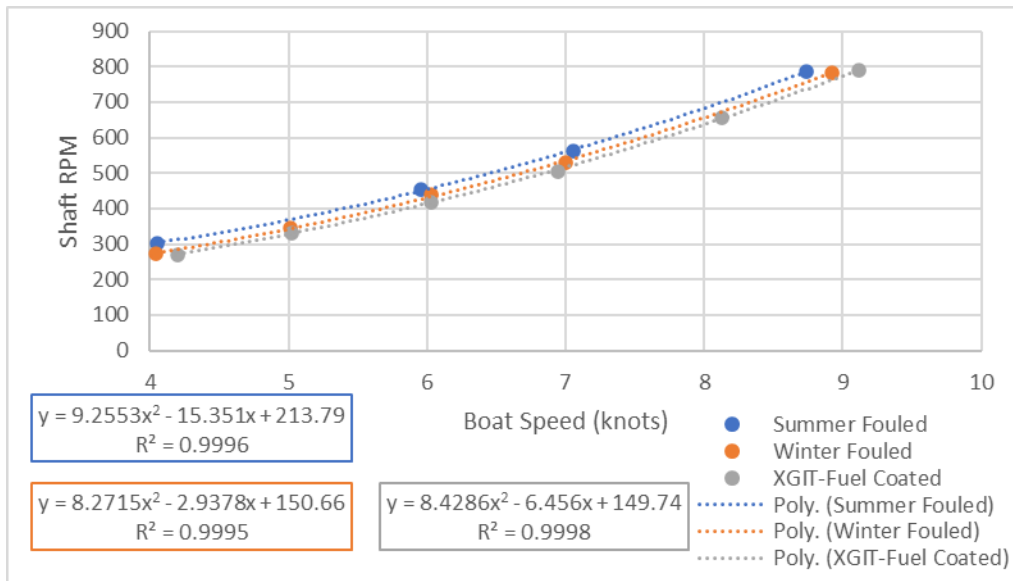


Figure 42: Shaft RPM vs. Speed for Vessel Bravo

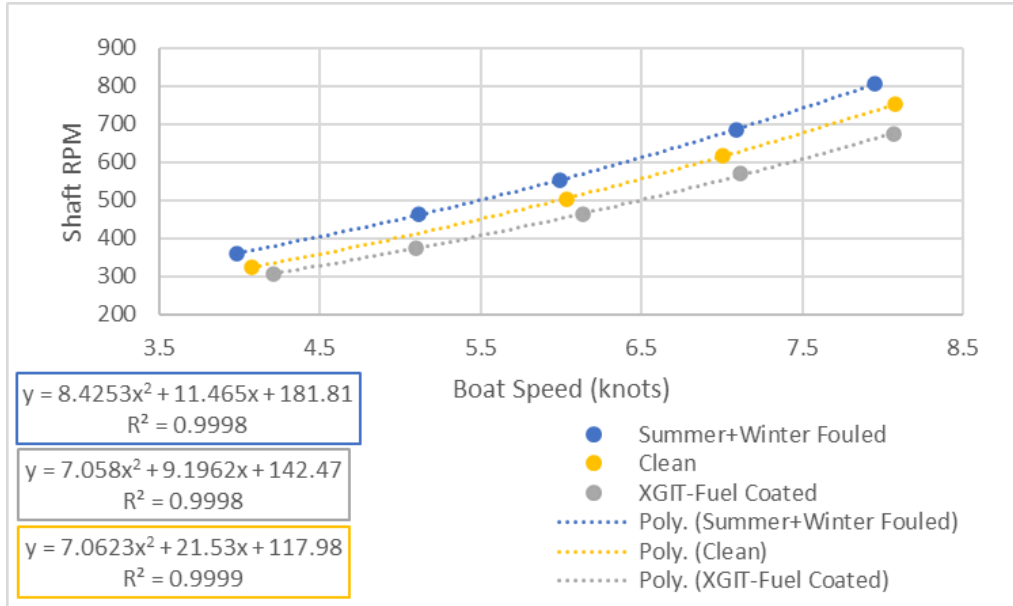


Figure 43: Shaft RPM vs. Speed for Vessel Charlie

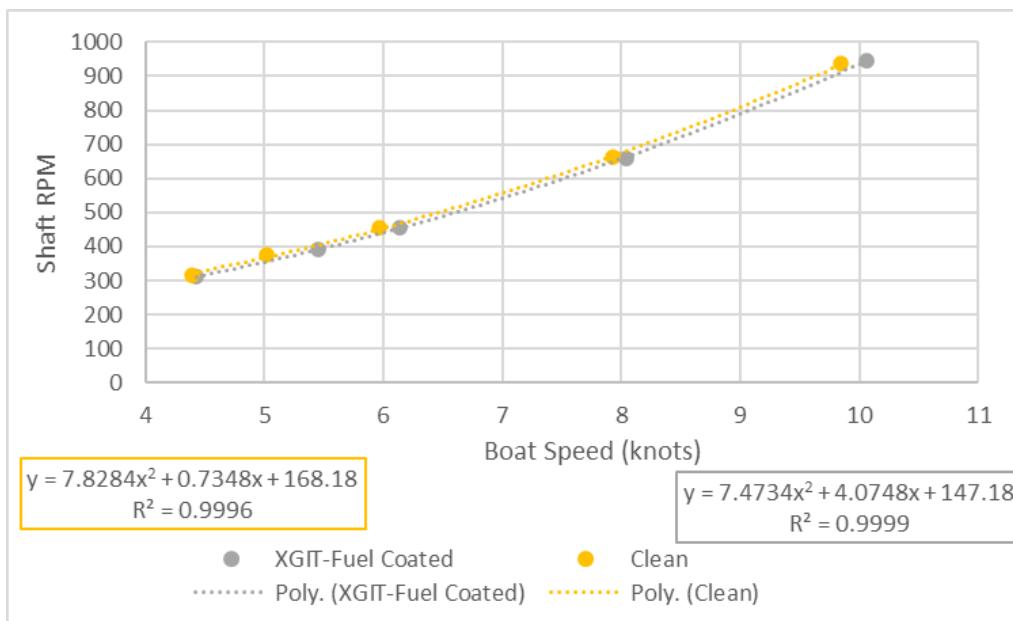


Figure 44: Shaft RPM vs. Speed for Vessel Delta

Vessel Photos and Sea Trial Dates

**Alpha**  
Gel Coat



**Bravo**  
Gel Coat



Figure 45: Photos of Alpha and Bravo after a season of summer fouling growth.

**Charlie**  
Gel Coat









**Delta**  
Gel Coat




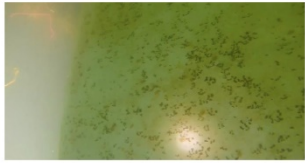

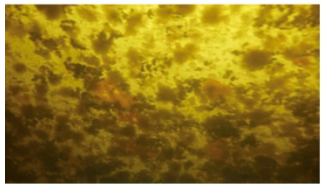
Figure 46: Photos of Charlie and Delta after a season of summer fouling growth.




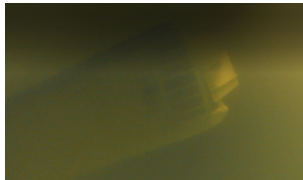
Table 25: Overview of all speed trial dates and vessel hull conditions.

Vessel Name	Sea Trial Date	Hull Condition	NSTM Rating	Image of Hull Condition
Charlie	21 Oct 2020	Clean	NSTM 0 Foul free surface	No photo as hull was cleaned 6 days prior to sea trial.
Bravo	28 Oct 2020	Summer Fouled	NSTM 50-70 Heavy layer of algae and barnacles (~7mm in height)	
Alpha	28 Oct 2020	Summer Fouled	NSTM 50-70 Heavy layer of algae and barnacles (~7mm in height)	
Alpha	3 June 2021	Winter Fouled	NSTM 30-40 Thin layer of slime and barnacles (~2mm in height)	

Bravo	10 June 2021	Winter Fouled	NSTM 30-40 Thin layer of slime and barnacles (~2mm in height)	
Bravo	24 June 2021	XGIT-Fuel Coated	NSTM 0 Foul free surface	
Alpha	24 June 2021	XGIT-Fuel Coated	NSTM 0 Foul free surface	



Charlie	1 Sept. 2021	Summer + Winter Fouled	NSTM 50-70 Composite fouling Tunicates 50mm in height, barnacles 5- 7mm in height, hydroids 1- 2mm in height	
Delta	1 Sept. 2021	Clean	NSTM 0 Foul free surface	No photo as hull was cleaned days prior to sea trial.
Charlie	6 Oct. 2021	XGIT-Coated	NSTM 0 Foul free surface	Missing photo
Delta	6 Oct. 2021	XGIT-Coated	NSTM 0 Foul free surface	Missing photo
Alpha	23 Jul. 2021	XGIT-Coated – Summer Fouled	NSTM 20-30 Patches of soft fouling growth (colonial tunicates)	
Bravo	23 Jul. 2021	XGIT-Coated – Summer Fouled	NSTM 20-30 Patches of soft fouling growth (colonial tunicates)	
Bravo	26 Aug. 2021	XGIT-Coated – Summer Fouled	NSTM 40-50 Patches of soft fouling growth (colonial tunicates & encrusting bryozoans)	
Alpha & Bravo	Jan. 2022	XGIT-Coated – Clean from Foul Release	NSTM 0-10 Surface is free of any visible	Bow area

		<p>&amp; Winter Season</p>	<p>growth, difficult to see any evidence of slime given the lighting in the underwater images.</p>	 <p>Mid vessel areas</p>   <p>Stern area</p> 
--	--	----------------------------	--	---

**Appendix B: Supplementary Fully Turbulent Flow Channel Data**  
Test Panel Images

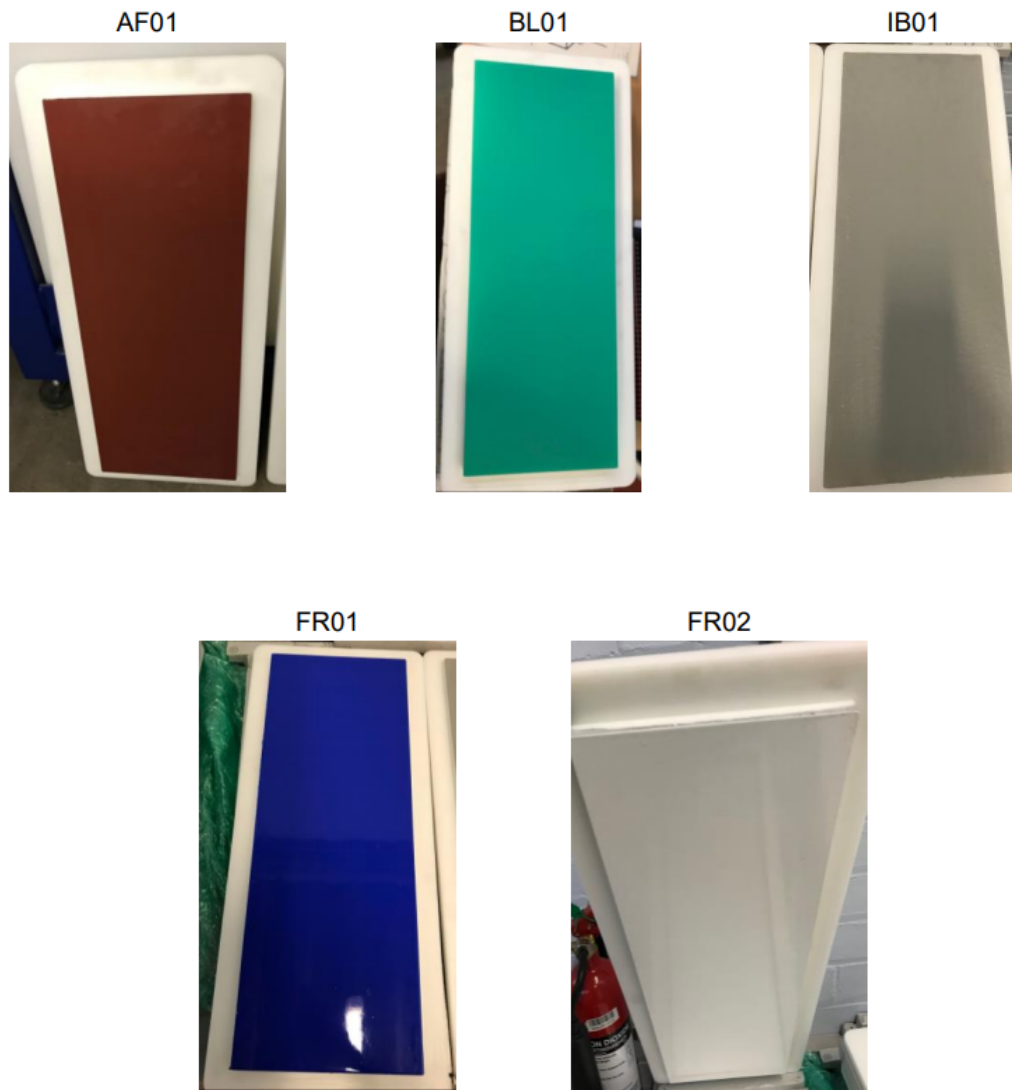


Figure 47: Images of each coated panel tested in the fully turbulent flow channel.

Added Resistance Diagrams

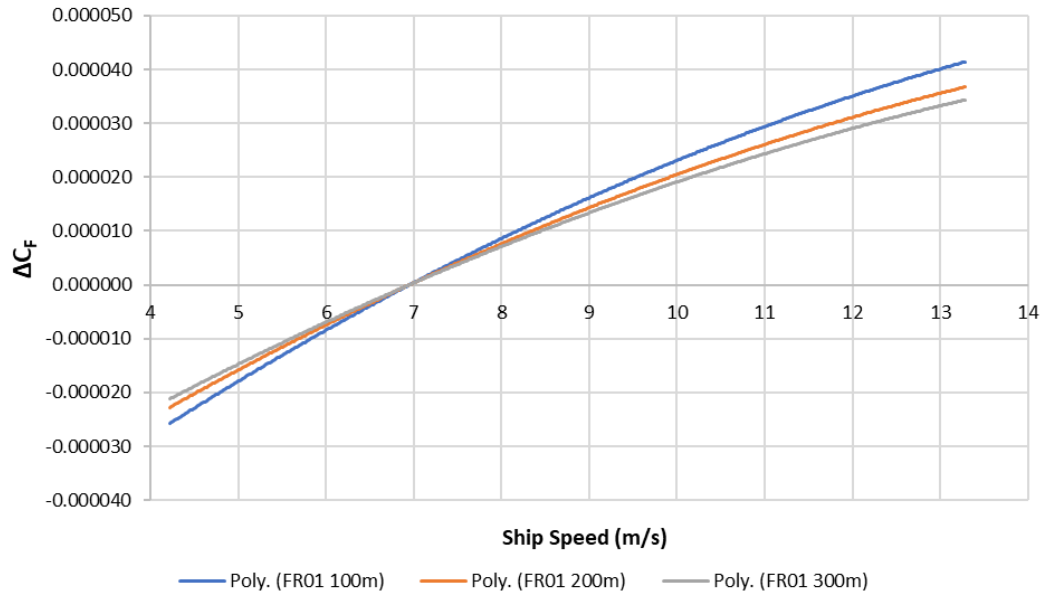


Figure 48: Added resistance diagram for FR01 for 100m, 200m and 300m ship lengths.

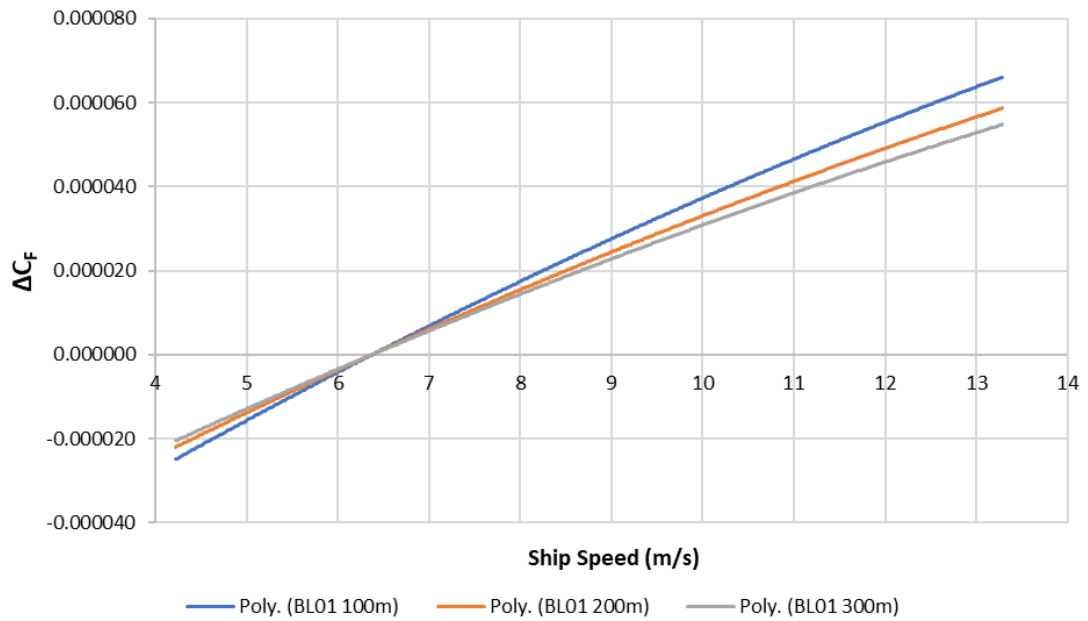


Figure 49: Added resistance diagram for BL01 for 100m, 200m and 300m ship lengths.

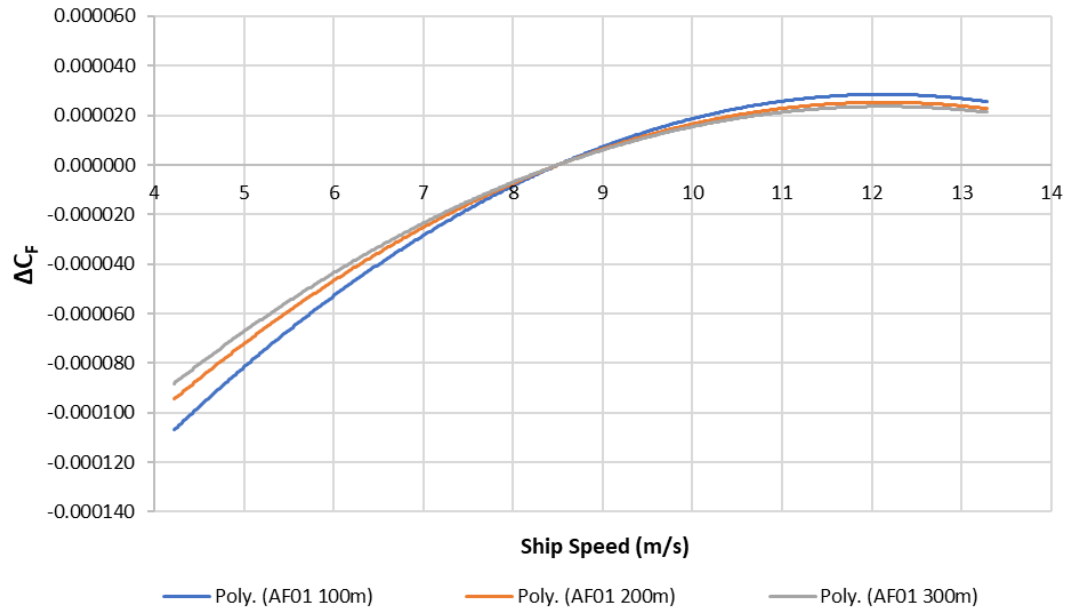


Figure 50: Added resistance diagram for AF01 for 100m, 200m and 300m ship lengths.

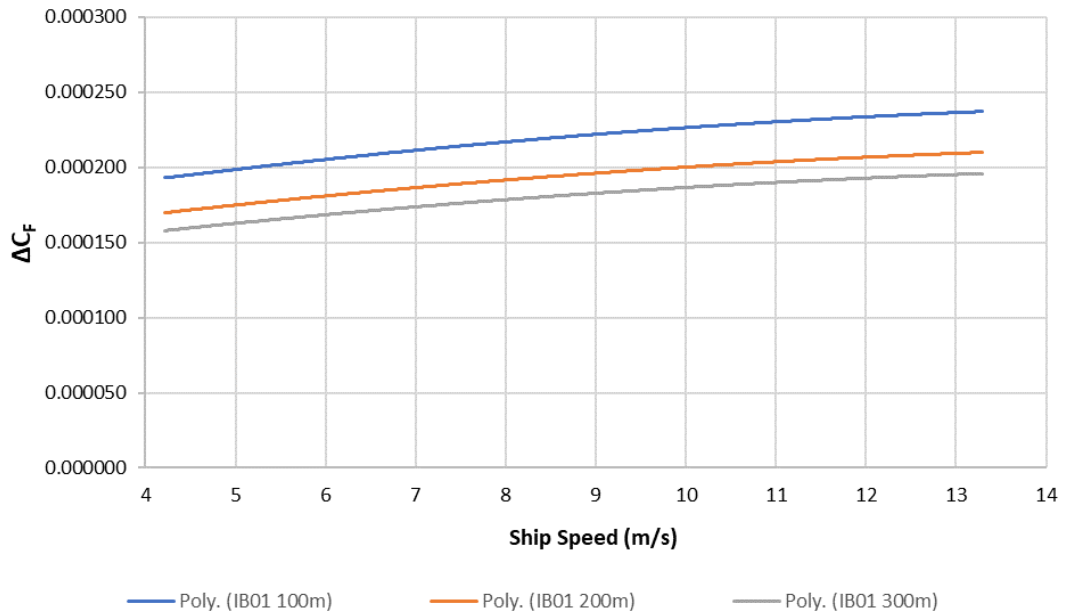


Figure 51: Added resistance diagram for IB01 for 100m, 200m and 300m ship lengths.

## Appendix C: Supplementary LCA Data

Table 26: OpenLCA inventory for INT1100SR hazardous raw material components.

Raw Material Component	Raw Material (kg)	Avg. Weight Fraction (%)
Poly(dimethylsiloxane)	1149.7	28.1%
Titanium dioxide	536.5	13.1%
Xylene	594.4	14.5%
Activated silica	168.6	4.1%
Ethyl benzene	287.8	7.0%
<b>Total</b>	<b>2737.0</b>	<b>67.0%</b>

Table 27: OpenLCA inventory for XGIT-Fuel hazardous raw material components.

Raw Material Component	Raw Material (kg)	Avg. Weight Fraction (%)
Methyl acetate	706.7	17.0%
Graphite	150.9	3.6%
Benzyl alcohol	75.5	1.8%
<b>Total</b>	<b>933.1</b>	<b>22.4%</b>

## BIBLIOGRAPHY

- AkzoNobel, 2017. Case Studies - Marine Coatings - AkzoNobel [WWW Document].  
URL <https://www.international-marine.com/cases> (accessed 3.22.22).
- AkzoNobel Sustainability, 2017. Avoiding Greenhouse Gas Emissions - The Essential Role of Chemicals - Case 10 - A comparative study of three fouling control systems for marine vessels.
- Anderson, C., Atlar, M., Callow, M., Candries, M., Townsin, R., 2003. The development of foul-release coatings for seagoing vessels. Proc. Inst. Mar. Eng. Sci. Technol. Part B, J. Mar. Des. Oper. 2003, 11–23.
- ASTM, 2020. Standard Test Method for Testing Antifouling Panels in Shallow Submergence [WWW Document]. URL <https://www.astm.org/standards/d3623> (accessed 3.28.22).
- Atlar, M., Ünal, B., Ünal, U.O., Politis, G., Martinelli, E., Galli, G., Davies, C., Williams, D., 2013. An experimental investigation of the frictional drag characteristics of nanostructured and fluorinated fouling-release coatings using an axisymmetric body. Biofouling 29, 39–52. <https://doi.org/10.1080/08927014.2012.745856>
- Augusto Paz-Villarraga, C., Fillmann, G., 2021. Biocides in Antifouling Paint Formulations Currently Registered For Use. <https://doi.org/10.21203/rs.3.rs-704342/v1>
- Ayer, N., Martin, S., Dwyer, R.L., Gace, L., Laurin, L., 2016. Environmental performance of copper-alloy Net-pens: Life cycle assessment of Atlantic salmon grow-out in copper-alloy and nylon net-pens. Aquaculture 453, 93–103. <https://doi.org/10.1016/J.AQUACULTURE.2015.11.028>
- Blanco-Davis, E., del Castillo, F., Zhou, P., 2014. Fouling release coating application as an environmentally efficient retrofit: a case study of a ferry-type ship. Int. J. Life Cycle Assess. 19, 1705–1715. <https://doi.org/10.1007/S11367-014-0780-8>
- Candries, M., Atlar, M., 2005. Experimental investigation of the turbulent boundary layer of surfaces coated with marine antifouling. J. Fluids Eng. Trans. ASME 127, 219–232. <https://doi.org/10.1115/1.1891148>
- Chen, L., Duan, Y., Cui, M., Huang, R., Su, R., Qi, W., He, Z., 2021. Biomimetic surface coatings for marine antifouling: Natural antifoulants, synthetic polymers and surface

- microtopography. *Sci. Total Environ.* 766.  
<https://doi.org/10.1016/J.SCITOTENV.2020.144469>
- Coleman, H.W., Steele, W.G., 1995. Engineering application of experimental uncertainty analysis. *AIAA J.* 33, 1888–1896. <https://doi.org/10.2514/3.12742>
- Corbett, J.J., Winebrake, J.J., 2011. Energy and GHG Emissions Savings Analysis of Fluoropolymer Foul Release Hull Coating.
- COVE, 2022. COVE Ocean - Centre for Ocean Ventures & Entrepreneurship [WWW Document]. URL <https://coveocean.com/> (accessed 3.27.22).
- Dafforn, K.A., Lewis, J.A., Johnston, E.L., 2011. Antifouling strategies: History and regulation, ecological impacts and mitigation. *Mar. Pollut. Bull.* 62, 453–465.  
<https://doi.org/10.1016/J.MARPOLBUL.2011.01.012>
- Demirel, Y.K., 2015. Modelling the Roughness Effects of Marine Coatings and Biofouling on Ship Frictional Resistance 1–231.
- Demirel, Y.K., Song, S., Turan, O., Incecik, A., 2019. Practical added resistance diagrams to predict fouling impact on ship performance. *Ocean Eng.* 186, 106112.  
<https://doi.org/10.1016/j.oceaneng.2019.106112>
- Demirel, Y.K., Uzun, D., Zhang, Yansheng, Turan, O., 2017. Life cycle assessment of marine coatings applied to ship hulls, in: *Maritime Energy Management (MARENER 2017)*.
- Ecoinvent Centre, 2018. ecoinvent Database – ecoinvent v3.5 [WWW Document]. URL <https://ecoinvent.org/the-ecoinvent-database/data-releases/ecoinvent-3-5/> (accessed 3.21.22).
- Finnie, A.A., 2007. Improved estimates of environmental copper release rates from antifouling products. <https://doi.org/10.1080/08927010600898862> 22, 279–291.  
<https://doi.org/10.1080/08927010600898862>
- Granville, P.S., 1987. Three Indirect Methods for the Drag Characterization of Arbitrarily Rough Surfaces on Flat Plates. *J. Sh. Res.* 31, 70–77.  
<https://doi.org/10.5957/jsr.1987.31.1.70>
- Granville, P.S., 1958. The Frictional Resistance and Turbulent Boundary Layer of Rough Surfaces. *J. Sh. Res.* 2, 52–74. <https://doi.org/10.5957/JSR.1958.2.4.52>
- Hearin, J., Hunsucker, K.Z., Swain, G., Stephens, A., Gardner, H., Lieberman, K.,



- Harper, M., 2015. Analysis of long-term mechanical grooming on large-scale test panels coated with an antifouling and a fouling-release coating. *Biofouling* 31, 625–638. <https://doi.org/10.1080/08927014.2015.1081687>
- Howell, D., Behrends, B., 2006. A review of surface roughness in antifouling coatings illustrating the importance of cutoff length. <https://doi.org/10.1080/08927010601035738>
- IMO, 2021. Further shipping GHG emission reduction measures adopted [WWW Document]. URL <https://www.imo.org/en/MediaCentre/PressBriefings/pages/MEPC76.aspx> (accessed 1.10.22).
- IMO, 2012. Annex 9, Resolution MEPC.213(63), 2012 Guidelines for the development of a Ship Energy Efficiency Management Plan (SEEMP).
- IMO, 2001. International Convention on the Control of Harmful Anti-Fouling Systems on Ships [WWW Document]. Afs/Conf/26. URL [https://www.imo.org/en/About/Conventions/Pages/International-Convention-on-the-Control-of-Harmful-Anti-fouling-Systems-on-Ships-\(AFS\).aspx](https://www.imo.org/en/About/Conventions/Pages/International-Convention-on-the-Control-of-Harmful-Anti-fouling-Systems-on-Ships-(AFS).aspx) (accessed 10.28.21).
- International Maritime Organization, 2021. Fourth IMO Greenhouse Gas Study.
- International Paint Ltd., 2011. Additional Information Theoretical and Practical Coverage [WWW Document]. URL <http://strandsindustrialcoatings.com/wp-content/uploads/2016/06/International-Paints-Theoretical-and-Practical-Coverage.pdf> (accessed 3.21.22).
- International Paint Ltd., n.d. Product Search - Marine Coatings [WWW Document]. URL <https://www.international-marine.com/productsearch> (accessed 3.26.22).
- ISO/TC 213, 2021. ISO - ISO 21920-2:2021 - Geometrical product specifications (GPS) — Surface texture: Profile — Part 2: Terms, definitions and surface texture parameters [WWW Document]. 3. URL <https://www.iso.org/standard/72226.html> (accessed 2.26.22).
- ISO 10890, 2010. Paints and varnishes — Modelling of biocide release rate from antifouling paints by mass-balance calculation.
- ISO 14040, 2006. ISO 14040:2006 Environmental management — Life cycle assessment

- Principles and framework.
- ISO 14044, 2006. ISO 14044:2006 Environmental management — Life cycle assessment — Requirements and guidelines.
- ISO 15016, 2015. ISO - ISO 15016:2015 - Ships and marine technology — Guidelines for the assessment of speed and power performance by analysis of speed trial data.
- ITTC, 2017. The Specialist Committee on Energy Saving Methods - Final Report and Recommendations to the 28th ITTC, in: Proceedings of 28th ITTC - Volume II.
- ITTC, 2011a. ITTC-Recommended Procedures Fresh Water and Seawater Properties.
- ITTC, 2011b. Specialist Committee on Surface Treatment – Final report and recommendations to the 26th ITTC, in: Proceedings of 26th ITTC – Volume II.
- Kim, S.M., Lee, Y.S., Kang, K.H., Yoo, K.S., 2014. The Analysis on the VOC Contents and Ozone Production Contribution of A Marine Paint in Korea . J. Korean Soc. Atmos. Environ. 30, 569–576. <https://doi.org/10.5572/KOSAE.2014.30.6.569>
- Lejars, M., Margailan, A., Bressy, C., 2012. Fouling release coatings: A nontoxic alternative to biocidal antifouling coatings. Chem. Rev. 112, 4347–4390. <https://doi.org/10.1021/CR200350V>
- Lin, S., Usino, D., 2014. Life cycle assessment of the use of marine biocides in antifouling paint A comparison of the environmental profiles between conventional copper-based and innovative Selektope paint.
- Lindholdt, A., Dam-Johansen, K., Olsen, S.M., Yebra, D.M., Kiil, S., 2015. Effects of biofouling development on drag forces of hull coatings for ocean-going ships: a review. J. Coatings Technol. Res. 415–444. <https://doi.org/10.1007/S11998-014-9651-2>
- Mapcarta, 2022. McGraths Cove Map - Nova Scotia, Canada [WWW Document]. URL <https://mapcarta.com/24485104> (accessed 3.25.22).
- Marino, A., Ilter, Y.K., Song, S., Shi, W., Atlar, M., Demirel, Y.K., 2019. Design specification, commission and calibration of the University of Strathclyde’s Fully Turbulent Flow Channel (FTFC) facility.
- Mitutoyo Corporation, 2016. Surface Roughness Tester User’s Manual SJ-201 [WWW Document].
- Muralikrishna, I. V., Manickam, V., 2017. Life Cycle Assessment. Environ. Manage. 57–

75. <https://doi.org/10.1016/B978-0-12-811989-1.00005-1>  
Naval Sea Systems Command, 2006. Waterborne underwater hull cleaning of navy ships.  
Nav. Ships' Tech. Man. 68pp.  
OECD.Stat [WWW Document], 2018. URL  
[https://stats.oecd.org/Index.aspx?DataSetCode=FISH\\_FLEET](https://stats.oecd.org/Index.aspx?DataSetCode=FISH_FLEET) (accessed 10.19.21).  
Oliveira, D.R., Granhag, L., 2020. Ship hull in-water cleaning and its effects on fouling-  
control coatings. *Biofouling* 36, 332–350.  
<https://doi.org/10.1080/08927014.2020.1762079>  
Oliveira, D.R., Lagerström, M., Granhag, L., Werner, S., Larsson, A., Ytreberg, E., 2021.  
HullMASTER – An Interactive Tool to Calculate Economic and Societal Costs and  
Benefits of Ship Hull Maintenance, in: 6th Hull Performance & Insight Conference  
HullPIC'21. pp. 95–111.  
Olmer, N., Comer, B., Roy, B., Mao, X., Rutherford, D., 2017. Greenhouse gas emissions  
from global shipping, 2013–2015 - International Council on Clean Transportation.  
Robertson, J.M., Martin, J.D., Burkhart, T.H., 1968. Turbulent flow in rough pipes. *Ind.  
Eng. Chem. Fundam.* 7, 253–265. <https://doi.org/10.1021/I160026A014>  
Rossini, P., Napolano, L., Matteucci, G., 2019. Biototoxicity and life cycle assessment of  
two commercial antifouling coatings in marine systems. *Chemosphere* 237.  
<https://doi.org/10.1016/J.CHEMOSPHERE.2019.124475>  
Safinah Group, 2021. The need for innovation in antifouling coatings. *PCE Int. Mag.*  
April - June.  
Schultz, M.P., 2007. Effects of coating roughness and biofouling on ship resistance and  
powering. *Biofouling* 23, 331–341. <https://doi.org/10.1080/08927010701461974>  
Schultz, M.P., 2004. Frictional resistance of antifouling coating systems. *J. Fluids Eng.*  
*Trans. ASME* 126, 1039–1047. <https://doi.org/10.1115/1.1845552>  
Schultz, M.P., Flack, K.A., 2013. Reynolds-number scaling of turbulent channel flow.  
*Phys. Fluids* 25. <https://doi.org/10.1063/1.4791606>  
Schultz, M.P., Myers, A., 2003. Comparison of three roughness function determination  
methods. *Exp. Fluids* 35, 372–379. <https://doi.org/10.1007/S00348-003-0686-X>  
Schultz, M.P., Walker, J.M., Steppe, C.N., Flack, K.A., 2015. Impact of diatomaceous  
biofilms on the frictional drag of fouling-release coatings. *Biofouling* 31, 759–773.

- <https://doi.org/10.1080/08927014.2015.1108407>
- Shin, Y.J., Kim, M.C., Lee, J.H., Song, M.S., 2019. A numerical and experimental study on the performance of a twisted rudder with wavy configuration. *Int. J. Nav. Archit. Ocean Eng.* 11, 131–142. <https://doi.org/10.1016/J.IJNAOE.2018.02.014>
- Shipping, T.C., Consultants, C., Lewis, J.A., 2007. Antifouling Performance Standards for The Maritime Industry Development of A Framework for The Assessment, Approval and Relevance of Effective Products 61.
- Sindagi, S., Vijayakumar, R., Nirali, S., Saxena, B.K., 2019. Numerical Investigation of Influence of Microbubble Injection, Distribution, Void Fraction and Flow Speed on Frictional Drag Reduction, in: *Proceedings of the Fourth International Conference in Ocean Engineering (ICOE2018)*. Springer, Singapore, pp. 293–318. [https://doi.org/10.1007/978-981-13-3119-0\\_17](https://doi.org/10.1007/978-981-13-3119-0_17)
- Song, S., Dai, S., Demirel, Y.K., Atlar, M., Day, S., Turan, O., 2021a. Experimental and theoretical study of the effect of hull roughness on ship resistance. *J. Sh. Res.* 65, 62–71. <https://doi.org/10.5957/JOSR.07190040>
- Song, S., Demirel, Y.K., Atlar, M., 2020a. Penalty of hull and propeller fouling on ship self-propulsion performance. *Appl. Ocean Res.* 94, 102006. <https://doi.org/10.1016/j.apor.2019.102006>
- Song, S., Demirel, Y.K., De Marco Muscat-Fenech, C., Tezdogan, T., Atlar, M., 2020b. Fouling effect on the resistance of different ship types. *Ocean Eng.* 216. <https://doi.org/10.1016/J.OCEANENG.2020.107736>
- Song, S., Ravenna, R., Dai, S., DeMarco Muscat-Fenech, C., Tani, G., Demirel, Y.K., Atlar, M., Day, S., Incecik, A., 2021b. Experimental investigation on the effect of heterogeneous hull roughness on ship resistance. *Ocean Eng.* 223, 108590. <https://doi.org/10.1016/J.OCEANENG.2021.108590>
- Sundaram, H.S., Cho, Y., Dimitriou, M.D., Weinman, C.J., Finlay, J.A., Cone, G., Callow, M.E., Callow, J.A., Kramer, E.J., Ober, C.K., 2011. Fluorine-free mixed amphiphilic polymers based on PDMS and PEG side chains for fouling release applications. *Biofouling* 27, 589–602. [https://doi.org/10.1080/08927014.2011.587662/SUPPL\\_FILE/GBIF\\_A\\_587662\\_SUP\\_19622516.PDF](https://doi.org/10.1080/08927014.2011.587662/SUPPL_FILE/GBIF_A_587662_SUP_19622516.PDF)

- Swain, G., 1999. Redefining antifouling coatings. *J. Prot. Coatings Linings*.
- Swain, G., Erdogan, C., Foy, L., Gardner, H., Harper, M., Hearin, J., Hunsucker, K.Z., Hunsucker, J.T., Lieberman, K., Nanney, M., Ralston, E., Stephens, A., Tribou, M., Walker, B., Wassick, A., 2022. Proactive In-Water Ship Hull Grooming as a Method to Reduce the Environmental Footprint of Ships. *Front. Mar. Sci.* 8, 2017. <https://doi.org/10.3389/FMARS.2021.808549/BIBTEX>
- Swain, G., Lund, G., 2016. Dry-dock inspection methods for improved fouling control coating performance. *J. Sh. Prod. Des.* 32, 174–185. <https://doi.org/10.5957/JSPD.32.3.150038>
- Swain, G.W., Kovach, B., Touzot, A., Casse, F., Kavanagh, C.J., 2007. Measuring the performance of today’s antifouling coatings. *J. Sh. Prod.* 23, 164–170. <https://doi.org/10.5957/JSP.2007.23.3.164>
- Takahashi, K., 2009. Release rate of biocides from antifouling paints. *Ecotoxicol. Antifouling Biocides* 3–22. [https://doi.org/10.1007/978-4-431-85709-9\\_1](https://doi.org/10.1007/978-4-431-85709-9_1)
- Tribou, M., Swain, G., 2015. Grooming using rotating brushes as a proactive method to control ship hull fouling. *Biofouling* 31, 309–319. <https://doi.org/10.1080/08927014.2015.1041021>
- UK Statutory Instruments, 2012. The Volatile Organic Compounds in Paints, Varnishes and Vehicle Refinishing Products Regulations 2012 [WWW Document]. URL <https://www.legislation.gov.uk/uksi/2012/1715/made> (accessed 3.22.22).
- UNCTAD, 2019. Review of Maritime Transport 2019, Review of Maritime Transport.
- US EPA, 2018. Complete List of VOC Exemption Rules | US EPA [WWW Document]. URL <https://www.epa.gov/ground-level-ozone-pollution/complete-list-voc-exemption-rules> (accessed 3.22.22).
- US EPA, 2017. 26 DEPARTMENT OF THE ENVIRONMENT - 11 AIR QUALITY Chapter 19 Volatile Organic Compounds from Specific Processes.
- USNA, 2002. Resistance and powering of ships [WWW Document]. Resist. powering ships. URL [https://www.usna.edu/NAOE/\\_files/documents/Courses/EN400/02.07 Chapter 7.pdf](https://www.usna.edu/NAOE/_files/documents/Courses/EN400/02.07 Chapter 7.pdf)
- Uzun, D., Demirel, Y.K., Coraddu, A., Turan, O., 2019a. Time-dependent biofouling growth model for predicting the effects of biofouling on ship resistance and

- powering. *Ocean Eng.* 191. <https://doi.org/10.1016/J.OCEANENG.2019.106432>
- Uzun, D., Demirel, Y.K., Coraddu, A., Turan, O., 2019b. Life cycle assessment of an antifouling coating based on time-dependent biofouling model, in: 18th Conference Computer and IT Applications in the Maritime Industries (COMPIT'19) At: Tullamore, Ireland.
- Van Rompay, B., 2012. Surface treated composites white book a proven, non-toxic, cost-effective alternative technology for underwater ship hull protection and biofouling control. Tahoka Press.
- VesselFinder, 2022. Free AIS Ship Tracker - VesselFinder [WWW Document]. URL <https://www.vesselfinder.com/> (accessed 3.21.22).
- Walker, J.M., Schultz, M.P., Flack, K.A., Steppe, C.N., Academy, U.S.N., 2014. Skin-friction drag measurements on ship hull coating systems 2–7.
- Woo, E.L., Karafiath, G., Borda, G., 1983. Ship-Model Correlation of Powering Performance on Uss Oliver Hazard Perry, Ffg-7 Class. *Mar. Technol.* 20, 35–52. <https://doi.org/10.5957/mt1.1983.20.1.35>
- Yeginbayeva, I.A., Atlar, M., 2018. An experimental investigation into the surface and hydrodynamic characteristics of marine coatings with mimicked hull roughness ranges. *Biofouling* 34, 1001–1019. <https://doi.org/10.1080/08927014.2018.1529760>
- Yeginbayeva, I.A., Atlar, M., Turkmen, S., Chen, H., 2020. Effects of ‘in-service’ conditions–mimicked hull roughness ranges and biofilms–on the surface and the hydrodynamic characteristics of foul-release type coatings. *Biofouling* 36, 1074–1089. <https://doi.org/10.1080/08927014.2020.1855330>
- You, D., Moin, P., 2007. Effects of hydrophobic surfaces on the drag and lift of a circular cylinder. *Phys. Fluids* 19, 081701. <https://doi.org/10.1063/1.2756578>
- Ytreberg, E., Åström, S., Fridell, E., 2021. Valuating environmental impacts from ship emissions – The marine perspective. *J. Environ. Manage.* 282, 111958. <https://doi.org/10.1016/J.JENVMAN.2021.111958>
- Zhang, Y., Yeginbayeva, I., Brink, A., 2021. Modelling and Simulation of the Effect of Antifouling Coating on Ship Resistance, in: 6th Hull Performance & Insight Conference HullPIC'21.
- Zhang, Z.P., Qi, Y.H., Ba, M., Liu, F., 2014. Investigation of silicone oil leaching in

PDMS fouling release coating by confocal laser scanning microscope. *Adv. Mater. Res.* 842, 737–741.

<https://doi.org/10.4028/WWW.SCIENTIFIC.NET/AMR.842.737>